EXPERIMENTAL STUDY OF NEAR ANODE PLASMA IN HOLLOW CATHODE CROSS FIELD DISCHARGES

By

RAMKRISHNA RANE

PHYS06201204015

Institute For Plasma Research, Gandhinagar

A thesis submitted to the
Board of Studies in Physical Sciences

In partial fulfillment of the requirements
for the degree of

DOCTOR OF PHILOSOPHY

of

HOMI BHABHA NATIONAL INSTITUTE

February 2019

Homi Bhabha National Institute

Recommendations of the Viva Voce Committee

As members of the Viva Voce Committee, we certify that we have read the dissertation prepared by **RAMKRISHNA RANE** entitled "EXPERIMENTAL STUDY OF NEAR ANODE PLASMA IN HOLLOW CATHODE CROSS FIELD DISCHARGES" and recommend that it may be accepted as fulfilling the thesis requirement for the award of Degree of Doctor of Philosophy.

SDeshpande

Chairman – Prof. S. Deshpande **Date : 07/06/2019**

SMukherjee

Guide / Convener - Prof. S. Mukherjee **Date : 07/06/2019**

Mainak

Co-guide - Dr. M. Bandyopadhyay **Date : 07/06/2019**

Examiner - Prof. Mridul Bose **Date : 07/06/2019**

PSharma

Member 1- Dr. P. Sharma **Date : 07/06/2019**

Member 2- Dr. G. Ravi **Date : 07/06/2019**

Final approval and acceptance of this thesis is contingent upon the candidate's submission of the final copies of the thesis to HBNI.

We hereby certify that we have read this thesis prepared under our direction and recommend that it may be accepted as fulfilling the thesis requirement.

Date: 07/06/2019

Place: IPR, Gandhinagar

Mainak

Dr. M. Bandyopadhyay

(Co-guide)

SMukherjee

Prof. S. Mukherjee

(Guide)

STATEMENT BY AUTHOR

This dissertation has been submitted in partial fulfillment of requirements for Ph.D. in Physical Sciences at Homi Bhabha National Institute (HBNI) and is deposited in the Library to be made available to borrowers under rules of the HBNI.

Brief quotations from this dissertation are allowable without special permission, provided that accurate acknowledgement of source is made. Requests for permission for extended quotation from or reproduction of this manuscript in whole or in part may be granted by the Competent Authority of HBNI when in his or her judgement the proposed use of the material is in the interests of scholarship. In all other instances, however, permission must be obtained from the author.

Rane

Ramkrishna Rane

DECLARATION

I, hereby declare that the investigation presented in the thesis has been carried out by me. The work is original and the work has not been submitted earlier as a whole or in part for a degree/diploma at this or any other Institution/University.

Ramkrishna Rane

List of Publications arising from the thesis

Journal:

1. **Controllable transition from positive space charge to negative space charge in an inverted cylindrical magnetron**

   R. Rane, M. Bandyopadhyay, M. Ranjan and S. Mukherjee *Phys. Plasmas* **23**, 013514, (2016).

2. **Experimental investigation of near anode phenomenon in inverted cylindrical magnetron discharge**

   R. Rane, P. Bandyopadhyay, M. Bandyopadhyay and S. Mukherjee *Phys. Plasmas* **25**, 063516, (2018).

3. **Electron sheath evolution controlled by a magnetic field in modified hollow cathode glow discharge**

   R. Rane, S. Chauhan, P. Bharathi, K. Nigam, P. Bandyopadhyay and S. Mukherjee *Phys. Plasmas* **25**, 093509, (2018).

4. **Comparative study of discharge characteristics and associated film growth for post-cathode and inverted cylindrical magnetron sputtering**

   R. Rane, A. Joshi, S. Akkireddy and S. Mukherjee *Pramana- J.Phys.* **92**, 55,(2019).

Conferences Presentations:

1. **The anode glow formation and its effect on thin film deposition in a Hollow Cathode Cylindrical Magnetron(HCCM) discharge**

   R.Rane, A.Joseph, S. Mukherjee. 33^{rd} *National Symposium on Plasma Science and Technology, PLASMA - 2018, December 4 to 7,2018* New Delhi, India.

2. **Magnetic field induced anode sheath transition in modified hollow cathode discharge**

   R. Rane, K Nigam, P Bharathi, A Joseph, S. Mukherjee.71^{st} *Annual Gaseous Electronics Conference, November 5 to 9, 2018*, Portland, USA.

3. **Magnetic field controlled transition from positive space charge to negative space charge in an inverted cylindrical magnetron**

   R. Rane, M. Bandyopadhyay, M. Ranjan, and S. Mukherjee.10^{th} *Asia Plasma and Fusion Association ,Dec- 2015*, Ahmedabad , India.

4. **Influence of magnetic field on near anode plasma properties of reflex plasma source**

   R.Rane, K. Nigam, A. Vaid, S. Mukherjee.32^{nd} *National Symposium on Plasma Science and Technology, PLASMA - 2017* Ahmedabad, India.

Ramkrishna Rane

In loving memory

of

Baba

(my Uncle)

Late Shri. Sabaji Rajaram Rane
- 17/01/2018

His love and support made my life gratifying. He passed away during my Ph.D. tenure.
His cheerful memories will last forever with me and my family.

ACKNOWLEDGEMENTS

First and foremost, I would like to acknowledge the efforts, love and sacrifices of my better half Mrs. Gayatri Rane. I also acknowledge and appreciate the support of my mother Smt. Savitri Rane, my brother Mr. Rajaram Rane and my other family members. The love of my daughter Ms. Gargi Rane always gives me more energy to work.

I cannot appreciate enough in words the contribution of my guide and mentor Dr. S. Mukherjee. He tutored me and built my strong base upon which I was able to work for my thesis. He always stood by my side during the ups and downs of my research work. His kind attitude helped me stay on track. He made it smooth for me to clear the hurdles of the research. He taught me not only the way of research but also encouraged me to keep fighting in bad situations. I feel lucky to get a guide like him. He will always remain my guide and mentor for the rest of my life.

I thank my Co-guide Dr. Mainak Bandyopadhyay, who always pushed me to do more. He gave me a different perspective and new solutions to tackle research problems.

I thankfully acknowledge chairman of my doctoral committee Prof. Shishir Deshpande and all the members of the doctoral committee for tirelessly reviewing and keeping my work on track and on schedule.

Dr. Pintu Bandyopadhyay and Dr. G. Ravi has played a crucial role in this thesis. They helped me to consolidate my work and present it properly. I also thank Mrs. Bharathi and Dr. Alphonsa Joseph for their help.

I would like to thank my friends at FCIPT specially Satyaprasad, Bala, Akshay, Kushagra, Mukesh who helped me a lot during my thesis work. I also thanks Bhavesh, Ghanshyam, Kaila bhai, Adam, Chirayu, Bhupendra and Gautam Vadolia for helping me timely with various things. I am very thankful to Samir, Niraj, Vidhi, Garima, Mangilal for fruitful discussion on plasma physics. I would like to acknowledge the Academic committee of IPR for the support. I am thankful to IPR Library, administration, accounts section, purchase department, stores department, workshop, computer center for providing best facilities during the thesis tenure.

I thank all of my friends and family members for their support.

Ramkrishna Rane

Contents

SYNOPSIS

The DC discharges having external magnetic field (B) perpendicular to the electric field (E)(i.e. cross field discharges) has applications in different areas like thruster, vacuum gauges, magnetron sputtering *etc* [1]. These cross field discharges are generally used in a diode mode with a cold cathode. These discharges are used in different geometries like cylindrical, planar and annular. The cylindrical magnetron discharges and Penning cells falls in the cylindrical category while circular and rectangular magnetrons are of planar geometry. The cylindrical magnetron has two types i.e. post cathode and hollow cathode or inverted magnetron. In post cathode, the central electrode is cathode while outer electrode is anode and for inverted or hollow cathode configuration it is vice versa. The basic physics and discharge structure of post cathode and hollow cathode cylindrical magnetron is well studied previously [2–4]. In these discharges, the magnetic field is such that the electrostatic confinement of electrons takes place along B. The trapped electrons have long path length which increases the probability of ionization of background gas. Hence the operation of these discharges at lower pressure is also possible as compared to un-magnetized discharges. Further these discharges in hollow cathode configuration are used in a wide variety of applications such as efficient light sources, electrons sources, ion sources, for nitriding, space propulsion, plasma-activated pre-treatment and coating processes [5]. The hollow cathode cylindrical magnetron and modified hollow cathode penning cell device are the two discharges of similar category. In these discharges, the plasma is enclosed or bound by the walls that are at the cathode potential. The inverted cylindrical magnetron is one of the cross field discharge in the hollow cathode configuration. It has been used widely to coat wires and fibers because of their enclosed geometry. The Penning discharge with modified hollow cathode is also a cross field discharge which can be used as a source for high density plasma, electrons and ions. The discharge region is formed by two plane electrodes at cathode potential and modified cylindrical anode at the center. In Hollow Cathode Cylindrical Magnetron (HCCM) and Penning cell discharge, E and B are perpendicular to each other near the anode. The magnetic field near the anode acts as a barrier to electron transport and which can lead to the formation of significant anode fall. In case of DC discharges the cathode fall and associated phenomena are well documented [6, 7]. However the anode region is not explored much especially in case of magnetized discharges. Even though plasma properties in cross field discharges has been studied previously, the discharge properties near the anode are also important considering the plasma surface interactions with conducting surfaces like anode.

Literature indicates that the anode region has been studied theoretically as well as experimentally in case of different types of discharges. The electron kinetics in the anode regions of a glow discharge has been studied by using Monte Carlo simulations [8]. As the anode is mostly the electron absorbing surface in the discharge, the diffusion of electrons was studied under the influence of electric field near the electron absorbing boundary [9]. Further the deformation of the electron distribution function in the near anode plasma was also studied at low pressure and low discharge currents [10]. The experimentally observed properties of the plasma in the anode region such as anode fall, anode dark space, anode glow has been confirmed by theoretical modelling [11]. The study of the anode region is not limited to glow discharge plasma, but there have been many studies of the anode region of the arc plasma also [12]. The anodic plasma was also studied by using auxiliary electrode in filamentary and inductively coupled plasmas. The electrode was biased positively above the plasma potential. The different sheath regimes have been demonstrated by selecting the electrode area appropriately [13–15]. The electron sheath can breakdown into the quasi neutral plasma whose potential drop is close to ionization energy of the background gas [16, 17]. Further anode region of the cross field discharges like Hall thruster, magnetron discharges etc became important due to their applications in electric propulsion as well as thin film deposition. In Hall thruster discharge, the anode sheath phenomenon has been studied experimentally with two types of anode sheaths i.e. electron repelling and electron attracting sheaths [18]. In this present work the study of anode sheath in two types of cross field discharges is presented. The sheath evolution is controlled by magnetic field rather than the bias voltage in hollow cathode cylindrical magnetron and modified Penning discharge.

The thesis involves the experimental study of the plasma properties near the anode of two types of cross field discharges in hollow cathode geometry. The effect of magnetic field on the global as well as plasma parameters near the anode has been investigated by using electrical probe and optical emission spectroscopy diagnostics. The study contains (i) Development of experimental setup and implementation of diagnostics (ii) Demonstration of transition from large cathode fall to strong anode fall controlled by magnetic field in cylindrical magnetron discharge. (iii) Influence of magnetic field on the evolution of anode glow and its stability and (iv) The transition from ion sheath to electron sheath near the anode in modified hollow cathode Penning discharge. (V) Effect of magnetic field on the oscillations of the anode glow.

The thesis is organized in different chapters as outlined below.

Organization of the thesis

Chapter-1 : ***Introduction.*** The introductory first chapter of the thesis outlines the motivation behind the study and defines the scope of the study. Brief introduction of the glow discharge, cross field discharges and anode region is provided. Literature survey about the study of anode region in magnetized and unmagnetized plasma is presented. The physical phenomenon near the anode in the DC glow discharge is discussed qualitatively. Different types of sheath regions at the anode is presented. The theory regarding behaviour of charged particle in magnetic field is also explained.

Chapter-2 : ***Experimental Setup and Diagnostic Techniques*** This chapter details the experimental set-up used for the study of near anode plasma. The plasma source i.e. hollow cathode cylindrical magnetron (HCCM)and modified hollow cathode Penning discharge is described. A detailed description of vacuum chambers, power supplies, vacuum pumping system and magnetic field generator is provided. The experimental procedure to produce the plasma is explained. Various relevant electric probe (e.g. single Langmuir probe, double probe, emissive probe) based diagnostics is discussed. Techniques to derive plasma parameters from various probes are explained in detail. The optical diagnostics using optical emission spectrometer is also described.

Chapter-3: ***Effect of magnetic field on discharge properties of HCCM*** In this chapter, the combined effect of magnetic field (B) and gas pressure (P) on the discharge properties in cylindrical magnetron has been investigated. In a HCCM source, the transition from positive space charge (i.e large cathode fall) to negative space charge (i.e large anode fall) due to magnetic field is demonstrated experimentally. It is observed that B/P ratio plays an important role in sustaining the discharge. It is also observed that at a comparatively high magnetic field and low operating pressure the discharge extinguishes and demands a high voltage to reignite the discharge. At higher magnetic field, floating potential is observed to increase slowly from cathode to anode and distribution of floating potential changes with magnetic field.

Chapter-4: ***Anode glow evolution in HCCM*** In this chapter it is shown that, the anode fall becomes prominent in presence of magnetic field. In addition, the plasma potential profile near the anode shows two distinct regions with potential difference of 10-15 V at the boundary of anode glow. It is also noticed that the anode glow expands radially as a function of magnetic field. The size of the anode glow increases with magnetic field in order to collect more electron current. The plasma density and electron temperature as measured by double Langmuir probe near the anode is observed to be higher as compared to the background plasma.

Chapter-5 : ***Response of the background plasma to anode sheath transition*** The magnetic field effect on anode glow evolution is studied in modified hollow cathode Penning discharge. The discharge showed an onset of anode glow at a critical applied magnetic field indicating the formation of electron sheath and a double layer. The discharge current initially decreases; however it starts to rise again as the anode spot appears on the anode. The critical magnetic field at which anode glow formation takes place is dependent upon operating pressure and discharge voltage. The plasma potential near the anode decreases during the transition from ion sheath to electron sheath. The plasma potential locks to the ionization potential of argon gas when anode spot is completely formed. A systematic study showed that during the transition, the electron temperature increases and plasma density decreases in the bulk plasma. The spectroscopy of the discharge showed presence of strong atomic and ionic lines of argon. The intensity of these spectral lines showed a dip during the transition between two sheaths. After the formation of the anode spot, oscillations of the order of 5-20 kHz are observed in the discharge current and floating potential due to the enhanced ionization and excitation processes in the electron sheath.

Chapter-6 : ***Anode glow Oscillations: Effect of magnetic field.*** An experimental investigation on the dynamics of floating potential oscillations in a modified hollow cathode discharge is presented over a wide range of magnetic fields. The current-voltage characteristics near the breakdown voltage show a hysteresis with two distinct discharge current regimes. The discharge transits from oscillation free high discharge current regime (beyond 4-5 mA) to a oscillating low discharge current regime (less than 1 mA). Depending upon the discharge parameters, low discharge current regime shows either the periodic or chaotic oscillation in the frequency range of 1-50 kHz. The frequency of periodic oscillation increases with the increase in magnetic field up to 90 Gauss and with further increase in magnetic field, broadband of frequencies is appeared in which the periodic oscillation becomes chaotic in nature..

Chapter-7 : ***Conclusions.*** Results are summarized in this chapter. The scope for future work from this study is also discussed. Our experiments clearly demonstrate the transition from positive space charge to negative space charge due to the magnetic field in hollow cathode cylindrical magnetron. We showed the formation and evolution of anode glow on the anode of the magnetized discharges. The different sheath regimes i.e ion sheath, electron sheath and anode spot near the anode are demonstrated by controlling the magnetic field rather than controlling the physical area of the anode.

List of Figures

List of Tables

1 Introduction

Plasma is a state of matter which consists of neutral atoms, charged particles like electrons and ions, active species of atoms and molecules *etc.* There are two major classes of plasmas viz. Thermal plasmas (hot) and Non-thermal plasmas (cold). Thermal plasmas are identified by local thermodynamic equilibrium and accordingly the temperature of electrons, ions, and neutral atoms is similar. In non-thermal plasmas the electron temperature is very high when compared to that of ions and neutral atoms. Non-thermal plasmas are generated at atmospheric pressure or at sub atmospheric pressure. The most common way to generate laboratory plasmas is by supplying electrical energy to the gaseous atoms at sub-atmospheric pressure. Different types of power supplies like direct current (DC), Radio Frequency (RF), microwave frequency are used for generating the plasma. The simplest and widely used non thermal plasmas are DC discharges.

1.1 Direct Current (DC) discharges

Plasmas generated by applying a DC voltage across two electrodes are typically called as a DC discharges. These discharges are of great significance in the study of low pressure non-thermal plasmas. Further, these discharges have major role in the plasma processing like deposition of thin films, surface activation and/or cleaning of materials, surface hardening by plasma nitriding *etc.* Because of their vast applications in plasma processing of materials, and since they are also used as electron/ion sources; these discharges are well studied for understanding the

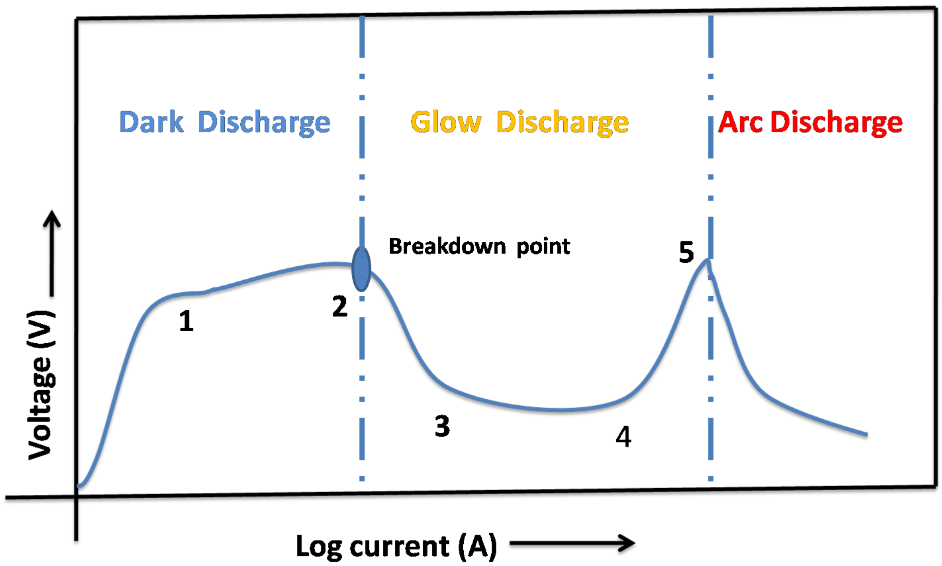

Figure 1.1: *Current Voltage characteristics of DC discharges showing dark discharge (region between point 1 and 2), Glow discharge (region between point 2 and 5) and arc discharge (after point 5)*

plasma behaviour during its interaction with surfaces. Fundamentals of physical processes occurring in DC discharges relevant to plasma processing have been widely studied by many researchers in the past. DC discharges are operated in a wide range of voltages and currents. Depending on the range of discharge voltage and discharge current, different operating regimes of the DC electrical discharges are identified and are shown in the Fig. 1.1. This curve is also well known as universal voltage-current characteristics of DC discharges. The region between point 1 and 2 is called as Townsend dark discharge which operates at very low currents and high voltages. At point 2 the discharge becomes self-sustained and visible. This discharge is typically known as glow discharge and is stable in the region from point 2 to 5. When this DC discharge operates at higher current values, the regime is known as Arc discharge region (region to the right side of point 5 in Fig. 1.1). Arc discharges are characterized by very high current densities and are useful in materials processing at higher temperatures. The region of interest in the present study is the glow discharge region and the studies are conducted in a typical range of discharge voltages ($300 - 800\ V$) and discharge currents ($10 - 500\ mA$).

1.1.1 DC glow discharge

A DC glow discharge is generally produced at sub atmospheric pressure by applying a potential difference across two electrodes. The electrodes of various shapes like planar, cylindrical are used for the formation of glow discharge. The simplest configuration consists of two metal plate/disc electrodes placed parallel and opposite to each other in a long cylindrical glass or quartz tube, which can be evacuated. In most cases, a few hundred volts of potential difference is required to generate and maintain a DC glow discharge plasma at sub-atmospheric pressure. Once the stable plasma is formed, it is observed that the gap between the two electrodes is divided into different regions as shown in Fig. 1.2. These regions are identified as Aston dark space, cathode glow, Crooks dark space, negative glow, Faraday space, positive column *etc* mentioned in order starting from the surface of the negative electrode (cathode). There are two more regions viz. anode glow and anode dark space (anode sheath) which are formed near the surface of positive electrode i.e anode [6]. The anode glow region is relatively more intense than the positive column. The anode glow is the boundary between anode sheath and the positive column region. The appearance and dimensions of each of the above mentioned regions depend on various operating parameters like background pressure, discharge current and inter electrode distance *etc*. Cathode sheath/Crookes dark space found near the surface of cathode, is a very important region and is always present in a DC discharge. Most of the applied DC voltage falls within small distance near the cathode and is called as cathode fall also. The ions present in the plasma (positive column region) travel towards cathode and once they approach cathode sheath region, they get accelerated due to this cathode fall and gain energy. These energetic ions hit the cathode resulting in the emission of secondary electrons from the cathode surface. The secondary electron emission yield is typically in the range of 0.05—0.2 and it depends on cathode material, gas used for plasma formation *etc*. These secondary electrons get accelerated in the cathode fall region and gain energy. These energetic electrons collide with neutral atoms and produce new electron-ion pairs. These newly produced electrons also indulge in collisions with neutral atoms and generates more electron-ion pairs. This multiplication of ion-electron pairs helps to self-sustain the DC glow discharge plasma. The detailed discussion of the gas breakdown and the electron avalanche mechanism in a DC

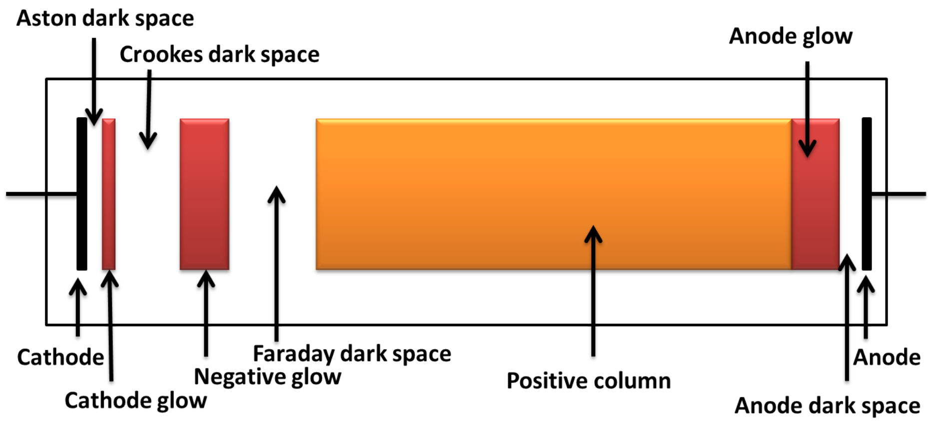

Figure 1.2: *Different dark and bright regions of DC glow discharge starting from cathode to anode*

discharge is already well described [7, 19].

1.1.2 Cross field DC discharges

As described earlier, plasma consists of charged particles and they can be easily effected by additionally applying magnetic field. Applying an external magnetic field to a simple DC discharge has a potential to increase the range of DC discharge applications. Direction of this externally applied magnetic field with respect to that of the DC electric field is very important. The discharges of this type in which electric and magnetic fields are perpendicular to each other, are generally refered as cross field discharges. Typical applications of these discharges are in thrusters, vacuum gauges and magnetron sputtering systems for thin film deposition [1].

In the beginning, the DC discharge with external magnetic field was explored as a vacuum gauge. In 1950s, an extended research in this field has helped to develop the inverted magnetron ionization gauges [20]. The research on the use of these cross field discharges for space propulsion applications was started in 1960s, which resulted in the development of useful devices like Stationary Plasma Thruster (SPT) and Thruster with Anode Layer (TAL). Further the magnetron sputtering systems were popularised for thin film deposition. Subsequently, the plasma sputtering process was developed so rapidly that it has become an established technique for depositing wide range of industrially important coatings [21].

Surface modification processes like plasma sputtering, plasma etching by using these discharges are getting more importance because they are superior in many features than their conventional counterparts. Plasma phenomenon like transport of charged particles in a magnetic field, instabilities, diffusion are studied in these discharges [1].

The cross field discharges are generally used in a diode mode. In these discharges, typically the plasma is generated between the cathode and anode by applying a DC high voltage across them in the presence of an externally applied magnetic field. The background pressure is typically maintained below 10^{-1} $mbar$ for generating the discharge. The important parameter that distinguishes these discharges from the conventional DC discharge is the externally applied magnetic field. When a charged particle moves in a direction perpendicular to the magnetic field lines, it will experience a force in a direction perpendicular to both the field lines and velocity of the particle. However, the velocity component parallel to the magnetic field lines remains unaffected by this force. The particle moves in a cyclotron orbit due to the action of magnetic field. The frequency of this circular motion is known as cyclotron frequency.

$$\omega = \frac{eB}{m} \tag{1.1}$$

ω is cyclotron frequency, e, B and m are charge, magnetic field and the mass of the particle, respectively. When particles travel along the magnetic field lines, they are forced to spiral around the field lines in a helical path. As the magnetic field strength increases, the radius of helix decreases and the total effective distance travelled by charged particle increases. The radius of the helix is an important length scale in magnetised plasmas which is also called as Gyro radius or Larmour radius and is defined as

$$r_g = \frac{mv_\perp}{eB} \tag{1.2}$$

r_g is gyro radius, e, B and $v_\perp$ are the charge, magnetic field and the perpendicular velocity of the particle, respectively.

From the above equation it is very clear that electrons and ions will have vastly differing gyro radii. In the case of electrons, the gyro radius is very small and hence they will travel effectively a long path before they get lost from the plasma. This increases the residence time of electrons in the plasma which increases the probability of ionization of the background gas. Hence the operation of these magnetised discharges is possible even at lower pressure as compared to other non-magnetised discharges. Where as in the case of ions, as they are highly massive (e.g. Ar+ ion to electron mass ratio is $m_i/m_e = 40 \times 1837$), their gyro radius is very much greater than that of electrons. Most of the times it is even greater than the discharge dimensions. As the electric field $\vec{E}$ and magnetic field $\vec{B}$ are perpendicular to each other in cross field discharges, the charged particles experience a $\vec{E} \times \vec{B}$ drift velocity

$$V_E = \frac{\vec{E} \times \vec{B}}{\vec{B}^2} \tag{1.3}$$

V_E is perpendicular to both $\vec{E}$ and $\vec{B}$. This velocity does not dependent on the mass and charge of the particle. The electrons and ions drift in the same direction. In case of spatially varying E field or B field, the particle motion becomes much more complicated.

1.1.3 Cross field DC discharges in hollow cathode configuration

The cross field discharges are generated with various electrode configurations, wherein the $\vec{E} \times \vec{B}$ drift path forms a closed loop. The configurations in practice are planar, cylindrical and annular geometries. The circular and rectangular magnetrons fall in planar category. The cylindrical magnetron discharges and Penning cell are of cylindrical category, while TAL thruster is of annular geometry. In all these geometries, the magnetic field is applied in such a way that the electrostatic confinement of electrons takes place along $\vec{B}$. Usually, in the Penning cell and the cylindrical magnetron devices, the $\vec{B}$ is axial and $\vec{E}$ is radial near the anode. Similarly in case of planar magnetron $\vec{E}$ is axial and $\vec{B}$ is radial near the surface of the cathode. The cross field discharges in cylindrical geometry are widely known as cylindrical magnetrons. The cylindrical magnetron also has two configurations i.e post-cathode configuration and hollow-cathode or inverted magnetron configuration. In the post-cathode configuration the central rod shaped electrode is maintained as cathode while the outer one is maintained as anode, whereas in the case of an inverted configuration it is vice versa. Fig. 1.3 shows schematic for the discharge in a cylindrical post-cathode and hollow-cathode configuration. The basic principle of these magnetron discharges has been explained by Thornton [2]. As mentioned previously these low pressure discharges are sustained by the secondary electron emission from the cathode by the ion bombardment. These emitted electrons are accelerated in the cathode sheath and enter into the plasma region where they are known as primary electrons. The primary electrons which enter into the plasma are trapped in cycloidal like paths because the applied magnetic fields (typically up to 500 *Gauss*) are sufficient enough to magnetise the electrons. These discharges exhibit a bright glow region next to the cathode where the energy exchange of primary electrons with neutral atom takes place. The electron neutral collisions in the presence of radial electric field causes the electrons to move towards the anode. In addition to the magnetisation effect experienced by the primary electrons (as described above), the electrons near the cathode surface will also experience a $\vec{E} \times \vec{B}$ drift which makes them travel around the cathode. This leads to an increase in ionization probability near the cathode surface, which results in more number of ions and hence more sputtering from the cathode.

The cylindrical magnetron sputtering technique is used for depositing thin films on cylindrical and tubular objects. In this technique an uniform magnetic field is applied in a direction parallel to the long axis of the cylindrical shaped cathode, using appropriate electromagnetic coils. Sometimes permanent magnets are also used for obtaining this magnetic field near the cathode surface. In the case of hollow cathode configuration, the material is sputtered from the inside surface of the tubular cathode. In this configuration the object to be coated (i.e. substrate) is enclosed by the cathode, and hence receives a high flux of sputtered material uniformly from all directions. Cathodes with larger diameter, and low aspect ratio can be used for depositing uniform coatings on even three dimensional objects without necessitating the rotation of the objects. In this configuration, most of the sputtered material either deposits on the substrate or redeposits on the cathode itself, enabling maximum utilisation of the cathode material. This configuration is also easy to scale up for industrial applications. Further, bombardment of various charged particles on the substrate is significant in the case of hollow cathode configuration which can be used for modifying the film properties.

As mentioned earlier, in this configuration $\vec{E}$ and $\vec{B}$ are perpendicular to each other near the surface of the anode. This condition acts as a barrier to electron transport and accordingly can increase the anode fall. This can ultimately alter the plasma properties near the anode. Further, in this configuration, generally the object to be coated is kept as anode itself or placed very near to the actual anode. Therefore, in both these cases, understanding the plasma behaviour close to anode becomes very important and useful for plasma application development. As discussed earlier, Penning cell also works on cross field discharge mechanism. In the Penning cell also $\vec{E}$ and $\vec{B}$ are perpendicular to each other near the anode surface. The geometry consists of two plate cathodes, facing each other, with a tubular anode placed between them [1]. The magnetic field, $\vec{B}$ is applied along the axis of the tubular anode. Researchers have worked on using this configuration, with necessary modifications, for developing high density plasma sources [22]. The modification consists mainly of reducing the aspect ratio of the tubular anode which is nothing but reducing the surface area of anode. The magnetic as well as electrostatic confinement of the electrons in this modified version gives higher plasma density. Although considerable research was carried out in this modified Penning cell discharge, little study was carried out on understanding the near anode plasma regions. Studying the discharge properties near the anode is important because the interaction of plasma with anode surface can affect the overall properties of bulk plasma.

In the following section the anode region of DC glow discharges is discussed briefly. Further it is also discussed on the past studies carried out with regard to anode region in different types of discharges.

1.2 Anode region of the DC discharge

The anode of the DC discharge is an important plasma boundary. In the region near to anode, a transition in potential takes place from the end of uniform positive column region to the surface of the anode. Electrons from the quasi neutral plasma (generally referred to as 'plasma') are lost to the anode through an interface located between anode and positive column. Fig. 1.4 shows a typical potential profile in between cathode and anode. As shown in Fig. 1.4, depending upon anode

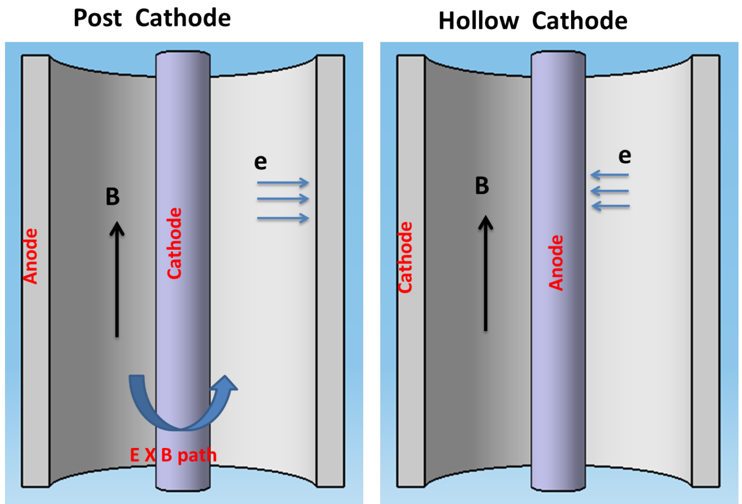

Figure 1.3: *Post-cathode and hollow-Cathode or inverted configurations of cylindrical magnetrons. The electrons are confined due to axial magnetic field*

condition, the potential near anode can be either positive or negative with respect to quasi neutral plasma. When this potential is lower than the plasma potential, it is called as negative anode fall and when it is higher than plasma potential it is known as positive anode fall. The negative anode fall repels electrons while the positive anode fall attracts them. These regions where steep changes in potential are observed (near the boundary), are typically called as sheath regions. Depending on whether it is negative or positive anode fall; ion or electron sheath would be formed respectively, near the anode surface. In the following section general sheath theory is explained.

1.2.1 Sheath theory

Sheath is a non-neutral region formed between the plasma region and a solid boundary. Sheath plays an important role in surface modification applications by plasma. It controls the flux and energy of the charged particles being lost from the plasma to any solid surface. Anode is one of such surfaces in a glow discharge plasma. One can control the loss of charged particles by controlling the sheath parameters. In order to maintain the quasi neutrality of the bulk plasma, the sheath electric field accelerates one type of species (negative or positive charge

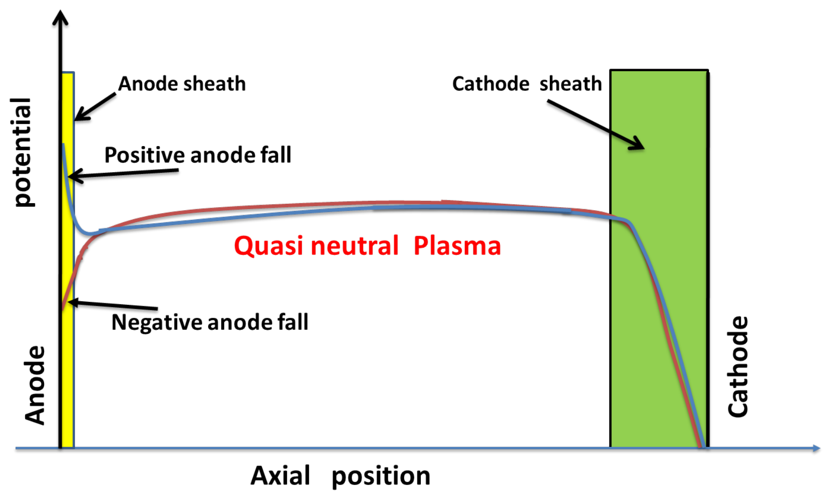

Figure 1.4: *Potential distribution of DC Glow discharge plasma showing positive and negative potential fall near the anode*

particles) while repelling the other. This ensures that the flux of positive and negative charges is lost from the plasma in almost equal quantities. The thermal flux of electrons is greater than that of ions because of the lower mass of electrons. Due to higher flux of electrons, the formation of an ion sheath at the boundary is necesary in order to balance the electron and ion current. Plasma potential adjusts itself near the surface of any solid boundary that comes in contact with plasma so that the electrons get repelled. The magnitude of plasma potential depends on the accumulated space charge in the sheath region. The langmuir probe is a simple example in which it can be cleary seen that ion or electron sheath is formed over the probe depending on the applied probe potential with respect to plasma potential. When the probe is biased negatively, with respect to plasma potential, ion rich sheath is formed on the probe. The electron sheath is usually formed when the probe is biased above the plasma potential. The ion sheath is also formed on any floating electrode in plasma. The floating surface acquires a negative charge because the mobility of electrons is higher compared to that of ions. In the bounded plasma discharges, which are studied in laboratories, the ion sheath formation is common due to the higher mobility of electrons. Hence, the ion sheath is well studied both experimentally [23, 24] as well as in theory and simulation [25–31].

In one of the important studies, it was shown that there exist a transition layer between the quasi-neutral plasma and the ion sheath. This transition layer is known as pre-sheath region and is necessary to maintain the continuity of ion flux [27]. By using Poisson's equation, it was established that ions need to flow into the sheath with a higher velocity known as Bohm velocity. It was shown mathematically by Bohm [27] that the ions going into the sheath should have a minimum velocity, given by

$$u_B = \sqrt{\frac{eT_e}{M}} \tag{1.4}$$

where M is mass of ion, T_e is electron temperature in eV and u_B is Bohm velocity. The required potential drop in the pre-sheath region for the acceleration of ions to this energy, was shown to be $\phi = T_e/2$. This potential drop was used in the Boltzmann relation to determine the density of ions at the sheath edge. This density was related to bulk plasma density as $n_s = 0.61n$, where n_s is the density at the sheath edge and n is the bulk plasma density.

Even though the above discussion of the sheaths is in context of maintaining quasi-neutrality of the bulk plasma, the high voltage sheaths are also formed e.g near the cathode of the discharge. A typical high voltage ion sheath is shown in Fig. 1.4. In case of higher negative potential much more than electron temperature, the current drawn by the electrode is almost ion current. These sheaths are mostly described by famous child law [7]. By using the sheath voltage(V) and width (d), the current density (J_0) is given by Child's Law

$$J_0 = \frac{4}{9}\epsilon_0\left(\frac{2e}{M}\right)^{1/2}\frac{V^{3/2}}{d^2} \tag{1.5}$$

where, ϵ_0 is the permitivity of the free space, M is the mass of particle. The ion sheaths are mostly encountered in DC glow discharge plasmas. However there are some situations in which sheath can be electron rich. When a small auxiliary electrode (e.g. Langmuir probe) is placed inside the plasma and biased above the plasma potential, it will draw electron current. The electrons get acccelearted due to positive potential and sometimes these energized electrons cause electron sheath to glow due to eletron-neutral collisions. When this electrode is biased above a certain critical potential, it develops a bright glow. The current passing through this electrode rises rapidly during formation of such a bright glow. This bright glow is due to the breakdown of the electron sheath into a quasi neutral plasma [14] and such structures were called anode spots or fireballs[16, 32–37]. The formation and stability of anode fireballs has been studied experimentally [16, 33, 35, 38] and theoretically [17, 32, 34, 39]. In the following section the previous studies carried out related to electron sheath on anode surface (also called as anode sheath), anode glow and anode spot are discussed.

1.2.2 Previous studies of anode region

Literature indicates that the anode region has been studied theoretically as well as experimentally in different types of discharges. The previous work carried out by many researchers regarding the plasma parameters in the anode region can be divided into two categories. One of them deals with the anode sheath occurring near any auxillary electrode placed in an already formed plasma. In these studies the axillary electrode was biased above the plasma potential. The second category deals with sheath formed near the discharge electrode i.e. anode itself. The electron kinetics in the anode region of a glow discharge has been studied using Monte carlo simulations [8]. As the anode is an electron absorbing surface in a discharge, the diffusion of electrons was also studied under the influence of electric field near the anode [9]. Further, the deformation of the electron distribution function in the near anode plasma was also studied at low pressure and low discharge currents [10]. The experimentally observed properties of the plasma in the anode regions such as anode fall, anode dark space, anode glow etc. has been confirmed by theoretical modelling [11]. Study of the anode region is not limited to glow discharge plasmas only, as many groups studied the anode region of arc plasma also [12]. Further, anode region of the DC discharges like Hall thruster was explored considering their applications in electric propulsion. In Hall thruster discharge, the anode sheath phenomenon has been studied experimentally with two types of anode sheaths i.e. electron repelling and electron attracting sheaths [18].

The anode spot or fireball and anode double layer were demonstrated by positively biasing a disc electrode which is immersed in a filamentary discharge argon plasma [16]. It was observed that the transition from luminious anode sheath to an anode spot takes place at a critical pressure. The dimensions of the anode fireball were estimated by equating the rate of ion production to the rate of ion loss in the surrounding plasma. It was also shown that the diameter of anode spot varies inversely with operating pressure. The rise time and fall time of the anode current oscillations were shown to be comparable to that of ionisation time in the anode sheath. If bias potential of the electrode exceeds some threshold value, then the electron attracting sheath transforms into thin anodic double layer due to the ionization in the sheath [40]. The evolution of plasma potential profile during this transformation was studied by numerical modelling. It was confirmed that these potential profiles are due to the increased ionisation in the electron sheath. It was shown that above a threshold voltage, plasma sheath becomes unstable and transition to double layer takes place.

In another study, it was shown that the sheath near a positive auxillary electrode immersed in a plasma can be either pure ion sheath, pure electron sheath or a double sheath [13]. A particular type of sheath formation depends on the electron collection area as well as ion collection area. Based on the ratios of these surface areas, the condition necessary for the formation of a particular sheath was established. In case of double sheath formation, the characteristics of global non-ambipolar flow was demonstrated where all the electrons were lost to one boundary and all ions to other boundary [13]. Hence it was concluded that the sheaths near the plasma boundaries are responsible for the global non ambipolar flow.

The equlibrum states of anodic double layer like double sheath, anode glow and fireball or fire rod were experimentally studied [14]. The potential profile for the electron sheath, anode glow and anode spot were measured near the baised electrode. In case of anode spot, the potential drop across the double layer formed at few cm away from the electrode. The transition from thin anode glow to thick anode spot was explained based on the physics of quasi neutrality. It was also shown that the critical electrode bias at which the transition from anode glow to anode spot takes place is inversely proportional to background pressure. It was also observed that the double layer potential drop was close to the ionisation potential of the background neutral gas. As most of the experiments with auxiliary electrode reported that the anode spot formation takes place at a bias potential in the range of $40 - 50\ V$ above the plasma potential [14, 36, 41], it is clear that the electrons can gain the required ionization energy ($\sim 15.7\ eV$ for argon) near this electrode.

Further, the experiments were performed by changing the area of positively biased electrodes. The objective of these experiments was to study the response of the bulk plasma to varying electrode area and thereby the type of sheath formed [15]. The bulk plasma parameters like plasma density, plasma potential, electron temperature *etc* were also measured . A sudden transition in the plasma parameter was observed due to the changes in the electrode area. The transition in the sheath plasma interface due to the changes in electrode area were compared with the previously predicted results of global non-ambipolar flow model [13]. Recently the characteristics of ion and electron sheaths were also studied in a low density, low temperature plasma [42].

Apart from experimental study, recently simulation studies of electron sheath and anode spot were also carried out [43–45]. Using PIC simulation it was shown that long pre-sheath exists near the electron sheath because of electron pressure gradient. Their results infer that the flow velocity of electrons was more than their thermal speed at the sheath edge [43]. In another PIC simulation study, the transition from ion sheath to electron sheath was also studied [44]. The anode spot formation at a bias potential above the plasma potential was also studied using 2D PIC simulations [45]. The ionisation in the sheath also results in various kinds of instabilities. The instabilities were studied by obsereving oscillations in electrode current [16] and other plasma parameters like floating potential. The growth and decay of anode fireballs has been studied by applying a pulsed bias to the grid electrode [35]. The experimental results also observed the ion acoustic waves and oscillations close to the plasma frequency due to fireball formation. Stenzel et al. [38, 46] also reported the dynamic behaviour of the so called inverted fireball which includes high frequency oscillations, light oscillations, transit time instability etc.

There are some experiments in which the anode double layers are produced in presence of external magnetic field. The effect of magnetic field on the shape, dimensions and stability of anode spot/fireball has been studied in a variety of discharges. The anode sheath and double layer in magnetised plasma was studied in filamentary discharges [47–49], inductively coupled plasma [50] and magnetically constricted anode source [51]. Mostly near the small electrode, the shape of the anode spot or fireball is spherical. However the magnetic field aligns the anode spot in its direction changing its shape to a cylindrical one [52]. The effect of the external magnetic field on the evolution of the anode spot was studied for argon and xenon discharge [49]. They observed that the anode fireball changes into a rod shaped anode spot above a certain externally applied magnetic field.

A simple model, earlier given by Song et al. [16] was used for studying the effect of magnetic field on the shape and size of the anode spot. They incorporated the effect of magnetic field in the form of modified particle fluxes through various boundaries. The anode double layers were also studied in strong magnetic fields [52]. They produced anode double layer by biasing the anode plate kept in the diverging magnetic field. The anode sheath and fireball were studied by using the permanent magnets behind the anode of DC discharge [51].

After giving a brief introduction of various types of anode sheath structures like pure electron sheath, anode glow, anode spot/fireballs etc. in magnetised and non magnetised discharges, the motivation and outline of the thesis is given below.

1.2.3 Motivation

As discussed above, plasma properties near the anode were mostly studied by using an auxiliary electrode and biasing it with reference to background plasma. The condition for formation of different structures like ion sheath, electron sheath, anode glow, anode spot *etc* near the auxiliary electrode are explored in above mentioned studies. In the magnetised discharges of hollow cathode configurations, anode is physically small. Additionally transverse magnetic field acts as barrier to electrons, particularly at low pressures and high magnetic fields.

Hence it is necessary to study

1) Whether the conditions near the anode of cross field DC discharges can lead to the formation of similar types of anode sheath structures as discussed above (near auxiliary electrode)

2) Whether the anodic structures can be controlled by tuning externally applied magnetic field in low pressure cross field discharges in hollow cathode geometry.

3) What is the impact of changes in anode sheath structure on the bulk plasma parameters.

Therefore, in the present thesis, two types of cross field discharges in hollow cathode configuration are studied for plasma parameters near the anode. The first type is hollow cathode cylindrical magnetron and other is modified hollow cathode Penning discharge. The hollow cathode cylindrical magnetron source is important for developing an industrial process like large area thin film deposition while the modified Penning discharge can be used as a high density plasma source, ion source *etc.*

1.3 Outline of the thesis

The present thesis includes the study of discharge properties of hollow cathode cylindrical magnetron and Penning discharge in modified hollow cathode configuration. The anode sheath formation and its stability has been investigated. It also reports on the effect of magnetic field over the near anode plasma characteristics. The global plasma response to the changes in the anode sheath structure is also studied. Chapter-2 describes the experimental set-up of the cylindrical magnetron system and modified hollow cathode Penning discharge system. It consists the description of power supplies, magnetic coils, diagnostics techniques like Langmuir probe, emissive probe, optical emission spectroscopy and concerned electronic circuits used for the measurements. In Chapter-3, the combined effect of magnetic field (B) and gas pressure (P) on the discharge properties of hollow cathode cylindrical magnetron has been investigated. The transition from positive space charge (i.e large cathode fall) to negative space charge (i.e large anode fall) due to magnetic field is demonstrated. Plasma parameters like electron temperature, plasma density, plasma potential profiles are measured and the results are discussed. Chapter-4 describes the experimental results of the anode fall measurements and anode glow characterisation. The origin and expansion of anode glow due to magnetic field is also discussed. In Chapter-5, the modified hollow cathode Penning discharge is studied. The magnetic field controlled transition of ion sheath to electron sheath near the anode is shown. The impact of this transition on the background plasma parameters is also discussed. The Chapter-6 reports the study related to effect of magnetic field on the discharge characteristics in the presence of anode glow oscillation. The Chapter-7 includes conclusion of the work carried out for the thesis. The future scope of this work is also discussed in this chapter.

2

Experimental set-up and Diagnostics

In this chapter the experimental set-up of hollow cathode cylindrical magnetron (HCCM) and modified hollow cathode Penning discharge are described. This chapter has two parts, the first part describes the vacuum system, magnetic field coils, power supplies and typical operation of both the devices while the second part gives the details of various diagnostics and its implementation. The main components of both the devices are the vacuum chamber, pumping system, power supplies, Helmholtz coil and various diagnostics. Section 2.1 describes the HCCM while Section 2.2 describes the modified hollow cathode discharge. The plasma diagnostics techniques are similar for both the devices and are explained in Section 2.3

2.1 Hollow Cathode Cylindrical Magnetron

2.1.1 Vacuum chamber and pumping system

The device consists of a stainless steel (SS) cylindrical vacuum chamber 50 *cm* in diameter and 150 *cm* long. A coil pair, called as Helmholtz coil was mounted in the central region of the chamber while the vacuum chamber was placed horizontally on the stand. The schematic of the vacuum chamber is shown in Fig. 2.1. It consists of many radial ports and was pumped via an ‘L’ shaped port from back end. A view port from front end as well as one radial view port were used to view the plasma formed inside the chamber. The other radial ports were used for mounting pressure gauges, Langmuir probe, emissive probe and the optical fiber. A cylindrical coaxial inverted electrode configuration as illustrated in Fig. 2.1 was used in the experiments. The central inner electrode consists of solid cylindrical copper rod of length 250 mm and diameter 15 mm. The end limiters of the central electrode were covered with teflon. The cylindrical main chamber was used as the other electrode. The experiments were performed in hollow cathode configuration in which the central electrode was used as anode while outer was used as cathode. The distance between central anode and outer cathode was around 240 mm. Fig. 2.2 shows the three dimensional view of the HCCM experimental device.

A base vacuum of 5×10^{-5} $mbar$ was achieved using a combination of rotary pump (300 l/min) and diffusion pump (2000 l/sec). The rotary pump takes about 30 minutes to pump down upto a pressure of 8×10^{-2} $mbar$ starting from atmospheric pressure. Once this pressure was achieved, the pumping from diffusion pump was started which takes about 60 $minutes$ to reach base pressure of 5×10^{-5} $mbar$. Pirani and Penning gauges were used for monitoring the pressure inside the vacuum chamber during pumping. The full range cold cathode gauge was used for monitoring pressure during the experiments. The working gas used for all of the experiments was argon. It was fed into the system using a gas dosing valve which was connected to one of the radial ports. Once the base vacuum was achieved, the gas dosing valve was turned on to maintain pressure in the range of 1×10^{-3} $mbar$ to 5×10^{-2} $mbar$ which was the entire pressure range that was used in the different sets of experiments. On the outer side of chamber, Helmholtz coil pair which contains 30 turns in each coil, was used to create a homogeneous magnetic field. The design of Helmholtz coil is discussed below.

2.1.2 Magnetic field by electromagnetic coil

Helmholtz coils were used to generate a uniform magnetic field up to 250 $Gauss$, parallel to the axis of the anode. It consists of two identical circular magnetic coils. They were placed symmetrically along a common axis, and were separated by a distance X equal to the radius R of the coil. Each coil carries an equal electrical current flowing in the same direction.

The magnetic field, B_x (in Tesla), at any point on the axis of the coil of a single

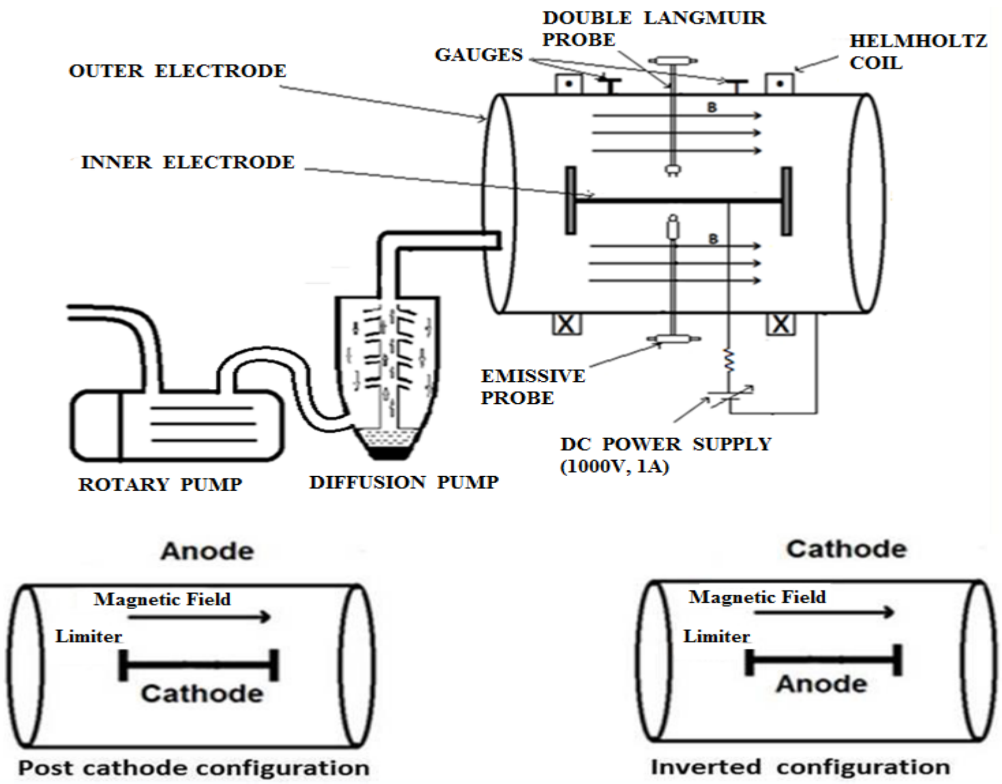

Figure 2.1: *The schematic of the vacuum chamber. It shows electrode arrangement and different ports for diagnostic and pumping system (diagram is not to the scale).*

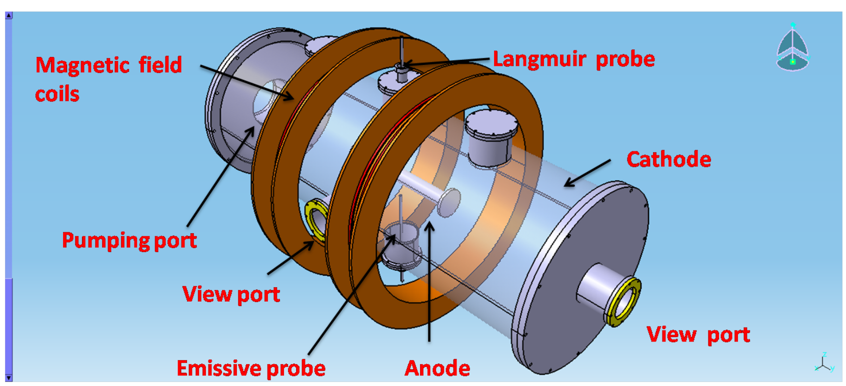

Figure 2.2: *3D view of the hollow cathode cylindrical magnetron system which shows magnetic field coils, anode and ports for mounting probes.*

loop is given by the following formula.

$$B_x = \frac{\mu_0 I}{2R}\left[\frac{1}{\left(\gamma^2+\gamma+\frac{5}{4}\right)^{\frac{3}{2}}}+\frac{1}{\left(\gamma^2-\gamma+\frac{5}{4}\right)^{\frac{3}{2}}}\right] \tag{2.1}$$

Where, B_x = magnetic field in Tesla, r = coil radius in meter, n = number of turns and I = current in the coil in Ampere. $\mu_0 = 1.26\times10^{-6}\ H/m$ is the permeability constant. γ is the ratio x/r, where x is the distance on the axis of the coil from the centre of the Helmholtz coil, and r is the radius of the coil. Setting $x = r$, which defines a Helmholtz pair, minimizes the non-uniformity of the magnetic field at the center of the coils. Therefore, a Helmholtz coil can be used for producing a nearly uniform magnetic field, in the region of interest. Under such conditions, the on axis magnetic field is defined by the following formula

$$B = \left(\frac{4}{5}\right)^{\frac{3}{2}}\frac{\mu_0 n I}{R} \tag{2.2}$$

For design purpose, the required magnetic field was fixed as 300 $Gauss$. Based on the radius of vacuum chamber, the required current and the number of turns were calculated. By substituting these values of B ($0.03\ T$) and R ($30\ cm$) in the above equation 2.2, value of nI was calculated which was found to be equal to 1000. After selecting the coil wire with a current carrying capacity of 300 A and suitable power supply, the required number of turns was calculated to be around 33. The externally wound Helmholtz coil is shown in the 3D view of the system (Fig. 2.2). In the experimental set-up, the magnetic field is measured at various coil currents and it is observed that for a given coil current the magnetic field is almost uniform both in radial(r) and axial(z) directions.

The magnetic field was measured by a Hall probe and found to be uniform along the axis. Fig. 2.3 shows the typical profile of the measured magnetic field in the radial direction at the center of the chamber. In the present experimental set-up the magnetic field used was in the range of 0 to 250 $Gauss$. Selection of this value is based on the fact that the applied magnetic field strength has to be sufficient enough to magnetize the electrons. For the above mentioned magnetic field (25 to 250 $Gauss$), the Larmor radius of the electrons ($1eV$) is 1 to 0.1 mm, which is very much less than the electron neutral mean free path at 10^{-3} $mbar$ pressure. Hence

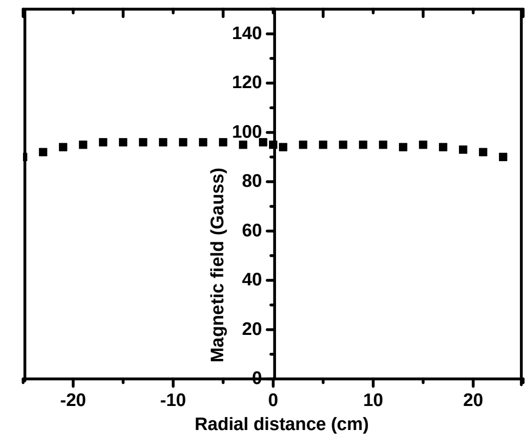

Figure 2.3: *Typical radial profile of the magnetic field. The magnetic field varies from 96 to 90 Gauss in the radial distance of 20 cm from the center of the chamber.*

electrons are surely magnetized. Also the electron cyclotron frequency is 700 MHz (at 250 *Gauss*) which is much higher than electron neutral collision frequency of around 50 MHz.

2.1.3 Power Supplies and discharge procedure

The discharge was powered by a 1000 V and 1 A DC power supply with a series resistor of 1 $k\Omega$. This resistor was used for limiting the discharge current during arcing phenomenon. In hollow cathode discharge formation, the positive terminal was connected to central electrode i.e anode while negative to the grounded cathode. The DC power supply of 50 V and 400 A rating was used for passing current through the electromagnetic coils. The vacuum chamber was first pumped to base pressure of 5×10^{-5} $mbar$, within 90 minutes. Then the argon gas was introduced in the chamber by using gas dosing valve to keep the chamber pressure in the range of 1×10^{-3} $mbar$ to 5×10^{-2} $mbar$. The discharge was obtained by slowly increasing the voltage from the DC power supply. The required magnetic field was applied by slowly increasing the coil current in the Helmholtz coil. Prior to any experiment, the magnetic field was measured by a Hall probe to obtain the calibration curve that was used to correlate the electromagnet coil current to the generated field. A half wave rectifier circuit is also used to bias the anode for acquiring the discharge characteristics like breakdown voltage, current magnetic field characteristics etc. A diode is used to rectify the output waveform of a step up transformer. The bias voltage is measured across the electrodes, while the discharge current is calculated by measuring the voltage across a resistor. The voltage and current waveforms are acquired in a digital storage oscilloscope using suitable voltage probes. In the following section the modified hollow cathode Penning discharge set-up is discussed.

2.2 Modified Hollow Cathode Penning Discharge

The schematic of experimental set up is shown in Fig. 2.4. It consists of a cylindrical shaped vacuum chamber made of glass tube of 200 mm diameter and 300 mm length. The stainless steel flanges at both ends of glass tube have feed- throughs for cathodes and ports for pumping and mounting pressure gauges. Two cathodes of 100 mm diameter each were made from stainless steel circular discs. The two cathodes were covered with teflon on the back side. Inter-cathode distance of 40 mm was fixed for all the experiments. The stainless steel anode in the form of a cube ($8 \times 8 \times 8$ mm^3) and in the form of a ring (100 mm outer diameter, 95 mm inner diameter and 5 mm thickness) was used during the experiments. Due to cubic shape of the anode, there is a clear distinction of the electron flux reaching the anode in the direction perpendicular to the magnetic field and parallel to the magnetic field. The ring shape was used in some experiments to keep all the electron flux perpendicular to magnetic field. This grounded anode was placed symmetrically with respect to the two plane parallel cathodes. The anode was mounted through a port on the upper side of the chamber. The three dimensional view of the modified hollow cathode system is shown in Fig. 2.5

The uniform axial magnetic field was produced by using a Helmholtz coils as described earlier. The coils were mounted symmetrically relative to the centre of the vacuum chamber. The average distance between the two coils was fixed at 100 mm, which is same as the radius of the coil. The coils were designed using similar calculations as discussed in Section 2.1. The magnetic field was varied precisely from 0 to 100 $Gauss$ by varying the coil current. A DC power supply of

32 V and 5 A was used to provide current in the coils. The chamber was evacuated by using rotary pump (150 l/min) and diffusion pump (300 l/sec) to the base pressure of 5×10^{-5} $mbar$. Then the working argon pressure was varied within the range of 0.05 to 0.125 $mbar$. The gas dosing valve was used to control the argon pressure in the chamber. The power was provided by a 600 V and 1.5 A DC power supply, which works in constant voltage mode. The negative of the power supply was connected to two cathodes while positive terminal was connected to anode which is grounded. The discharge voltage was varied in the range of $300 - 600$ V. The discharge voltage was measured using digital voltmeter of the power supply while current was measured using a series resistor in the circuit. The cylindrical Langmuir probe was mounted in such a way that it measures plasma properties near the anode. During Optical Emission Spectroscopy (OES) measurements, the light collecting system was mounted in front of the glass chamber so that it collects emitted light from the plasma.

2.3 Diagnostics

The plasma was characterised by using electrical probes like single, double Langmuir probe and emissive probe. The optical diagnostics like Optical Emission Spectrometer and photo diode detector were also used for identifying argon emission lines and measuring the intensity of argon lines.

2.3.1 Single Langmuir Probe

The Langmuir probe is perhaps the simplest diagnostic tool which is used for measurement of plasma parameters like plasma density, electron temperature and local plasma potential in low temperature plasmas. It is a small metal probe introduced into the plasma such that perturbation to the plasma is minimal. The shape of metal probe can be cylindrical, planar or spherical. The probe is biased to different voltages and the corresponding current drawn by the probe is measured. The graph of the measured current versus applied probe bias is known as current-voltage characteristic of the probe. The analysis of this current (I)- voltage (V) curve gives information about plasma parameters. Apart from simplicity, the other benefit of this technique is that it is used for localised measurement of the plasma

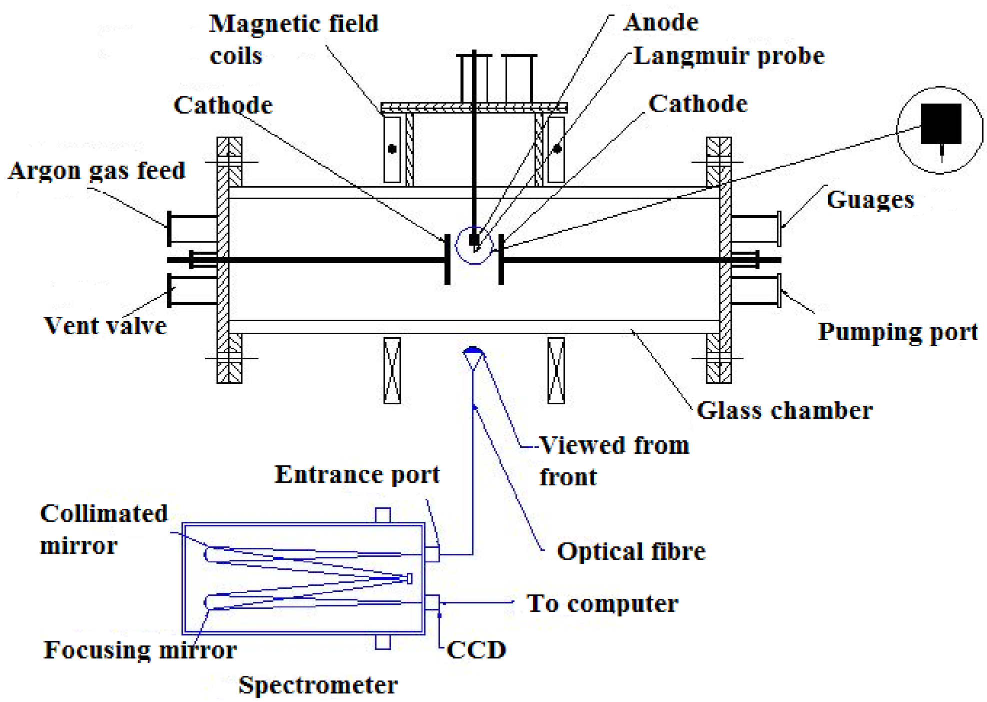

Figure 2.4: *Schematic of the modified hollow cathode discharge. It has two planar cathodes and cubical anode. The axial magnetic field is applied externally. The schematic also shows arrangements for collecting light signal form the plasma.*

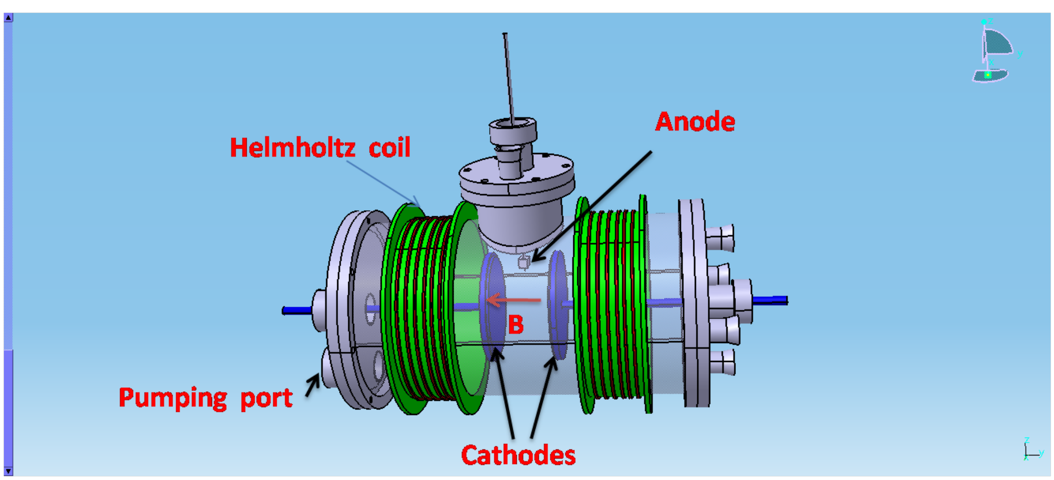

Figure 2.5: *3D view of the modified hollow cathode Penning discharge set-up.*

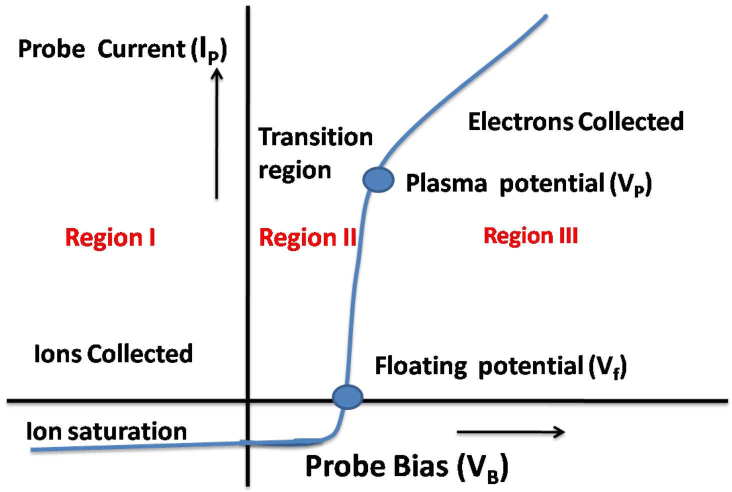

__Figure 2.6:__ Schematic of typical Langmuir probe I-V curve. The three regions are identified as ion saturation (region I), electron retarding (region II) and electron saturation region (region III), each gives specific information about the plasma. V_B is the probe bias and I_p is the current flowing through the probe.

parameters. Fig. 2.6 shows schematics of typical Langmuir probe characteristics. It shows three regions depending upon the nature of the collected particles from the plasma. Since the electrons and ions are not mono energetic, the probe collects only ion current, only electron current or both depending upon applied potential. The bias voltage of the probe V_B is always measured with respect to the laboratory ground or one of the electrodes of the discharge like anode. V_P is the plasma potential with respect to the laboratory ground potential. By applying the standard Langmuir probe theory, the equations of the current collected in all the three regions are discussed below.

When the probe bias is equal to the plasma potential, there is no electric field between the probe and the plasma. The probe will collect any particle randomly coming from the plasma. However, as the random flux of electrons is very high compared to ions, net current collected by the probe will be electron current. Even at higher positive bias, the probe draws more electron current. Ideally as per Langmuir probe theory, this current should remain constant, however practically this does not happen. With increasing bias voltage, the sheath expansion happens which increases the collection area and hence the increase in total electron current. The exact saturation of electron current is not observed during the measurement.

The electron saturation current is given by

$$I_{es} = enA\sqrt{\frac{kT_e}{2\pi m}} \tag{2.3}$$

where A is the probe area, n is plasma density, e is elementary charge, k is the Boltzmann constant, T_e is electron temperature, m is the mass of electron. The voltage at which saturation of electron current starts is called as local plasma potential. If the probe is biased below the plasma potential, it starts repelling electrons due to electric field between probe and plasma. Considering Maxwell Boltzmann distribution for velocity of electrons, the electron current in this region is given by

$$I_e(V_B) = I_{es}exp\left(\frac{-e(V_P - V_B)}{kT_e}\right) \tag{2.4}$$

In this region, ions and electrons both are collected by the probe. Depending upon the potential difference between the probe and plasma, the low energy electrons get repelled first and then high energy electrons. Hence the current collected in this region depends on the electron energy. With further reduction of V_B the electron current reduces and becomes comparable to ion current. Hence at one particular probe voltage below the plasma potential, both ion and electron current become equal and cancel each other. The situation arises when no current flows through the probe. This potential at zero probe current is known as floating potential of the plasma. Hence any electrically isolated object in plasma, which cannot carry current will float at this potential. When the bias voltage of the probe is sufficiently negative with reference to plasma potential V_P, the probe collects ion saturation current, I_{is}. In the ion sheath, most of the electrons, especially of low energy, are repelled. Taking into account the Bohm theory which is discussed in chapter 1, the ion saturation current is given by

$$I_p = I_{is} = 0.61enA\sqrt{\frac{kT_e}{M}} \tag{2.5}$$

where M is the mass of ion. This equation is effectively used to determine the plasma density (n), since a quasi neutral plasma has equal number of electrons (n_e) and ions (n_i), $n_i = n_e = n$. All of the above equations hold for collision-less sheath theory. Also the Bohm sheath criterion is applicable to cylindrical probe for thin sheath where $(r_p/\lambda_d) >> 1$, and λ_d is the debye length and is a measure of the sheath thickness. The r_p is probe dimension. In case of thick sheath, the other ion collection theories exist [53–56].

Electron temperature and Plasma density

The electron temperature was determined by using I-V characteristics in the electron repelling region (the region between plasma potential and floating potential). If the electron energy distribution is Maxwellian, the probe current in this region will be an exponential function of voltage divided by the electron temperature. However the probe current in this region also contains ion saturation current. Hence the ion current part has to be removed first. In actual measurements, ion current does not get saturated. Hence considering the thin sheath approximation, the ion current part is fitted to a straight line. This straight line is then extrapolated to the current axis. The intersection point on the current axis is considered as ion saturation current. The electron current is calculated by subtracting the ion saturation current from the probe current. It is clear from equation 2.4 that, the natural logarithm of the current in the electron retarding region should give a straight line. If we take plasma potential as a reference point then taking log of equation 2.4 gives

$$ln(I_e) = \frac{eV_B}{kT_e} + constant \tag{2.6}$$

This is a linear equation of nature $y = mx + c$, here x is V_B and m is e/kT_e. Hence the inverse of the slope for the straight line in the $ln(I_e)$ vs V_B curve directly gives the electron temperature in eV. Once T_e is known, the plasma density n is readily obtained from equation 2.5 which is applicable in the thin sheath limit.

Plasma potential and Floating potential

The floating potential(V_f) is the probe potential at which probe draws zero current. This point can be easily identified by observing the voltage at which zero current occurs. The floating potential is few volts negative below the plasma potential. The plasma potential is roughly determined by using the knee point in the Langmuir probe I-V characteristics. It is also found out from the $ln(I)$ vs V_B plot. The linear portion of electron retarding region and electron saturation region are extrapolated.

The intersection point of the extrapolated lines is the plasma potential. There is another method to estimate the plasma potential which is called as inflection point method. In this method the first or second derivative of the probe current with respect to bias voltage is taken. The inflection point of the first derivative is the location of plasma potential, while the zero crossing of the second derivative gives the plasma potential. In order to minimise error in the determination of plasma potential by using these various methods, the emissive probe is mostly used for the measurement of the plasma potential.

2.3.1.1 Double Langmuir probe

As mentioned above the single Langmuir probe is biased with reference to one of the electrode or the grounded chamber. When the cathode of the discharge is grounded and anode is floating positive, the plasma potential measured with reference to ground will be near the discharge voltage which will be very high. Generally during the single Langmuir probe measurement, the required sweeping voltage is few volt positive and few volt negative than the plasma potential. However, a high sweeping voltage is required for probe biasing if plasma potential is very high. In such cases, the use of double Langmuir probe is more suitable. For double Langmuir probe measurement, separate reference electrode is not required. Also, there is minimum perturbation to the plasma because the maximum current drawn by the probe is equal to ion saturation current. The double Langmuir probe is mostly used for space plasma where there is no reference avialble for probe measurements. The double Langmuir probe system consist of two identical Langmuir probes biased with respect to each other. The probes are electrically floating with reference to ground or any other electrode. The theory of double Langmuir probe, its advantages and limitations in different types of plasmas are documented in the literature [57–59].

Fig. 2.7(a) shows the typical double probe circuit. Both the probes are floating because the power supply connected to the two probes is floating from the laboratory ground and plasma. The Fig. 2.7(b) shows the typical I-V curve measured by using double Langmuir probe in our system. The two probes are exactly identical in material and dimensions. Hence the current drawn by one probe must be equal to the current from the second probe. The probe current is always limited to the

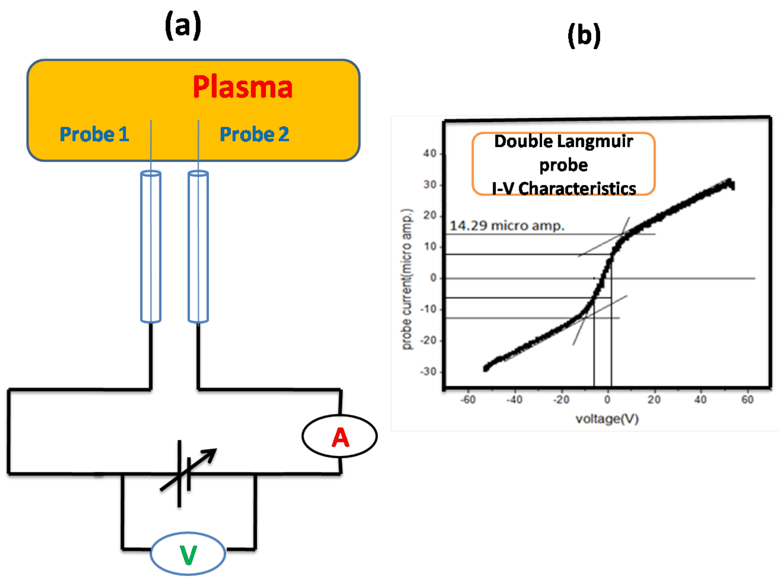

Figure 2.7: *(a) Circuit diagram of a typical double Langmuir Probe. The voltage source is completely floating. Probe 1 and Probe 2 are two probes immersed into the plasma.(b) Typical I-V characteristics of double Langmuir probe obtained from our experimental data.*

ion saturation value. The current collected by the probe is a small fraction of discharge current.

$$I_{P1} = -I_{P2} \tag{2.7}$$

where, I_{P1} and I_{P2} are the current through probe 1 and 2, respectively. The estimation of the current collected by the probes is given below. By using floating potential definition

$$I_{P1} = I_{is1}\left(1 - \exp(1 - \frac{eV_1}{kT_e})\right) \tag{2.8}$$

$$I_{P2} = I_{is2}\left(1 - \exp(1 - \frac{eV_2}{kT_e})\right) \tag{2.9}$$

$$V_d = V_1 - V_2 \tag{2.10}$$

$$I = I_{P1} - I_{P2} \tag{2.11}$$

Rearranging above equations, the current in the double Langmuir probe can be written as,

$$I = I_{is} tanh\Bigg(-\frac{eV_d}{2kT_e}\Bigg) \tag{2.12}$$

where, V_d is the voltage of a probe with respect to the other probe. From above equation the electron temperature can be calculated as below,

$$\Bigg(\frac{dI}{dV_d}\Bigg)_{V_d=0} = \frac{eI_{is}}{2kT_e} \tag{2.13}$$

$$\frac{kT_e}{e} = T_e(eV) = \frac{I_{is}}{2} \times \frac{1}{\text{slope at } V_d = 0} \tag{2.14}$$

Once T_e is obtained from the above equation, it is easy to obtain plasma density using equation 2.5. The double probe cannot be used to measure the plasma potential because the whole double probe system is floating.

2.3.1.2 Designing of the Langmuir probe

Even though the measurements from Langmuir probe is easy, the designing of the probe is crucial. In order to decide a suitable dimensions of the probe, it is necessary to consider first the range of parameters which has to be measured. Apart from that, operating conditions like pressure, magnetic field, contamination of the probe *etc* has to be considered. Depending upon the plasma parameters and operating conditions, there are different working regimes of Langmuir probe. Based on these regimes, the analysis of the Langmuir probe data is done. The regimes are defined by the characteristics probe dimension (probe radius r_p), mean free paths (λ_e and λ_i), Debye length(λ_d) and temperature of the electrons and ions. The region which is considered for our experiment is collision-less, thin sheath, weakly magnetised plasma in which

$$\lambda_{i,e} >> r_p >> \lambda_d \tag{2.15}$$

and when the plasma is confined by weak magnetic field

$$r_{ce} << r_p, r_{ci} >> r_p \tag{2.16}$$

where r_{ce} and r_{ci} are the electron and ion gyro radius respectively.

The estimation of the above parameters in case of our experimental conditions is detailed here. For the operating pressure of 1×10^{-2} to 1×10^{-3} $mbar$, the ion mean free path falls in the range of $10 - 100$ mm which is greater than the probe diameter of 0.70 mm. The formula for electron debye length is given by $\lambda_{De} = 740\sqrt{T_e/n_e}$ cm, where T_e is in eV and n_e is in cm^{-3}.

For $n_e = 10^9 - 10^{10}$ cm^{-3} and $T_e = 1$ eV the debye length is $\lambda_d = 0.2 - 0.07$ mm, Hence, for the expected plasma parameters the debye length will be smaller than the probe dimension of 0.75 mm diameter. The length of the Langmuir probe was taken as 8 mm to avoid the end effects. In our work, for hollow cathode cylindrical magnetron plasma, a Langmuir probe of 0.75 mm diameter was used where plasma density was in the range of 10^9 cm^{-3} while for modified Penning hollow cathode a Langmuir probe of 0.25 mm diameter was used where the plasma density and operating pressures were one order higher. The gyro radius of thermal ions at 50 $Gauss$ magnetic field is around 30 mm which is greater than probe dimension. Hence the plasma density was measured using the ion saturation current. A thin probe of 0.125 mm radius was used for electron temperature measurement at maximum magnetic field of 50 $Gauss$. The gyro radius of electron at $T_e = 1$ eV temperature and 50 $Gauss$ is around 0.5 mm which is much greater than the probe radius. Hence the effect of magnetic field on the Langmuir probe measurements could be neglected at low magnetic fields. Total area of Langmuir probe was taken as $A = 2\pi rl + \pi r^2$, where r and l are radius and length of the Langmuir probe, respectively.

The Langmuir probe is made from Tungsten (W) metal wire. Tungsten has high melting point as well as the sputtering yield of Tungsten is very less. The metal wire was fitted in a ceramic tube. A teflon coated copper wire is connected to the probe and is taken out through a SS pipe. The SS pipe is connected to vacuum port through vacuum feed-through. The probe movement inside the plasma chamber is also possible by using teflon based feed-through. In order to sputter clean the Langmuir probe, it was negatively biased for 30 minute before every measurement. The design of double Langmuir probe is similar to the single Langmuir probe. Only difference is that two identical probe tips are fixed in a glass tube. The circuit diagram is shown in Fig. 2.7. The separation between two probes was 10 mm which ensures that the sheath of one probe does not overlap the sheath of the other probe. The glass tube was connected to SS pipe in which the conducting wires of the two probes passes.

Effect of the magnetic field

In the presence of magnetic field, it becomes difficult to apply simple collisionless theory for Langmuir probe analysis. The motion of the electrons and ions gets deflected due to magnetic field. The Langmuir probe measurements in the magnetic field are affected by change of the trajectory of charged particle in magnetic field. The magnetised charged particle move along the magnetic field lines. The length scale which decides the motion of the particle is gyro or Larmor radius of the particles r_g. If the gyro radius is greater than probe radius $r_g >> r_p$, the standard Langmuir probe theory of the non magnetised discharge can be applied. In case of $r_g << r_p$, the electron current is decreased because of diffusion normal to the magnetic field is smaller than the diffusion parallel to the magnetic field. As the larmour radius of ions is much greater than the electrons, the ion current part of the Langmuir probe characteristics is not affected much. Hence the ion current part is used for plasma density determination in the case of low magnetic field where ions are not magnetised. Further in the electron retarding region, the probe repels low energy electrons at the negative voltages. Hence the measurement of electron temperature from this region at low magnetic field can produce minimum error. If the ion Larmour radius is also less than probe radius, then Bohm current will flow mainly parallel to the magnetic field. Practically in such cases, the probe area considered is the area projected to the surface perpendicular to field lines. In our case, the Larmour radius of ions was larger than probe radius at maximum magnetic field of 50 *Gauss*, hence the ion saturation current was considered for density determination.

2.3.2 Emissive Probe

Emissive probe is extensively used for the measurement of plasma potential. It can measure plasma potential reliably under various conditions e.g sheath, double layer *etc*, where the conventional cold Langmuir probe measurement will results in errors [60, 61]. The emissive probe is essentially a thin hot wire loop, usually made up of Tungsten metal. It is heated sufficiently so that the thermionic emission of

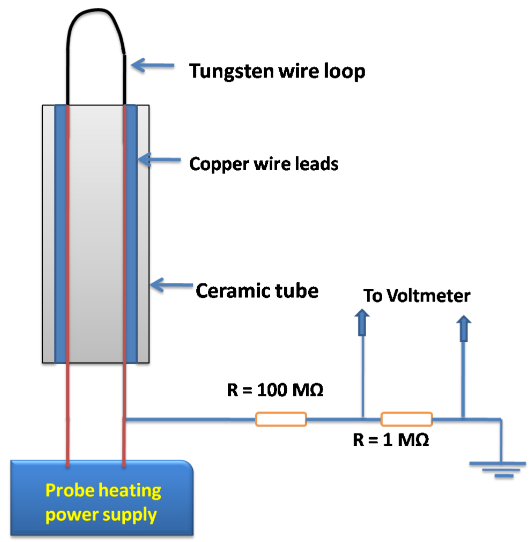

Figure 2.8: *Schematic of the emissive probe construction.* 0.125 *mm thin Tungsten (W) wire is taken and bent into a loop, which is simply press fit in to the double bore ceramic tube. The ceramic tube is filled with many thin copper threads to increase the conductivity inside the ceramic.*

electrons takes place. The temperature limited emission current can be given by,

$$I_{em} = AT_w^2 \ S \ exp\left(\frac{e\phi_w}{T_w}\right) \tag{2.17}$$

where, A is Richardson's constant, ϕ_w is the work function of the wire, T_w is the temperature of the wire and S is surface area of the wire.

The principle of operation of emissive probe is simple. When the bias voltage of the probe is more negative than the plasma potential, the electrons which are emitted by the probe are collected by the plasma. However, there is no net emission of electrons when the bias voltage is much more positive than the plasma potential. Using this principle, the plasma potential is determined. The emission from the probe is not affected by the flow of plasma or the electron temperature. The first use of emissive probe was reported by Langmuir [62].

Further practical and widespread use of emissive probe was started after the work of Kemp and Sellen Jr [63]. One of the simple and widely used technique to determine the plasma potential by using emissive probe is saturated floating potential method. In our experiment too, we had used this technique to obtain

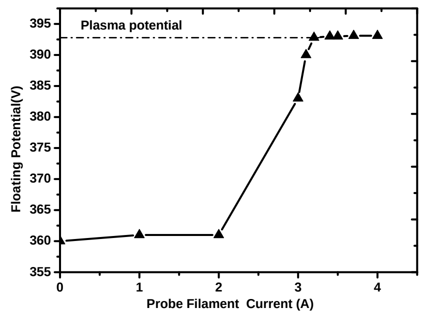

Figure 2.9: *It shows floating potential at increasing current in the emissive probe. Once emission starts, the floating potential quickly rises and saturates at the local plasma potential.*

the plasma potential. For each measurement, the heating of the emissive probe was increased until the floating potential gets saturated. It is shown below mathematically how the floating potential during the strong emission will give plasma potential. It is known that by equating the ion current and the electron current , the relation between plasma potential and floating potential of cold probe would be

$$V_P = V_f + T_e ln(\frac{I_{es}}{I_{is}}) \tag{2.18}$$

V_P is plasma potential, V_f is floating potential, I_{es} is electron saturation current, I_{is} is ion saturation current. Now applying similar relation to emissive probe

$$V_P = V_{f,em} + T_e ln(\frac{I_{es}}{I_{is} + I_{em}}) \tag{2.19}$$

I_{em} is the emission current of the emissive probe . The $V_p = V_{f,em}$ is the actual floating floating potential of the probe which depends upon the emission current.

$$\left(\frac{V_P - V_{f,em}}{T_e}\right) = ln\left(\frac{I_{is} + I_{em}}{I_{es}}\right) \tag{2.20}$$

Thus when emission current just compensates the electron saturation current, the floating potential becomes equal to plasma potential.

Considering the temperature requirement during the operation of the emissive probe, thin Tungsten wire is generally used for the probe because it has high melting point (3695 K). There are different ways to increase the temperature of the probe e.g. Joule heating, Laser heating, Indirect heating etc. The probe heating is mostly done by passing current in the wire. Tungsten wire was made into a loop, and then is fixed into the double bore ceramic tube as shown in Fig. 2.8. The emissive probe breaks frequently after few operations. To solve this problem, the ceramic tube was filled with copper wires along with tungsten wire to prevent unnecessary heating [64]. The life span of the emissive probe was improved by using this technique. A few amperes of current in the emissive probe heats upto a temperature suitable for thermionic emission. The floating potential of the probe is measured by connecting the probe to ground through a high resistance. The emission of the emissive probe is increased by increasing the wire (probe) current or temperature until the floating potential saturates. The typical saturation floating potential is shown in Fig. 2.9 which is measured in our experimental arrangement.

2.3.3 Optical Emission Spectroscopy

This diagnostic technique was used to identify the argon emission lines from plasma near the anode. The light was collected using a light collection system fixed at one of the radial ports of the chamber. In the experiment, the light collection system was placed such that it collects the radiations from the near anode plasma. The optical probe has plano convex lens (diameter:50 mm and focal length of 150 mm) assembled in a small tube with a SMA (Sub Miniature version A) termination for connecting a 0.6 mm silica fiber (numerical aperture :0.22). The spectra were recorded with a 0.5 meter imaging spectrograph (Acton Research Corp., USA) having a 1200 l/mm grating and equipped with a CCD (Charge Coupled Device) detector (Princeton instruments, USA). All the recordings are obtained with entrance slit opening of 50 micron for which the achievable wavelength resolution is $\sim$ 0.05 nm. The argon spectra (400 nm to 900 nm) are recorded for different discharge parameters and intensity variation of prominent argon lines is studied.

3

Plasma characterisation of hollow cathode or inverted cylindrical magnetron

As mentioned in the Chapter 1, the cylindrical magnetron in inverted configuration is one type of hollow cathode cross field discharge. An extensive experimental and theoretical study of the cylindrical magnetron discharge in post cathode configuration (i.e. central cathode and outer anode) has been reported by Straaten *et al.* [3, 4]. In their work, it was shown that the ratio of magnetic field(B) to pressure(P) plays an important role in deciding discharge properties in post cathode configuration. Further a comparative study of cylindrical DC magnetron discharge in post cathode and hollow cathode configuration (i.e. central anode and outer cathode) has been studied experimentally and theoretically [65]. These studies are focused on lab scale systems with outer electrode having dimensions of few cm. However experimental studies are required to understand plasma properties in the hollow cathode configuration with large cathode diameter. Particularly, the operation of discharge at low pressure and high magnetic field in large diameter cylindrical configuration is important to develop an industrial scale process as large area thin film deposition by sputtering. In this chapter, study of effect of magnetic field on discharge characteristics of Hollow Cathode Cylindrical Magnetron (HCCM) is reported. The effect of magnetic field on breakdown voltage, current- voltage characteristics, discharge current was studied. The measurements of plasma potential, electron temperature and plasma density were carried out. Finally the transition from positive space charge to negative space charge due to magnetic field is shown.

3.1 Study of discharge characteristics

3.1.1 Effect of magnetic field on the breakdown voltage

In crossed field DC discharges, the magnetic field significantly affects the breakdown characteristics of the discharge. The effect of magnetic field on breakdown voltage for perpendicular electric and magnetic field has been studied by many researchers in the past. Blevin *et al.* considered bulk properties of electron avalanche and determined the electron energy, drift velocity and expression for ionization coefficient in the presence of magnetic field [66]. The value of second Townsend coefficient in the presence of magnetic field was deduced by Sen and Ghosh [67–69]. They concluded that the expression for equivalent pressure as deduced by Blevin and Haydon, can explain the observed results at low pressure and for low values of magnetic field (below 50 $Gauss$) but for higher magnetic field, the variation of second Townsend coefficient in a magnetic field also has to be taken into consideration. Effect of magnetic field in cylindrical diode configuration has also been studied [70]. It was shown that magnetic field strongly affects the characteristics of the left hand side of the breakdown curve. They have reported that electrical breakdown voltage decreases with increasing magnetic field. Marija has explained the breakdown characteristics in perpendicular electric and magnetic fields taking into account not only the influence of magnetic field on the first but also on second Townsend coefficient [71].

In this section, results of the experiments to study the effect of magnetic field on breakdown voltage of the HCCM discharge are described. The working pressure of argon gas in the chamber was varied in the range of 5×10^{-3} - 5×10^{-2} $mbar$ by feeding argon gas using gas dosing valve. Anode was biased with 10 ms sinusoidal half wave to ignite the discharge. A simple half wave rectifier circuit was used to produce a 10 ms sinusoidal continuous waveform. The circuit consist of transformer to step up the line voltage and diode to make a half wave. A schematic of the power supply used for measurement of breakdown voltage is shown in Fig. 3.1. A Tektronix make 1000X probe was used for voltage measurement while the voltage

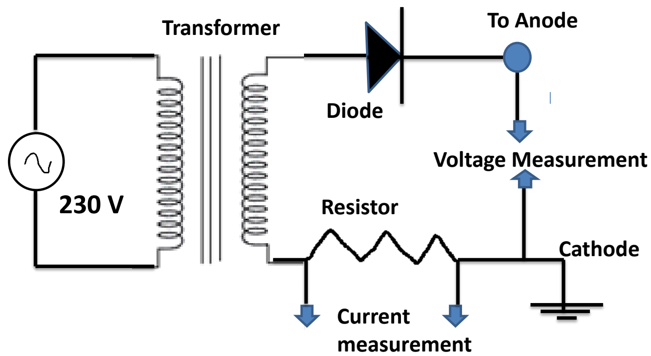

Figure 3.1: *Half wave rectifier circuit for measurements of breakdown voltage. The voltage and current waveforms are measured by using oscilloscope. The measurements are done with reference to grounded cathode.*

drop across the resistor in series of the circuit was used for current measurement.

Figure 3.2 shows the waveforms of the bias voltages for different magnetic fields. In this case, the operating pressure of 1×10^{-2} $mbar$ is kept constant for magnetic field ranging from 50 to 250 $Gauss$. The discontinuity in the waveform corresponds to the breakdown point. It can be clearly seen in the Fig. 3.2 that breakdown point moves towards higher voltages when the magnetic field increases from 50 $Gauss$ to 250 $Gauss$. This is because the electron gyro radius reduces with increasing magnetic field. At a given applied voltage, when ionisation mean free path $\sim 5-10$ mm (at 1×10^{-2} $mbar$) is less than gyro radius of energetic electrons, they gets accelerated and helps in ionisation. But with increase in magnetic field, the gyro radius of the secondary electrons liberated from cathode decreases and becomes less than the ionisation mean free path. In that scenario, ionization probability decreases. The secondary electron can be recaptured to cathode also. They will not gain sufficient energy for ionization. Hence ionization will take place at higher voltage where gyro radius is comparable to or more than mean free path again due to higher energy. Hence for constant pressure, breakdown voltage increases with magnetic field. The breakdown voltages are also measured for three different operating pressures which is shown in Fig. 3.3.

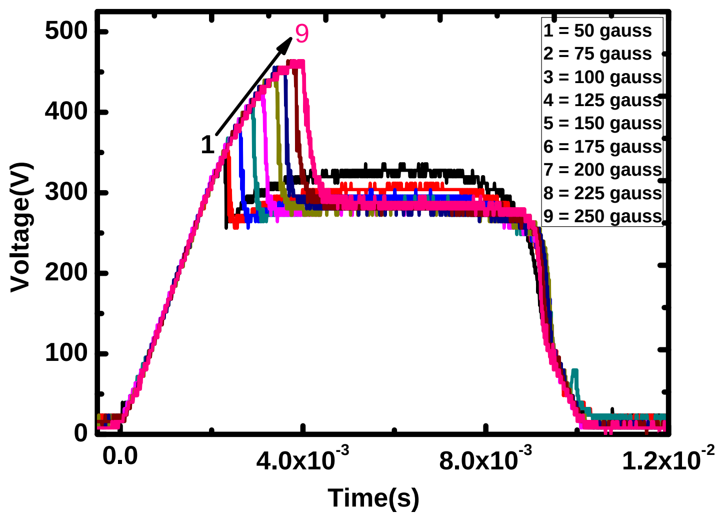

Figure 3.2: *Magnetic field effect on breakdown voltage at 1×10^{-2} mbar pressure. The point at which the voltage is reduced drastically is taken as breakdown voltage. The discharge current starts flowing at this point.*

At a given magnetic field, the breakdown voltage decreases with increase in pressure. This is again because at a higher pressure, collisions increases and ionization mean free path gets decreased and become comparable to or less than the gyro radius. This helps to initiate the discharge. Therefore both magnetic field as well as pressure play a major role in breakdown phenomenon and have a direct relationship with discharge voltage.

Typically at 50 $Gauss$ and 1×10^{-2} $mbar$ pressure, the breakdown voltage is $\sim 340\ V$ and for 150 $Gauss$ it increases to $\sim 400\ V$. This phenomenon can be explained by equivalent pressure concept in presence of magnetic field. Effect of magnetic field is equivalent to an increase of pressure P to P_e such that

$$P_e = P[1 + C_1(\frac{B^2}{P^2})]^{\frac{1}{2}} \tag{3.1}$$

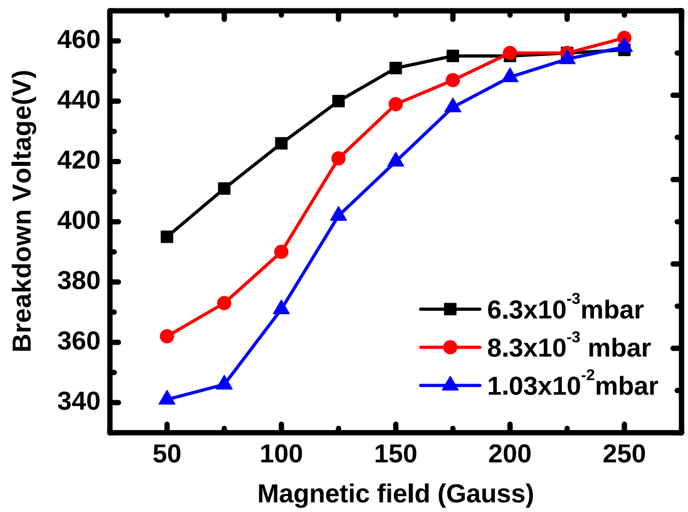

Figure 3.3: *Breakdown voltages at varying magnetic field for three different operating pressures.*

Where B is magnetic field intensity, C_1 is a constant and can be given by

$$C_1 = [\frac{e}{m}\frac{L}{u}]^{\frac{1}{2}} \tag{3.2}$$

L is the mean free path for electron neutral collision and u is velocity of electron of mass m. According to this equation, it has been previously reported [69] that the breakdown voltage in the presence of magnetic field is more than in absence of magnetic field. As per Equation 3.1, the equivalent pressure depends upon B^2/P^2. From our experiments, the breakdown voltage versus B^2/P^2 for three different pressures is plotted and shown in Fig. 3.4. It can be seen that all three curves of Fig. 3.3 almost collapse into single one. Basically, the graph shows breakdown voltage dependence on B/P. Hence, it can be concluded that as the equivalent pressure increases due to increase of magnetic field, the breakdown voltage also increases [72].

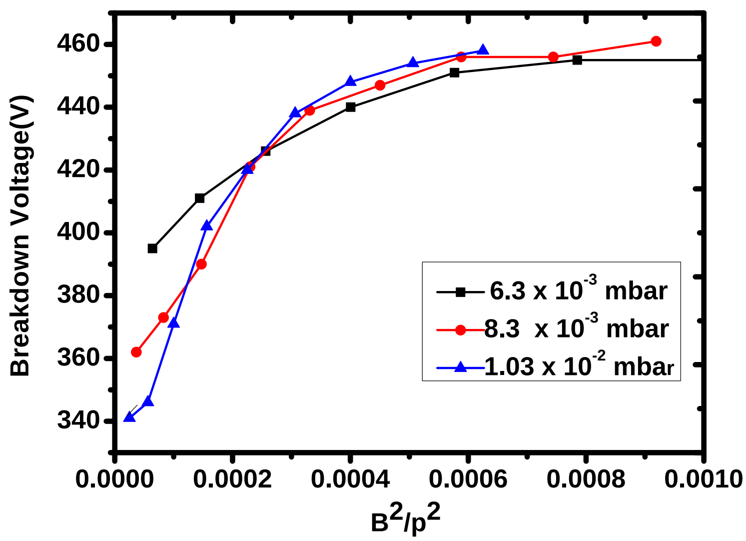

Figure 3.4: *Breakdown voltage vs B^2/P^2 at different operating pressures.*

3.1.2 Current-magnetic field characteristic of the discharge

Once the breakdown takes place, the current starts flowing between the two electrodes. The dependence of this discharge current on the magnetic field was also studied. The discharge current waveforms for different values of magnetic field under a constant pressure of 1×10^{-2} $mbar$ are plotted in Fig. 3.5. It shows that the discharge current is delayed because the corresponding breakdown point is moved towards higher voltages due to magnetic field. The variation of peak discharge current with magnetic field for four different pressure levels has been plotted in Fig. 3.6. The nature of the curve shows the rise of the discharge current with magnetic field, attaining a maximum value and then gradually decreasing. As expected, at higher magnetic field, electron experiences more ionization collisions as its path length increases and hence discharge current increases with magnetic field. Similarly, as shown in Fig. 3.6, the discharge current is more at higher pressure due to more ionizing collisions. But this increase in magnetic field is maintained until 150 $Gauss$, and then the discharge current starts decreasing. At sufficiently high magnetic field, there is decrease in electron mobility which leads to decrease in the cathode fall voltage. According to classical fluid theory, for an operating

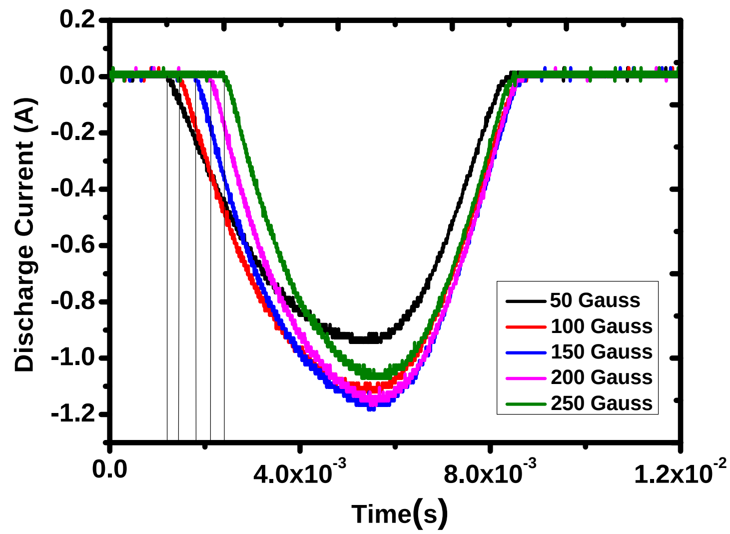

Figure 3.5: *Waveforms of discharge current at different magnetic field. These waveforms are measured simultaneously along with voltage measurement.*

pressure of 1×10^{-2} $mbar$ and magnetic field of 150 $Gauss$, mobility coefficient decreases severely as compared with the absence of magnetic field [3, 4]. Electron flux reaching the anode is reduced due to less ionization near cathode and hence discharge current starts decreasing. This observation of reduction in discharge current at higher magnetic field indicates the possibility of gradual transition to high impedance negative space charge mode. Hence in order to study the discharge current behaviour in detail, a different combination of magnetic fields and pressures were selected which is discussed in following Section.

3.2 Positive and negative space charge modes in HCCM

In cylindrical magnetron discharge plasma, the radial potential structure has been studied analytically by Pekker [73] for long discharges. Further the potential structure was studied using particle in cell simulation for short magnetron discharges [3, 4]. In all these studies, it was found that the steady state discharge will exhibit a gradual transition from positive space charge (PSC) mode to negative space charge

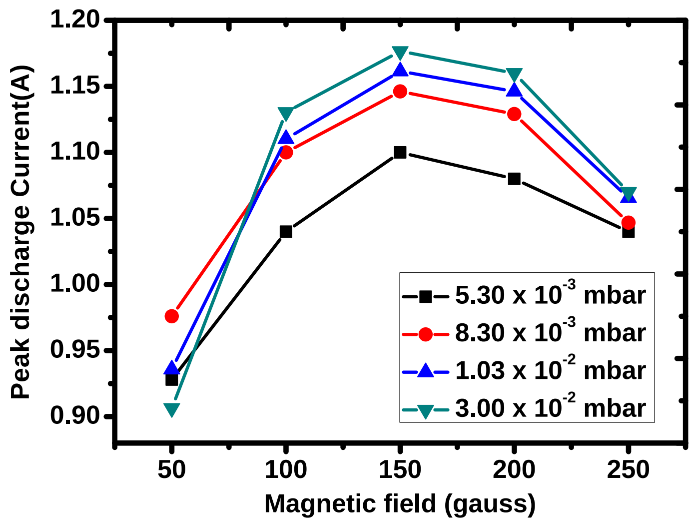

Figure 3.6: *Magnetic field effect on discharge current for different operating pressures.*

(NSC) mode if either pressure is reduced or magnetic field is increased. The PSC is associated with strong cathode fall and negligible anode fall while NSC shows expressive anode fall and less cathode fall. Hence the experiments were performed at low pressure to observe the above transition in HCCM.

3.2.1 Steady state discharge current dependence on magnetic field at low operating pressure

The different combinations of magnetic fields and pressures were selected for a fixed value of applied DC voltage. Fig. 3.7 shows discharge current variation with magnetic field for different values of operating pressures. It is observed that the discharge remains at high discharge current regime up to a critical value of B/P. However, when B/P ratio exceeds this critical value, discharge is converted into low discharge current regime. As shown in Fig. 3.7, for 600 V applied voltage, this critical ratio is approximately 75 kgauss/mbar. According to classical fluid theory of electrons and ions colliding with background neutral atoms, mobility and diffusion coefficients of charged particle can be expressed as [3, 4]

$$\mu_B = \frac{\mu}{1 + (\frac{\omega_c}{\nu})^{1/2}} \tag{3.3}$$

and

$$D_B = \frac{D}{1 + (\frac{\omega_c}{\nu})^{1/2}} \tag{3.4}$$

Where μ and D are mobility and transport coefficient in absence of magnetic field. ω_c is the cyclotron frequency and ν is the collision frequency with neutral species. The μ_B and D_B are mobility and transport coefficient in presence of magnetic field.

At operating condition $p \sim 10^{-3}$ $mbar$ and $B \sim 50$ to 250 $Gauss$, the denominators in the above equations are very large (around 10000) for electrons since $(B/P) \propto (\omega_c/\nu)$. Hence the electron transport coefficient and mobility across the magnetic field is expected to be reduced sufficiently as compared to their value in absence of magnetic field. Also the distance between cathode and anode was very large compared to the electron-neutral mean free path. As ions remain relatively unmagnetized compared to that of electrons under this specific discharge conditions, the ion transport coefficient also relatively remains unaffected. In the above equation, (ω_c/ν) is an important parameter which is equivalent to B/P. Simulation studies for post cathode cylindrical magnetron by Straten et.al [3, 4] suggests that at a higher magnetic field and lower operating pressure, normal positive space charge is difficult to sustain and hence discharge transits to high impedance negative space charge mode. In our case, it was observed that at critical value of B/P, as the electron mobility and transport coefficient across the magnetic field was reduced drastically rendering it difficult for discharge to remain in positive space charge mode.

According to classical fluid theory, when the mobility and transport coefficient across the magnetic field is reduced, discharge should not sustain in positive space charge mode. In our case we had observed this phenomenon for a magnetic field (50 to 250 $Gauss$) which is in good agreement with the classical fluid theory. For a detailed description of this phenomenon, we divided and analysed Fig. 3.7 into three different regions. In the first region (R-I), the discharge current increases

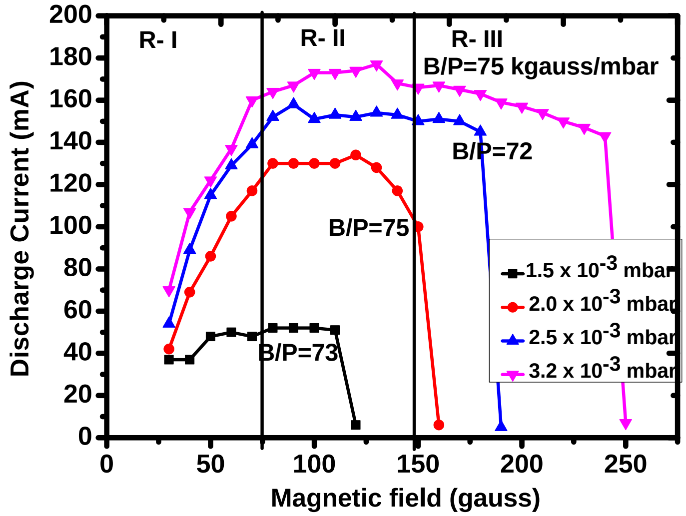

Figure 3.7: *Discharge current vs magnetic field at different pressures. B/P value marked on the graph is transition point.*

with the magnetic field. In this region, discharge operates in a positive space charge mode in which sufficient cathode fall is present. The escape probability of the electrons from the cathode is more due to cathode fall. The radial velocity of electron is greater than ion velocity in this region. In second region (R-II), saturation in the discharge current was observed. This saturation is due to the electron space charge near the anode. This should results in steep field gradient near the anode and less field near the cathode. The escape probability of electron from the cathode is decreased limiting the discharge current [74]. In third region (R-III), discharge current decreases abruptly because of short cathode fall. Electrons cannot gain sufficient energy from the electric field to cause ionization until they are accelerated in the steep field gradient near the anode. Hence all the ionization occurs in a narrow region close to the anode. In the presence of the magnetic field, electron drift in the radial direction depends upon collisional process. At higher pressure this probability increases as a result discharge current increases. In Fig. 3.7, it is observed that for $P = 1.5 \times 10^{-3}\ mbar$, saturated discharge current is $\sim 50\ mA$ which increases to $160\ mA$ for $3.2 \times 10^{-3}\ mbar$. But for same operating pressure, with sufficiently low applied voltages, current will

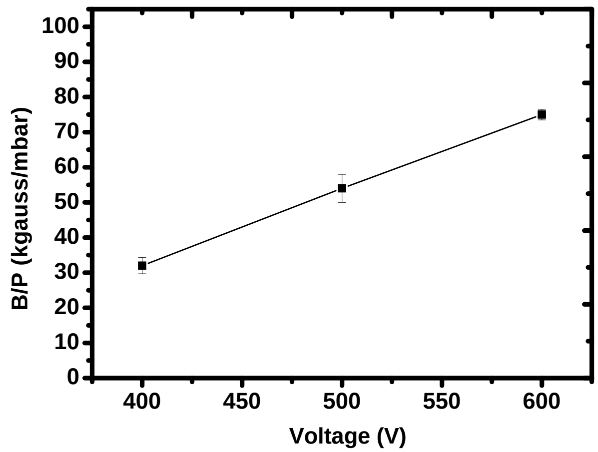

Figure 3.8: *B/P ratio at different discharge voltages.*

decrease with increasing magnetic field. In our case for applied voltage of 600 V at operating pressure of $3.2 \times 10^{-3} mbar$, discharge current starts decreasing after 150 $Gauss$ and at 250 $Gauss$, it transforms into negative space charge. At higher magnetic field and lower voltages very little number of electrons are able to escape from the cathode. For a given pressure, the escape velocity depends upon applied voltage and magnetic field. For sufficiently high voltage, electron radial velocity will be high, so this transition will occur at high magnetic field while for lower voltages, transition can take place at low magnetic field. Fig. 3.8 shows B/P ratio for transition for different applied voltages. The B/P ratio or (ω_c/ν) ratio varies linearly with applied discharge voltage. In our system it was observed that, for an applied DC voltage of 400 V, the discharge would transit into negative space charge mode if B/P ratio becomes more than 32 kgauss/mbar and for 600 V if B/P was more than 75 kgauss/mbar. The radial velocity of electrons is large in PSC mode. Hence in order to maintain high electron velocity, the magnetic field should be low while operating at low pressures.

3.2.2 Effect of magnetic field on floating potential and plasma potential distribution

The measurement of potential distribution between anode and cathode was necessary to support the above observation of negative space charge at higher magnetic fields. Hence the floating potential and plasma potential measurement were carried out at different magnetic field. Fig. 3.9 shows floating potential measured by Langmuir probe at different radial positions from cathode to anode. Floating potential is measured with reference to grounded cathode. In case of low magnetic field, floating potential is almost constant from cathode to anode and its value is high, typically 320 V at 50 $Gauss$ and 1×10^{-2} $mbar$ pressure, but at higher magnetic field, potential distribution changes. Potential value increases towards anode, it becomes more and more positive towards anode. However, overall value of the floating potential also reduces. The increased magnetic field reduces the mobility and diffusion of electrons across the magnetic field, while ions diffuse easily across the magnetic field. This results in floating potential gradient near anode region due to electron space charge, which is an indication of transforming the positive space charge discharge into negative space charge, and is discussed below.

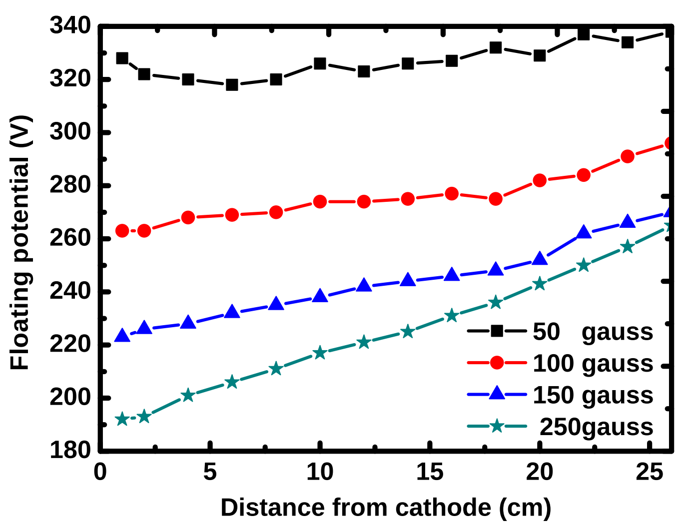

Figure 3.9: *Floating potential distribution at 450 V and* 1×10^{-2} *mbar pressure.*

Table 3.1: *Dependence of transition from PSC to NSC on different operating parameters*

Parameter	Constant B and V	Constant P and B	Constant P and V
P	Low P	—	—
B	—	—	High B
V	—	—	Low V

As explained in previous subsection, discharge transforms into low discharge current regime, i.e., 2 to 3 mA at higher value of magnetic fields. In order to understand these two discharge current regimes, plasma potential measurement by using emissive probe is done for both these discharge current regimes. Fig. 3.10 shows plasma potential distribution for both discharge current regimes obtained from emissive probe measurement. Curve 1 is at magnetic field for 100 $Gauss$ and curve 2 is for 210 $Gauss$ for constant applied voltage of 425 V. Comparison of these two potential distributions shows changes expected from space charge reversal. For normally occurring positive space charge, steep voltage gradient occurs in a narrow region near cathode, while for negative space charge, voltage gradient occurs close to the anode. Fig. 3.10 shows positive space charge behaviour at 100 $Gauss$, but it shows negative space charge behaviour at 210 $Gauss$ or more. Hence, based on the behaviour of discharge current (Fig. 3.7), floating potential (Fig. 3.9), and plasma potential profile (Fig.3.10), it can be stated that discharge is transforming to negative space charge at higher magnetic field. In the positive space charge mode, the plasma with reddish glow filled up the entire inter electrode space. In the negative space charge mode, a bluish glow was observed around the anode. The detailed plasma parameters measurements of the discharge in positive space charge mode are discussed in following section.

The Table 3.1 shows the dependence of transition from PSC to NSC on discharge parameters. In present experimental set up, the transition takes place at decreasing pressure (P)(typically in 10^{-3} mbar range), increasing magnetic field (B)(higher than 100 Gauss) and decreasing voltages (V)(less than 600 V).

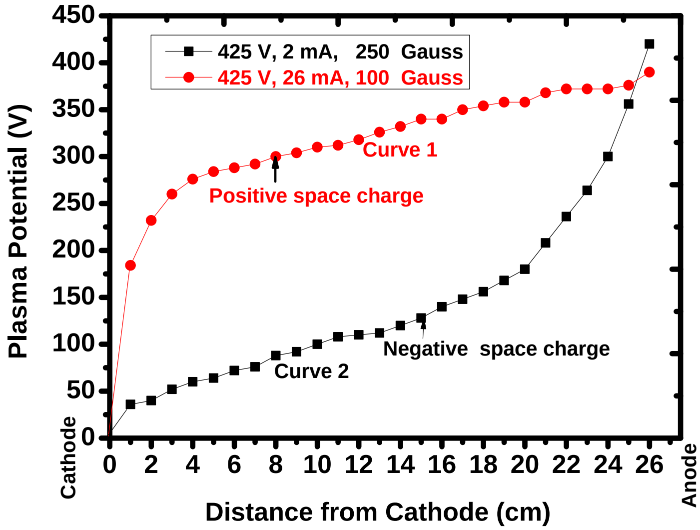

Figure 3.10: Plasma potential profile at two different magnetic fields and constant applied DC voltage of 425 V and pressure 4.5×10^{-3}*mbar showing the difference in two current regimes*

3.3 Plasma parameters measurements of Hollow Cathode Cylindrical Magnetron

As mentioned earlier, the hollow cathode as well as post cathode cylindrical magnetron are used for sputter deposition. The plasma parameters of post cathode magnetron has been measured by using cylindrical langmuir probe [75–77]. The plasma parameters of the hollow cathode configurations were also measured and compared with post cathode [65]. It is expected that the discharge characteristics of hollow cathode configuration will differ from the post cathode even though the principle of operation is same. The understanding of these differences will help in the technological application of thin film deposition. Hence the following section reports on the studies of the plasma parameters for hollow cathode configurations.

3.3.1 Current voltage characteristics

It is well known that the discharge current- voltage characteristics is directly associated with the ionization processes in various plasma discharges. Hence before measuring plasma parameters, the current(I)- voltage(V) characteristics of the discharge was measured at different magnetic fields. The measurements were done at 5×10^{-3} $mbar$ pressure, and at four different axial magnetic fields varying from 50 to 200 $Gauss$. The I-V characteristics of the hollow cathode magnetron configuration is shown in Fig. 3.11. At a fixed magnetic field and operating pressure, the relation between discharge current and discharge voltage was found to be $I \propto V^n$, where the value of n is in the range of 7.5 to 8.5. The fitted I-V characteristics curve, in this case, for a magnetic field of 100 $Gauss$ is shown in inset of Fig. 3.11. The value of n is related to efficiency of electron confinement [2, 78]. Hence the value of n increases with the magnetic field. Previously it is also shown that for magnetron discharges, the functional form of the relationship $I \propto V^n$ is equivalent to Child's law when the large variation of sheath thickness with voltage is taken into account [78].

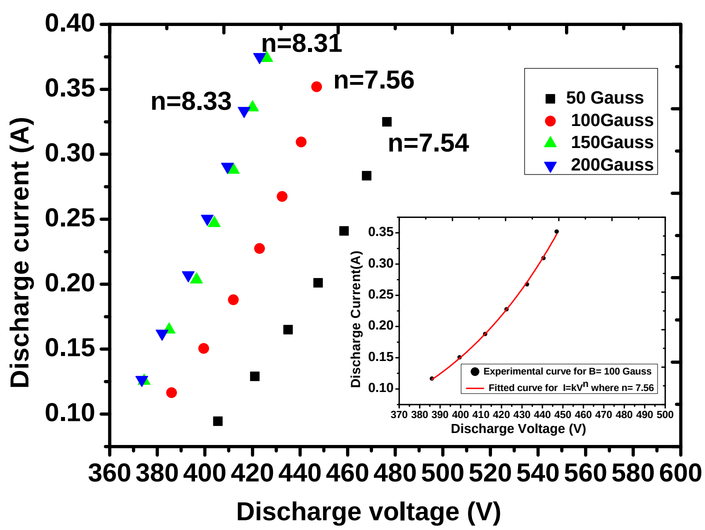

Figure 3.11: *Current-voltage characteristics for HCCM. The inset shows the fitted I-V curve at magnetic field of 100 Gauss.*

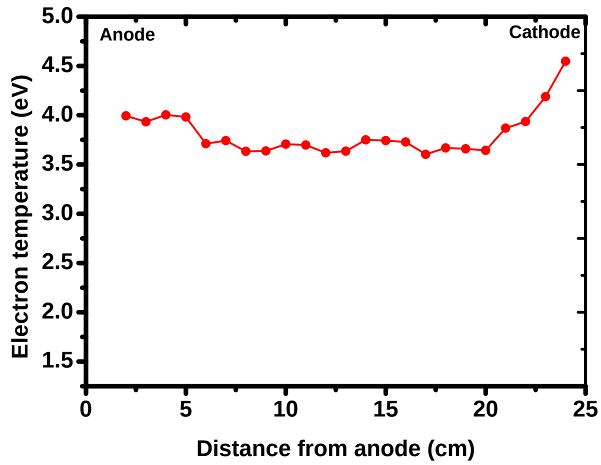

Figure 3.12: *Electron temperature measurements from anode (left) to cathode (right) at 100 Gauss magentic field.*

3.3.2 Electron temperature measurement

The electron temperature is measured by using double Langmuir probe. As the plasma potential with reference to cathode was very high, plasma parameter measurement by using single Langmuir probe became difficult. The radial profile of electron temperature is shown in Fig. 3.12. The electron temperature was determined from the I - V characteristics of the double Langmuir probe. All measurements were conducted at constant discharge voltage of 400 V, operating pressure of 5×10^{-3} $mbar$ and magnetic field of 100 $Gauss$. The electron temperature is found to be decreasing with the distance away from cathode upto 4 cm and becomes constant after that in the intermediate region. The electron temperature goes on decreasing radially away from the cathode because the electrons lose their energy in collisions and ionization while travelling away from cathode. However, the slight rise in electron temperature near the anode is observed.

3.3.3 Plasma density measurement

The radial profile of plasma density for hollow cathode magnetron discharges are shown in the Fig. 3.13. The experimental conditions like discharge voltage, operating pressure, and magnetic field were maintained same as mentioned in previous

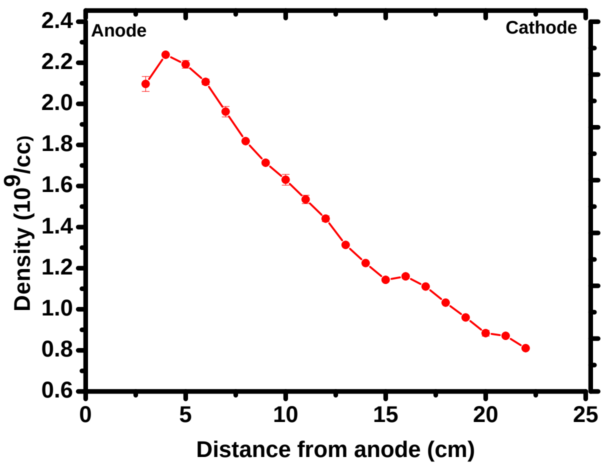

Figure 3.13: *Radial profile of plasma density at 100 Gauss magnetic field.*

section of electron temperature measurement. The plasma density is higher near the anode and decreases towards cathode. The maximum plasma density was observed at $3-4$ cm away from the anode. This is because, the electrons get trapped in the area close to and surrounding the anode so that most of the ionization and excitation occurs in that area.

3.4 Summary

In a Hollow Cathode Cylindrical Magnetron, where electric and magnetic fields are perpendicular to each other, electron transport across the magnetic field is reduced at low pressure and at higher magnetic field. Hence, at higher magnetic field and low pressure, high breakdown voltage is required for discharge ignition. The B/P ratio plays an important role in sustaining the discharge. The magnetic field changes the potential distribution in between cathode and anode and makes it less positive at higher magnetic field. It is demonstrated that there is sharp transition from normally occurring positive space charge to high impedance negative space charge at higher values of magnetic field to pressure ratio, B/P, which varies linearly with applied voltage. In case of large diameter cylindrical magnetron and in the operating pressure range of 10^{-3} $mbar$ which is generally taken for sputtering process, very high magnetic field is not useful for effective sputtering as discharge transforms into negative space charge mode. One has to operate the process in high discharge voltage and low magnetic field so that discharge remains in positive space charge mode. As an example, in our 500 mm diameter hollow cathode cylindrical magnetron for $400 - 600\ V$ and $10^{-3}\ mbar$ pressure range, one can use maximum 150 $Gauss$ magnetic field so that discharge remains in positive space charge mode. For large hollow cathode cylindrical magnetron, magnetic field and pressure have to be optimized properly for a given discharge voltage, so that the discharge remains in positive space charge during sputtering process because positive space charge mode is most appropriate for efficient sputtering. A sharp transition from positive space charge to negative space charge is identified which can be controlled precisely by three experimental parameters, i.e. magnetic field, pressure and applied voltage. The higher plasma density is observed near the anode even though it is expected more near the cathode region. Also the electron temperature is comparable to the near cathode region. These observations indicated that in HCCM significant ionisation is expected near the anode. A detailed investigation of near anode plasma parameters even at low magnetic field is necessary. The experimental investigation of near anode phenomenon in HCCM is reported in next Chapter.

4

Near anode phenomenon in HCCM discharge

In Chapter 3, while performing the plasma characterisation of HCCM, it is shown that the plasma potential near the anode becomes more negative with increasing magnetic field. It is also observed that the plasma density is higher near the anode as compared to other regions of the discharge. For discharges in hollow cathode configuration like HCCM, the anode is enclosed by the cathode. Generally, during the deposition of thin film, either the anode itself is used as a substrate or another substrate is kept near the anode which receives high rate of coating flux from the cathode. The main advantage of HCCM is that it offers large substrate area, fast deposition rates and efficient use of target material. The investigation on the control of particle flux and energy in inverted or hollow cathode magnetron was carried out by Todoran *et.al.*[79]. It is obvious that the plasma condition near the anode has a significant role to play in modifying the growth of the thin film. Hence, the basic understanding of the plasma near the anode of the HCCM discharge is essential considering its application for thin film deposition. The discharge region near the anode in magnetised plasma has been studied for filamentary discharges [47, 48, 80], inductively coupled plasma [50] and planar magnetron discharges [51]. In most of the above studies the anodic plasma is produced by biasing an auxiliary electrode above the plasma potential which essentially changes the properties of background plasma near the electrode [81].

In this chapter, an experimental investigation of the near anode plasma of

HCCM discharge has been presented over a range of discharge parameters in the background of argon gas. The formation of anode glow and its characterisation at low magnetic field for different operating pressures was carried out. The effects of the magnetic field and operating pressure on the evolution of anode glow were experimentally investigated. Further to study the emissions of argon lines from the anode glow, the OES measurements were carried out.

4.1 Plasma potential profiles at different magnetic fields

The radial profiles of the plasma potential and the potential near the anode (anode fall) were measured at different magnetic fields. The anode fall basically determines the anodic sheath behaviour. The negative anode fall attracts ions while positive anode fall attracts electrons. The plasma potential in the region between cathode and anode was measured by using an emissive probe. Fig. 4.1 shows the variation of the plasma potential in radial distance from the cathode in the absence of magnetic field and in the presence of magnetic fields of 50 and 100 $Gauss$. During this set of experiments, the operating pressure of argon gas and applied voltage were fixed at 5×10^{-3} $mbar$ and 600 V, respectively. It is clear from the Fig. 4.1 that in absence of magnetic field, the plasma potential remains almost constant between cathode and anode except a strong fall near the cathode. This indicates very less electric field in the positive column. It is also seen that in absence of magnetic field, the measured plasma potential in the positive column region as well as near the anode is approximately 10 V below the anode potential. This plasma potential profile without external magnetic field is similar to the conventional DC glow discharge plasma where the positive column shows a constant plasma potential. However, in case of applied external magnetic field of 50 $Gauss$ and 100 $Gauss$, the plasma potential decreases and become less positive as shown in Fig. 4.1. The plasma potential becomes more negative with respect to anode in case of 100 $Gauss$ magnetic field. Interestingly, there also exists a finite potential gradient in between the electrodes in presence of magnetic fields, which becomes higher with the higher magnetic field. The plasma potential is around -40 V near the anode (1 cm from the anode). The electron confinement is more in presence of magnetic field. The electron Larmour radius (~ 1 *mm* at 50 *Gauss* for 4 *eV* electron temperature) is less than the electron neutral mean free path (~ 100 *mm* at 5×10^{-3} *mbar*). The rate of electron loss to the anode decreases as compared to the loss rate of ions to the cathode. Hence plasma potential becomes less positive.

Based on the above experimental observations, the anode fall (i.e. potential near the anode) was also measured near to the anode with increasing magnetic field. The plasma potential near the anode surface was measured by keeping the emissive probe 1 *cm* away from the anode for a range of magnetic fields, where the electrons are magnetized. Fig. 4.2 shows the variation of this localized plasma potential with

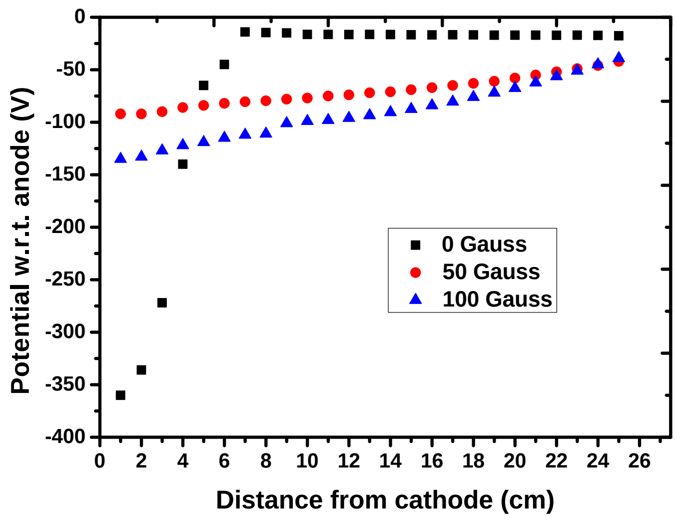

Figure 4.1: *Plasma potential profile in absence and presence of magnetic fields of 50 and 100 Gauss.Here the potentials are shown with reference to anode in order to show the reduction in the plasma potential. The measurements are performed at constant operating pressure and DC voltage.*

reference to anode where the operating pressure and discharge voltage were set to 5×10^{-3} *mbar* and 600 *V* respectively. It is observed that the potential difference becomes more negative with the increasing magnetic field. For example, the plasma potential is -15 *V* in absence of magnetic field whereas it becomes ~ -36 *V* at 10 *Gauss* magnetic field. With further increase of magnetic field the potential drop increases slowly and becomes approximately -45 *V* at 100 *Gauss* magnetic field. The magnetic field reduces the electron mobility in the radial direction which results in the decrease of available electron flux to anode. The voltage drop is developed to induce the electron current collection at anode. This is apparently a consequence of the transverse magnetic field. The transverse electron flux to anode is given by

$$\Gamma_{e_\perp} = -D_\perp \frac{dn_e}{dr} \tag{4.1}$$

where

$$D_\perp = \frac{D}{1 + (\frac{\omega^2}{\nu^2.})} \tag{4.2}$$

Where, $D_\perp$ is transverse diffusion coefficient, $\frac{dn_e}{dr}$ is electron density gradient in radial direction, ω is electron cyclotron frequency and ν is electron collision frequency. For a magnetic field of 100 $Gauss$, ω becomes 1.75×10^9 rad/s. The electron atom collision frequency at a pressure of 5×10^{-3} $mbar$ gives $\nu = 2 \times 10^7$ /s. Thus $\frac{\omega}{\nu}$ become $\sim$ 100 and as a result of which the radial electron current transport can be expected to be reduced significantly. With increasing magnetic field, the transverse electron flux reaching to the anode decreases and hence the anode fall voltage also increases to balance the global current in the discharge. Therefore, the magnetic field plays an important role to decide the anode fall voltage which is controlled by the electron flux reaching to the anode. If the anode fall voltage becomes greater than ionization potential, the ionization will take place in the anode sheath region and anode glow formation takes place. The anode glow evolution with magnetic field is discussed in following section.

4.2 Anode glow evolution with magnetic field

In absence of magnetic field, there is no visible glow on the anode surface. It was observed that in absence of magnetic field or even for low magnetic field (upto a few Gauss), a low intensity faint discharge was formed in between the two electrodes. As soon as transverse magnetic field (more than $4-5$ $Gauss$) was applied, luminous thin anode sheath was formed around the anode, with a thickness of approximately $2-3$ mm. The sheath become visible due to the excitation of neutral gas atoms within the sheath which is nothing but thin anode glow. With further increase in

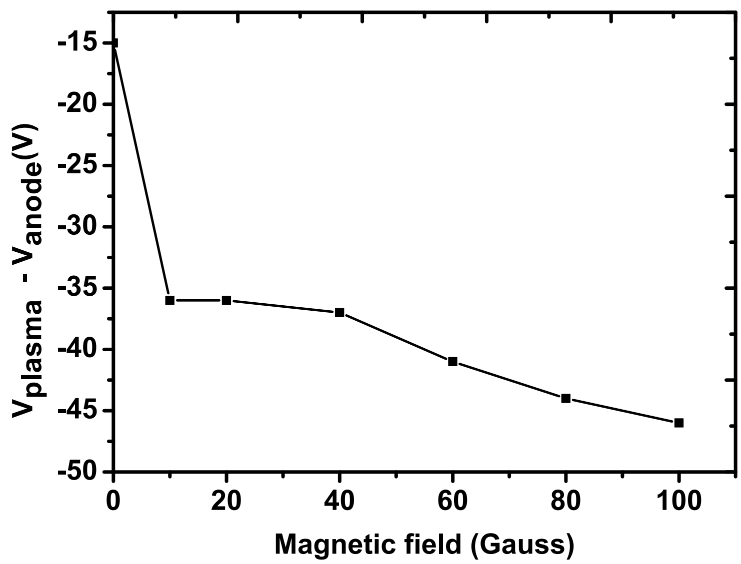

Figure 4.2: *Plasma potential variation with magnetic field near the anode. The difference between anode potential and plasma potential is shown to represent the positive anode fall near the anode.*

magnetic field, one or more anode spot formation takes place at the end points of anode. The electric field converges electrons at the edges and as a result anode spot formation starts there. The anode spot expands with further increase in magnetic field called as anode rods. Initially with increasing magnetic field (5 to 15 *Gauss*), the glow expands axially i.e along the magnetic field. For further increase in magnetic field beyond 15 *Gauss*, the radial expansion of the glow takes place. The discharge current variation with magnetic field is shown in Fig. 4.3. It is clear from this figure that the discharge current shows two different regimes depending on the values of magnetic field. In region-I (i.e 5 to 15 *Gauss*), the discharge current increases linearly with magnetic field with smaller slope. In this region the glow expands axially along the magnetic field and covers the anode surface. However, beyond 15 *Gauss* in region-II, the discharge current increases with faster rate due to the radial expansion of the glow near the anode.

Fig. 4.4 shows the images of discharges near the anode for different values of magnetic fields. Fig. 4.4 (a–d) shows these images of anode glow for $0, 10, 20$ and 40 *Gauss* magnetic fields at operating pressure of 5×10^{-3} $mbar$. Whereas Fig. 4.4 (e–h) shows the same at higher operating pressure of 2×10^{-2} $mbar$. It is observed

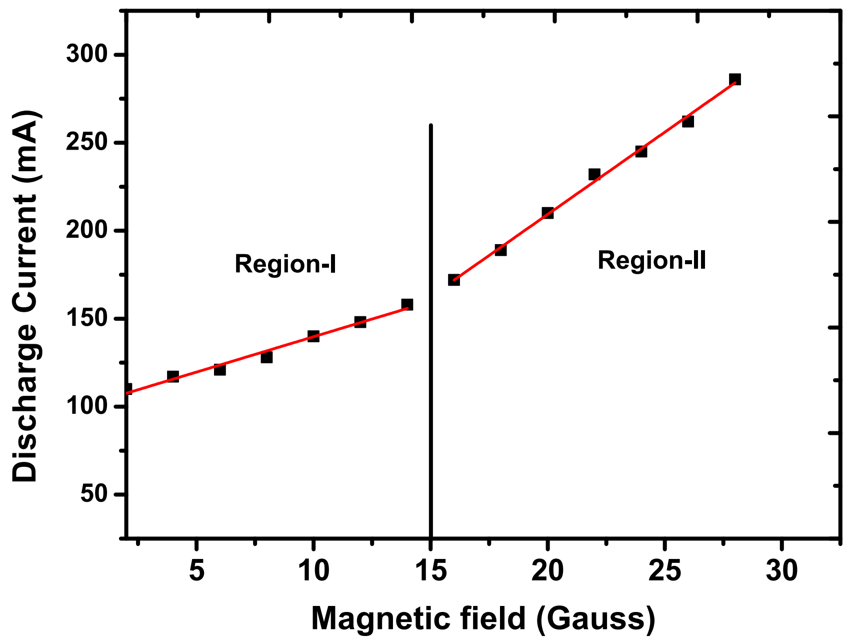

Figure 4.3: *The discharge current variation with magnetic field. The anode spot expands axially in the region I while it enlarges in radial direction in region II.*

that the size of the anode glow increases with magnetic field for both the pressure values. However, the anode glow contracts in case of higher pressure. In past, it is reported that if the ratio of electron collecting surface area (A_a) of anode to the ion collecting surface area (A_c) of cathode becomes less than $(\frac{m_e}{M_i})^{\frac{1}{2}}$ ($\sim 3.7 \times 10^{-3}$ for argon) and the electrode bias above the plasma potential is greater than the ionization potential, the glow initiates to form near the auxiliary anode surface [82]. In the present set of experiments, the anode to cathode area ratio is $\frac{A_a}{A_c} \sim 3.5\times10^{-3}$. In presence of transverse magnetic field the electron flux reaching to the anode across the magnetic field decreases. Hence, the effective anode area for the collection of electrons gets reduced in presence of transverse magnetic field which essentially develops the voltage drop and subsequent excitation and ionisation near the anode surface. Once the ionization takes place near the anode, the effective anode area for the collection of electrons increases. At higher magnetic field or low pressure, in order to balance the flux, the electron collection has to take place over a larger portion of the anode surface. Hence, for lower operating pressure and higher magnetic field as the transverse electron flux decreases the effective anode collection area increases. As a result, the radius of the cylindrical anode glow around the anode increases with the magnetic field as reflected in Fig. 4.4. It is clearly seen that with the increase of magnetic field, the effective anode area enhances significantly (for both the cases of neutral gas pressure) in order to collect more electrons from the background plasma.

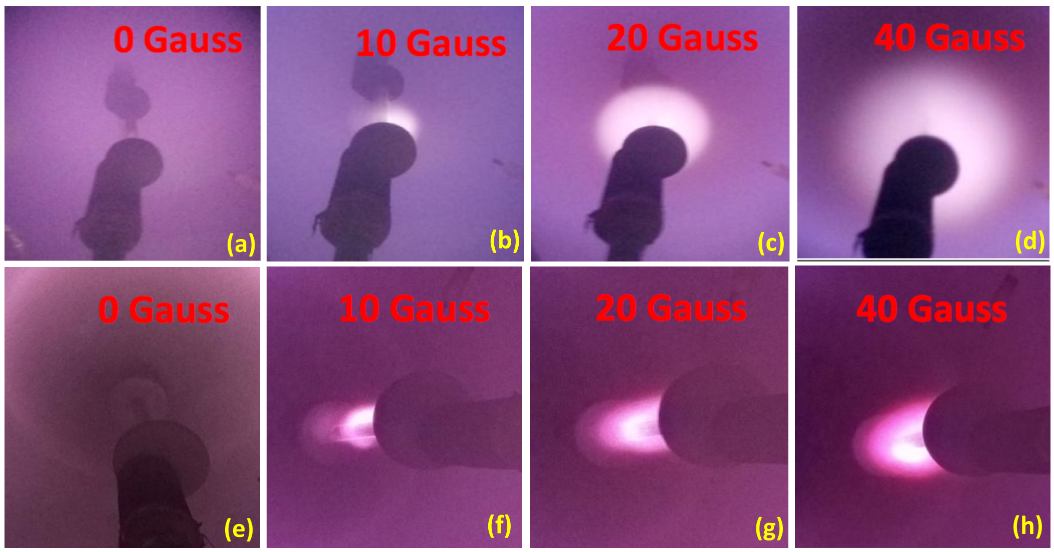

Figure 4.4: *Anode glow images at different magnetic field for* 5×10^{-3} *mbar and* 2×10^{-2} *mbar pressures. The images (a) to (d) are at pressure* 5×10^{-3} *mbar while (e) to (h) are at pressure* 2×10^{-2} *mbar.*

4.2.1 Expansion of anode glow

The size of the anode glow depends upon the discharge parameters like voltage, background pressure and applied magnetic field. The radial boundary of the anode glow was determined by processing the still images which are captured at different discharge parameters. The algorithm for image processing was developed. The central anode dimensions was used as reference object. The Fig. 4.5 shows the variation of the radius of anode spot at different voltages for a given magnetic field of 30 $Gauss$ and neutral gas pressure of 5×10^{-3} $mbar$. Similarly, Fig. 4.6 shows the variation in the size of anode glow and discharge current with different magnetic field for constant discharge voltage of 500 V and pressure of 5×10^{-3} $mbar$. It is observed that the size of the glow increases with both the voltage as well as with magnetic field. In addition, the Fig. 4.6 shows that the variation of discharge current and size of the anode glow follows the same trend, which essentially infer that the discharge current increases due to the increase of effective electron collection area.

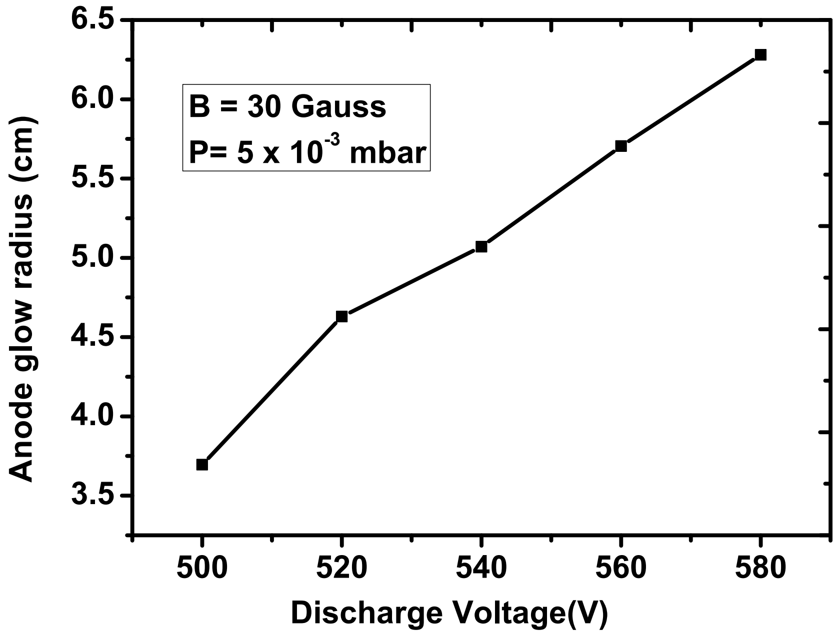

Figure 4.5: *The anode glow size variation with discharge voltage at fixed magnetic field. The radial boundary of the anode glow is considered as glow radius.*

4.2.2 Plasma parameters of the anode glow

Visually bright anode glow observed near the anode along a distance of few *cm* from the anode was due to the acceleration of electrons. These electrons create this secondary plasma which has different plasma parameters than the background plasma. Usually this near anode plasma has higher plasma density and electron temperature. In order to confirm this, the plasma parameters like plasma potential, ion saturation current and electron temperature were measured in this anode glow.

Fig. 4.7(a-c) displays the variation of plasma parameters e.g. plasma potential, ion saturation current and electron temperature with the distance from anode for the expanded anode glow which is developed on the anode surface at 40 *Gauss*. The plasma parameters were measured for two different pressure values

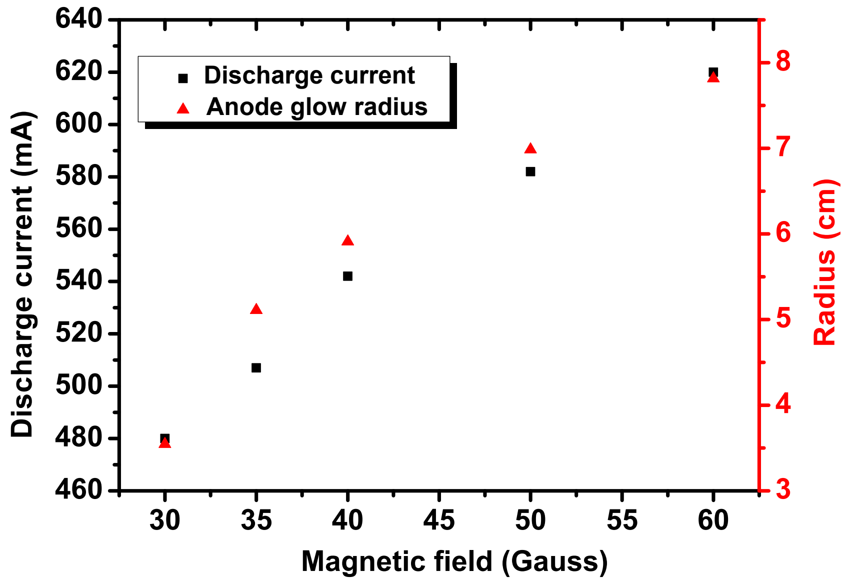

Figure 4.6: *The anode glow size variation with magnetic field at fixed discharge voltage. The radial boundary of the anode glow is considered as glow radius.*

5×10^{-3} $mbar$ (left) and 2×10^{-2} $mbar$ (right). Fig. 4.7(a) shows that the potential measured by the emissive probe is higher near the anode and it decreases monotonically when emissive probe comes out in the background plasma region (away from the anode) and finally attains approximately a constant value. This potential drop from anode to plasma becomes distinguishable at higher pressures. The ion saturation current and electron temperature as measured by double Langmuir probe are shown in Fig. 4.7(b) and Fig. 4.7(c) respectively. The electron temperature and the ion saturation current show their maximum value near the anode and then decreases gradually thereafter. At the outside of anodic glow region the density and electron temperature becomes almost half of the value compared to the glow region. However, it is worth mentioning that the maxima of electron temperature and ion saturation current get shifted towards the anode when the pressure was raised to the higher value because of the reduction in size of the anode glow. As explained in previous section, when the anode is made effectively smaller or magnetically constricted, it produces an intense glow near the anode. In this situation, the newly developed anodic glow/spot keeps on supplying the ions into the background plasma. These anode spots/glow not only produces positive ions but also effectively increases the anode area for collecting more electrons from the background plasma to conserve the same flux.

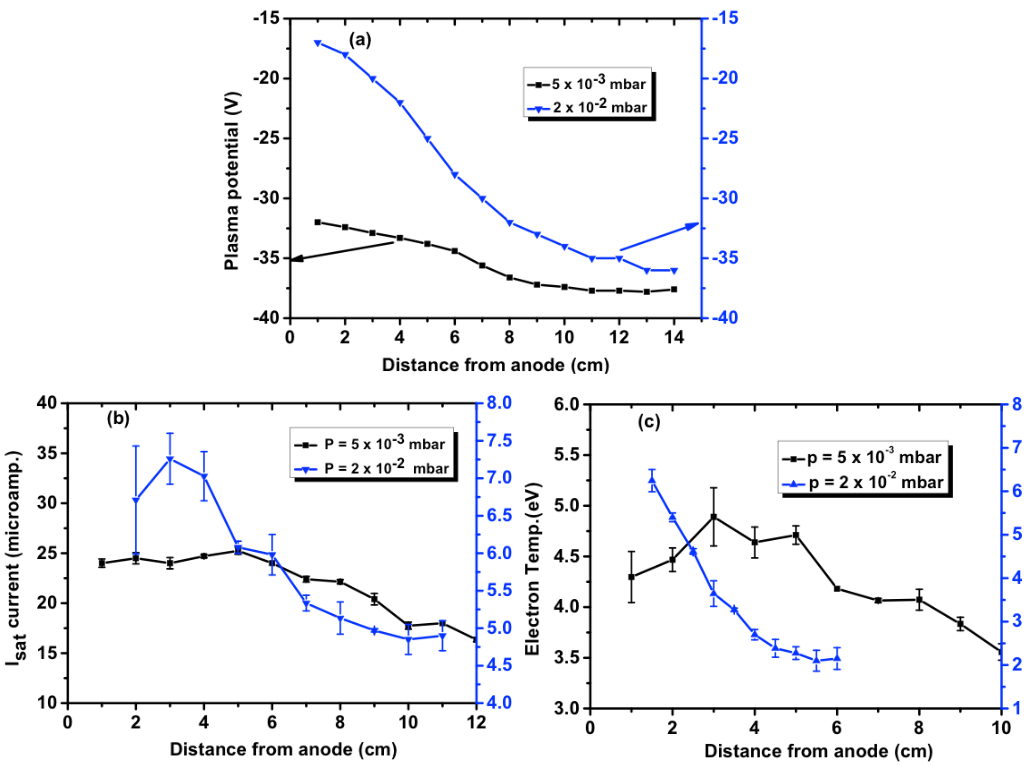

Figure 4.7: *Variation of (a) Plasma potential (b) Ion saturation current and (c) Electron temperature for* 5×10^{-3} *and* 2×10^{-2} *mbar pressures.*

4.2.3 Optical emission spectra of anode glow

The intensity of anode glow was observed to be higher than the surrounding background plasma. The emission of argon lines from this intense glow was measured by using optical emission spectrometer. The light collecting system was mounted on one of the radial port of the chamber such that the lens captures light coming from the anodic glow which is schematically shown in Fig. 4.8. The one end of optical fiber was connected to light collecting system while other end was connected to spectrometer. The argon spectra were collected at different operating pressures, magnetic fields and discharge voltages also. The Fig. 4.9 shows typical argon spectra at two different operating pressures and at constant voltage

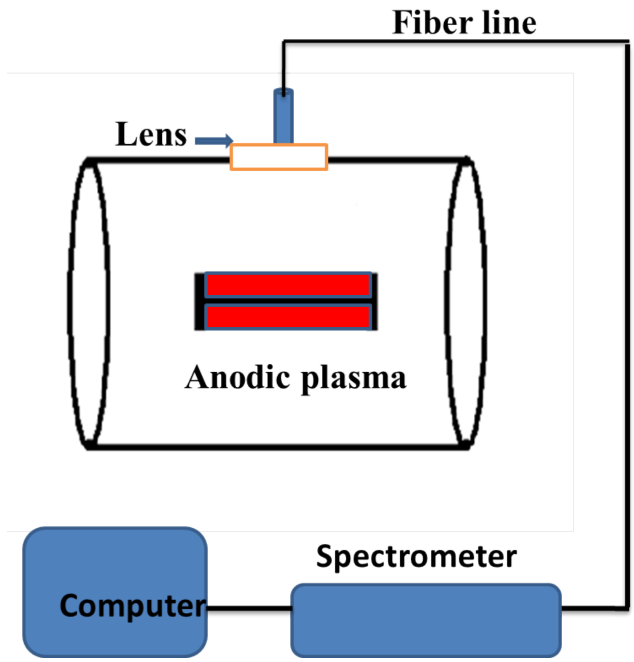

Figure 4.8: *Schematic of OES measurements.The optical fiber collects lights from one of the radial port of HCCM system.*

of 700 V and magnetic field of 100 $Gauss$. It is observed that the intensity of argon lines is more at higher operating pressure. The intense argon lines in the range of $650 - 950$ nm are identified from the spectrum acquired at pressure i.e 3.6×10^{-3} $mbar$. The Fig. 4.10 shows the intense argon lines of the spectrum. The observed intense lines are due to the strong emissions from excited argon atoms (ArI). These optical emissions come mainly from depopulation of the $4P$ levels via multiple $4P$–$4S$ transitions. The most prominent argon atomic transitions were observed at 811.53 nm and 750.38 nm. Certain argon spectral lines like 750.38 nm and 751.46 nm, 800.61 nm and 801.47 nm, 810.36 nm and 811.53 nm were very close to each other.

Fig. 4.11 shows energy level diagram with the transition levels of the intense lines observed in the spectrum [83]. The electron configuration of the ground state argon atom is $1S^2 2S^2 2P^6 3S^2 3P^6$. The observed intense lines are due to the transitions of electrons between first two excited level configurations of argon atoms [83]. The first excited level configuration i.e 4S contains 4 levels i.e $1S_2$,

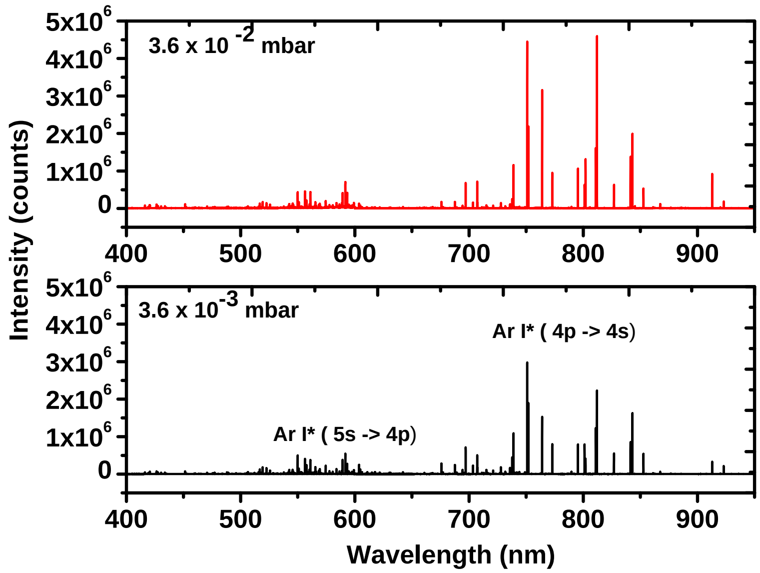

Figure 4.9: *Typical Argon Spectra recorded at two pressures of* 3.6×10^{-3} *and* 3.6×10^{-2} *for constant voltage of* $700V$ *and magnetic field of* 100 *Gauss.*

$1S_3$, $1S_4$ and $1S_5$ with $J = 1$, 0, 1 and 2 respectively. Next excited level i.e 4P configuration has 10 levels which are labelled as $2P_1$, $2P_2$, $2P_3$–,–$2P_{10}$. Transitions from the 2P levels to the 1S levels are the only dipole allowed radiative decay channels of the 2P levels [83]. The optical transitions from the $1S_5$ (J=2) and $1S_3$ (J=0) into the ground state (J =0) are dipole forbidden. Hence these two levels are metastable levels. The others resonance levels $1S_2$ (J=1) and $1S_4$ (J=1) decay optically into ground state. However re-absorption of the resonance photons by nearby atoms in ground state level leads to re-population of $1S_2$ and $1S_4$ levels which results in increasing effective life time of these states. Due to the longer life times, the population of atoms in metastable and resonance levels is more. The strongest emission is observed at 750.39 nm and 811.53 nm. The argon 750 nm line is sensitive to the high energy electron portion of the electron energy distribution function (EEDF) and the production of the 811.53 nm is sensitive to low energy electrons [84]. In addition, the argon 750.39 nm ($2P_1$ to $1S_2$) and 811.53 nm ($2P_9$ to $1S_5$) are generally selected to monitor $1S_5$ metastable fraction. The metastables can become an importnat source of ionisation if the metastable density is high enough. Considerable increase in ionisation occurs via the excited

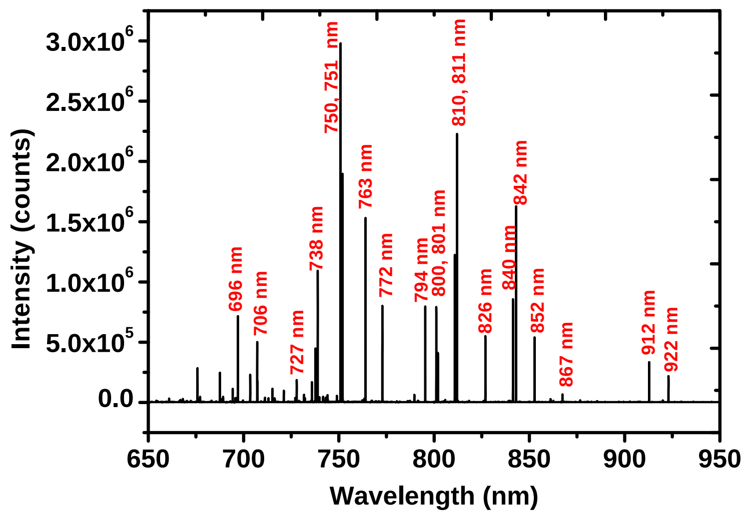

Figure 4.10: *Intense Argon lines in the range of* 650 *nm to* 950 *nm observed at* 3.6×10^{-3}.

levels, especially the 4P levels. Therefore, the intensities of these two lines i.e 750.39 nm and 811.53 nm were measured at increasing discharge voltages and magnetic fields. The Fig. 4.12 shows intensity variation with discharge voltage at fixed operating pressures of 3.6×10^{-2} $mbar$ and magnetic field of 100 $Gauss$. Similarly Fig. 4.13 shows intensity variation with magnetic field at fixed discharge voltage of 700 V. It is observed that the intensity of these lines increases with discharge voltage as well as magnetic field. The argon 750 nm is created by direct electron excitation from the ground level and could be a good representative of the ion density in the plasma [84, 85]. Hence increase in intensity of 750 nm line with voltage and magnetic field can be attributed to the enhanced ionisation near the anode due to the energetic electrons near the anode. The role of argon metastable ionisation in the near anode plasma can be studied in future.

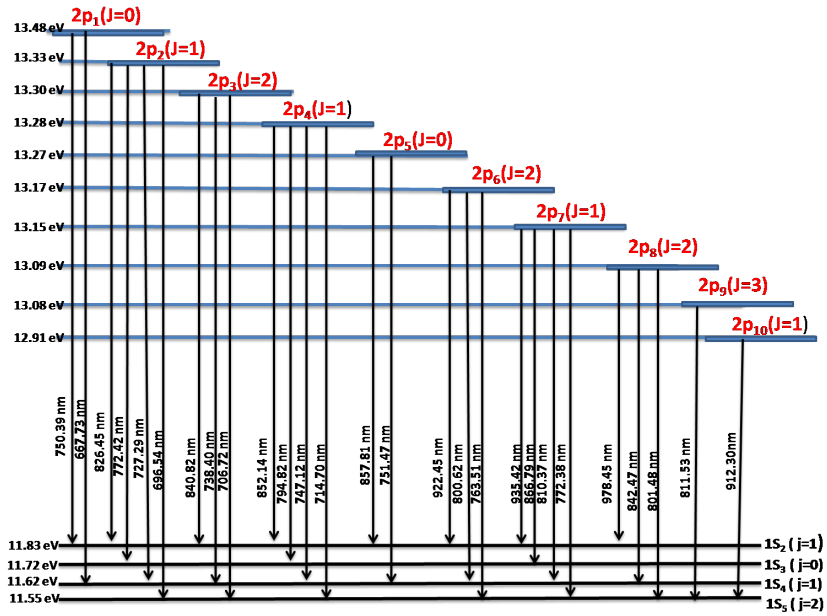

Figure 4.11: *Energy level diagram of argon showing 2P to 1S transitions. The shown energies levels are relative to the ground state of argon atom.*

4.3 Qualitative theoretical explanation of the phenomenon near the anode

The potential profiles obtained in the experiments indicates the cathode fall (shown in Fig. 4.1) as well as a significant anode fall (shown in Fig. 4.7(a)) in presence of transverse magnetic field. To understand this type of cross field discharges, the non-local electron kinetics in inhomogeneous electric field was studied in past with the help of Boltzmann kinetic equation for the distribution function of electrons [65, 86]. The theoretical approach to solve Boltzmann equation for cylindrical magentron in both post and hollow cathode cylindrical configurations was discussed by Golubovskii et al. [65].

By using Boltzmann kinetic equation, Golubovskii *et al.* determined the electron distribution functions with the help of appropriate boundary conditions [65, 86]. In their work the electron distribution funcation (EDF) was calculated using measured potential profiles. The discharge conditions like operating pressure, magnetic field strengths as well as magentron configuration in the present set of

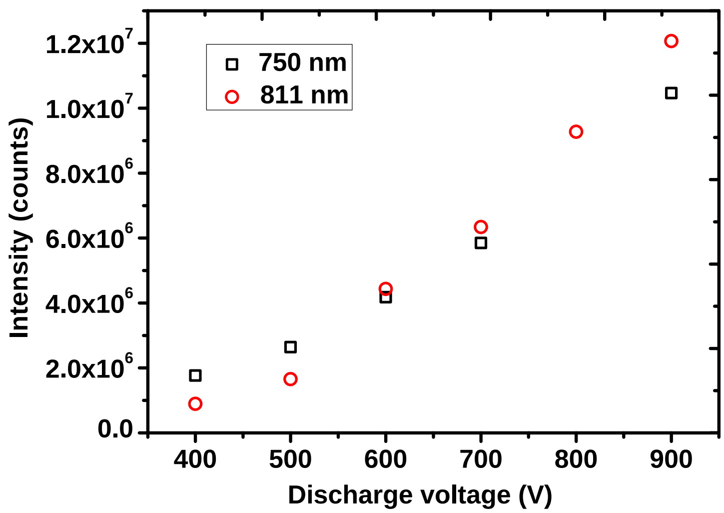

Figure 4.12: *Intensity variation with discharge voltage of Ar 750 and Ar 811 lines. The operating pressures was kept as* 3.6×10^{-2} *mbar and magnetic field as* 100 *Gauss.*

experiments were similar to the work carried out by Golubovskii et al.[65]. A notable anode fall of $\sim 40 - 50$ V has also been observed in our experiments which is similar to their results. Therefore, based on the analysis of EDF carried out by Golubovskii et al., our experimental findings are explained as follows. The potential profile and hence the radial electric field in the discharge column essentially influences the electron density and their energies. Near the cathode region, formation of energetic electrons takes place due to a strong electric field. This electric field $\sim 300 - 500$ V/cm comes from the strong cathode fall as shown in Fig. 4.1. These fast electrons then enter into the positive column from the cathode fall and lose their energy due to frequent inelastic collisions, which leads to depletion of energy of electrons. Furthermore, a strong electric field in the anode fall accelerates the electrons near the anode region. As a result the population of energetic electrons get enhanced in the anode region. In case of sufficient electric field in the anode region, the electrons accelerate toward the anode and electron impact ionisation/excitation takes place. Our experimental observation of higher ion saturation current and electron temperature (shown in Fig. 4.7(b) and 4.7(c))

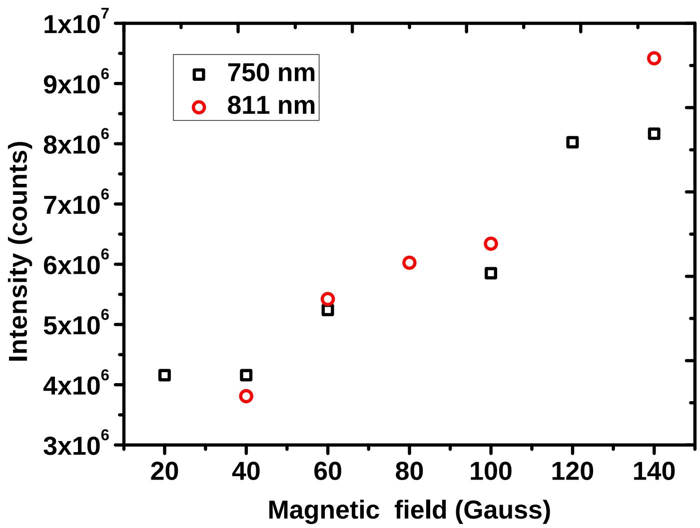

Figure 4.13: *Intensity variation with magnetic field for Ar750 and Ar811 lines. The operating pressures was kept as* 3.6×10^{-2} *mbar and discharge voltage as* $700\ V$.

near the anode compared to positive column region is similar to the theoretical prediction in case of hollow cathode or inverted cylindrical magnetron discharge [65].

4.4 Summary

The effect of magnetic field on the plasma propeties near the anode has been studied. The strong anode fall was observed in presence of magnetic field of around $5-10\ Gauss$. The plasma potential measurement shows that the bulk plasma potential was below the near anode potential. The finite potential gradient observed in the positive column and near anode region in presence of magnetic field indicates an increase in electric field. This electric field distribution basically influences the macroscopic characteristics of the discharge especially in the anode region [65]. The formation of anode glow on the anode surface is observed due to the sufficient anode fall near the anode. The size of the anode glow increases with magnetic field. The ion density and electron temperature in the glow region was more as compared to rest of the background plasma. The light emission from the anode glow shows intense lines of argon in the wavelength range 700 nm to 950 nm. The anode glow/spot formation due to magnetic field in large hollow cathode cylindrical magnetron device can modify the film properties when the substrate is kept near the anode during deposition.

Even though the formation of anode glow or spot due to magnetic field has been studied in this chapter, it is necessary to study how the background plasma responds when the changes near the anode takes place. In order to study the systematic variation of anodic structure at different magnetic field a experimental set-up with modified cathode and anode geometry is used. The detailed study of anode sheath transition and its effect on bulk plasma parameters are reported in next chapter where the modified hollow cathode set up is used.

5

Response of the background plasma to anode glow formation

In Chapter 4, it is shown that the transverse magnetic field is responsible for anode glow formation in Hollow cathode cylindrical magnetron (HCCM) discharge. It was seen that, as soon as the transverse magnetic field is applied, the anode sheath turns into anode glow/spot. It was also noticed that, the discharge current slightly decreases before rising again during anode glow evolution indicating that the changes in the anode sheath may affect the background plasma. Hence it was necessary to study the influence of changes in anode structures on the global plasma parameters. In order to study this, modified hollow cathode discharge was used. The experimental set-up of modified hollow cathode discharge is already described in Chapter 2. The schematic of experimental set-up is again shown in Fig. 5.1. In case of HCCM, it was difficult to study the transition from ion sheath to electron sheath and anode glow. The reason for this being that as soon as the magnetic field was applied the anode glow was formed. It was therefore necessary to vary the magnetic field with fine resolution. Hence, the studies concerned with the effect of externally applied and precisely controlled magnetic field on the transition of anode sheath is taken up; and the results and observations are discussed/presented in this chapter. The response of the bulk plasma to this transition is studied by using a Langmuir probe and optical diagnostics.

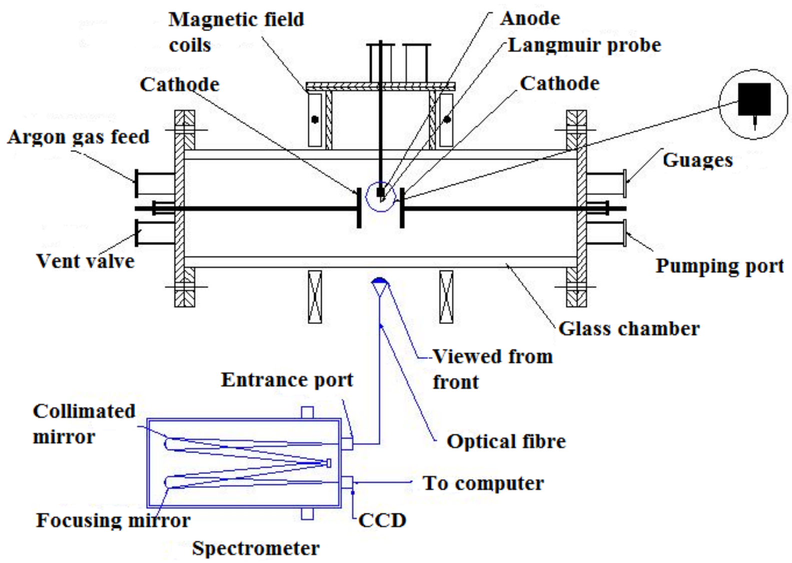

Figure 5.1: *Schematic of the modified hollow cathode Penning discharge. It shows cubical anode at the center. The spectrometer is used measure the emissions of argon lines from the plasma.*

5.1 Experimental observations

The distance between two cathodes was fixed at 40 mm while the cubical anode is mounted at the center. In order to carry out the experiments, the chamber was initially evacuated to a base pressure of 5×10^{-5} $mbar$ by using a combination of rotary and diffusion pumps. Then the argon gas was introduced in the chamber by using a gas dosing valve. The pressure was raised to an operating pressure of $5 - 8 \times 10^{-2}$ $mbar$. The plasma was formed by applying a DC voltage between the cathodes and the anode. Both the cathodes were kept at same potential while the anode was kept at ground potential. The magnetic field was varied by varying the current flowing through an electromagnetic coils wound over the experimental chamber. The experimental observations regarding the effect of magnetic field on different plasma parameters are discussed below.

5.1.1 Images of near anode plasma at different magnetic field strengths

Initially, it was tried to record the effect of change in magnetic field on the plasma near anode, by capturing digital photographs. As the chamber is small and made out of glass, it was easy to capture images. The images of the anode glow captured at various magnetic field values - at a consant discharge voltage of 500 V and an operating pressure of 8×10^{-2} $mbar$ are shown in Fig. 5.2. When the applied magnetic field strength was low (i.e in between 10 and 15 $Gauss$), there was no visible glow on the anode. This situation is indicating that the anode was able to collect the required electrons from the plasma while retarding the rest, which is a standard ion sheath case. When the magnetic field was increased to 20 $Gauss$, a faint glow near the anode starts appearing. Further increase in magnetic field upto 25 $Gauss$, results in a clear formation of the anode spot. Increasing magnetic field further results in larger anode spot (fireball) that covers the surface of the anode and extends out in to the surrounding plasma. At magnetic field of 20 $Gauss$, the gyro radius of electrons is ~ 1 mm (at 1 eV temperature) and gyro radius of ion is around 50 mm (considering ions at room temperature). Though ions are not magnetized, at this magnetic field, electrons are fully magnetised. From the

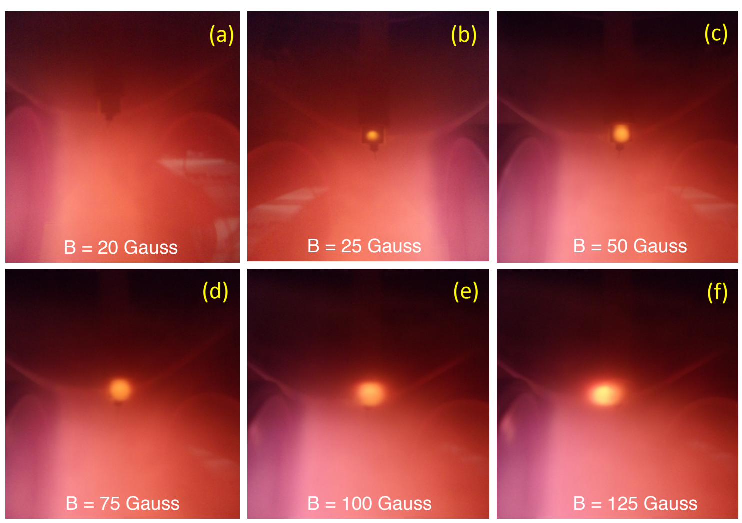

Figure 5.2: *Still images of the anode glow for different magnetic fields at discharge voltage of* 500 V *and background pressure of* 7×10^{-2} $mbar$.

work of other groups, as well as our studies presented in Chapter 4, it is clear that the formation of anode glow/spot is the result of the collisional ionization in the electron sheath [14, 40, 87]. Therefore, the electron sheath must be formed prior to the anode spot formation. In such case, the electrons are accelerated in the electron sheath. If the potential is high enough it will ionize the background gas, the electrons so produced are quickly absorbed by the anode, leaving behind the positive ion charge. Conde *et.al.*[40] have shown that if the collisions are frequent it will result in neutralization of negative space charge hence, forming the glowing fireball region. Such fireball is usually separated from the bulk plasma by a double layer having potential equal to the ionizing potential of the gas [14, 16, 34, 88]. In order to justify these visual observations of the anode sheath evolution the measurements of discharge current, plasma potential and plasma density measurements are carried out which are discussed below.

5.1.2 Discharge current response

The discharge current obtained at different discharge conditions is a very good indicator of plasma source behaviour. The discharge current was measured by measuring the voltage drop across the resistor kept in series of the main electrical circuit. Variation of the discharge current (I_d) with the externally applied magnetic field at a fixed operating pressure of 7×10^{-2} $mbar$ and discharge voltage of 500 V is shown in Fig. 5.3. Initially at low magnetic field values, the discharge current (I_d) shows an increasing linear trend (i.e. region I of Fig. 5.3) as magnetic field is increased. This increase in I_d is a result of better confinement and increased collisions due to cyclotron motion of electrons which increases overall electron and ion density inside the plasma. This nearly linear increase in I_d however stops at about 20 $Gauss$ and from thereon the trend reverses. The discharge current decreases with a further increase of magnetic field up to 25 $Gauss$ (region II, Fig. 5.3) before once again showing a positive trend (region III of Fig. 5.3). Region III of Fig. 5.3 shows localized glow known as anode spot (see Fig. 5.2).

The above transition between different regions was also studied at different discharge conditions. Fig. 5.4 shows the variation of discharge current at different operating pressures while the discharge voltage was kept constant. The critical magnetic field required to induce transition from one region to another is observed

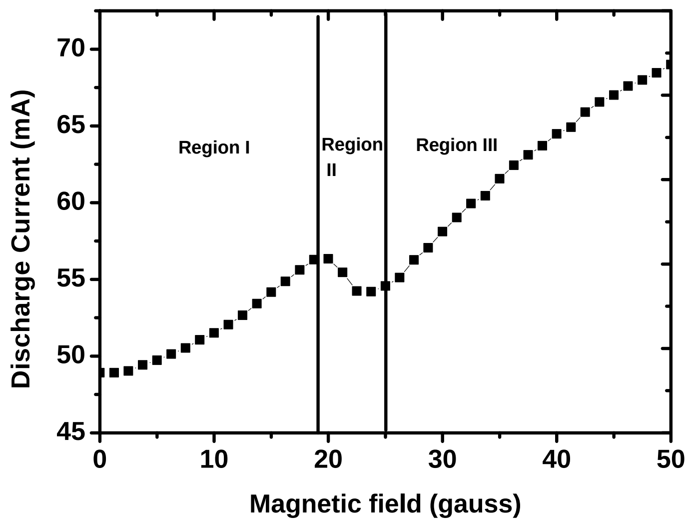

Figure 5.3: *The typical behaviour of the discharge current with increasing magnetic field.*

to increase with increasing operating pressure. This suggests that the ratio of electron neutral collision mean free path (λ_{en}) to the electron larmor radius (r_L) has an important role to play in the transition. Similarly, Fig. 5.5 shows the variation of the discharge current at different discharge voltages at a given operating pressure. In this case as well, it is observed that the critical magnetic field for transition increases with the increased applied voltages.

The increase in operating pressure as well as applied voltage results in higher electron-neutral collision frequency as well as the discharge current. The electrons will be magnetised sufficiently when electron cyclotron frequency is greater than the collision frequency. Hence it can be qualitatively said that the higher magnetic field is required for the transition from region I to region II with increasing operating pressure and discharge voltage. The above observed behaviour of discharge current should also reflect in plasma density and potential measurements. In order to confirm this fact, plasma potential and plasma density responses were also studied.

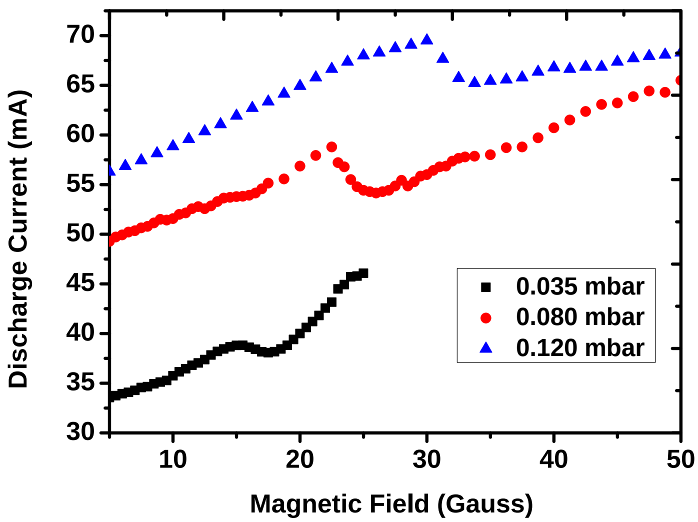

Figure 5.4: *Discharge current with increasing magnetic field for different background pressures at constant discharge voltage of 500 V.*

5.1.3 Plasma potential response

In order to measure the plasma potential and floating potential, a Langmuir probe was placed near the anode at 10 mm distance from the anode surface. The probe bias voltage at which the second derivative of probe current becomes zero is considered as plasma potential whereas, the floating potential is a potential at which the net flux of electrons and ions at the probe becomes equal and hence net current collected by the probe becomes zero. The plasma potential and floating potentials were measured at different externally applied magnetic field values while the discharge voltage was maintained constant. The results are shown in Fig. 5.6. It is observed that in region I i.e. upto the magnetic field of 20 $Gauss$, the plasma potential is few volts positive ($\sim$ 2 V) with reference to the anode potential. The plasma potential and floating potential remain almost constant till the magnetic field value reaches up to 20 $Gauss$. When the magnetic field was increased beyond 20 $Gauss$, the plasma potential is observed to systematically decrease initially (region II) and becoming constant again (region III) when the magnetic field was very high. These observations can be explained as follows.

Plasma potential of bulk plasma (measured with respect to the anode) indicates

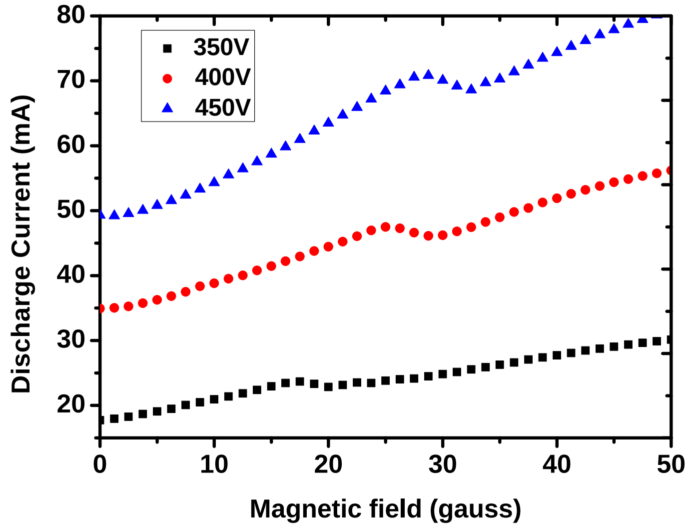

Figure 5.5: *Discharge current with increasing magnetic field for different discharge voltages at constant pressure of* 9×10^{-2} *mbar.*

the type of sheath formed at the anode surface. In case of a typical ion sheath, the anode (or any other electrode) is negative with respect to the plasma potential. This is the case in the region I of Fig. 5.6. Ion sheath is generally formed as a result of imbalance between discharge current and electron flux reaching the anode from the plasma. In simplest case it can be argued that the ion sheath forms when the thermal electron flux (J_e) at anode is larger than the discharge current (I_d), i.e. $AJ_e > I_d$, where A is area of the anode. Similarly, when $AJ_e < I_d$ is satisfied the electron sheath appears at the anode. In such cases the plasma potential becomes negative with respect to the anode (or any other electrode). This situation arises in region II and III of Fig. 5.6. Interestingly the potential difference between the anode and the plasma is 14 V which is close to the ionization potential of the argon. This observation has been verified by repeating the experiment by replacing argon gas with helium. In this case the potential difference was measured as $\sim$ 24 V which is again close to the ionisation potenial of helium gas. It has been reported numerous times that during the fireball formation at the anode, the potential difference between the anode and the plasma is always close to the ionization potential of the gas used for the discharge [14, 16, 34, 88]. The visual

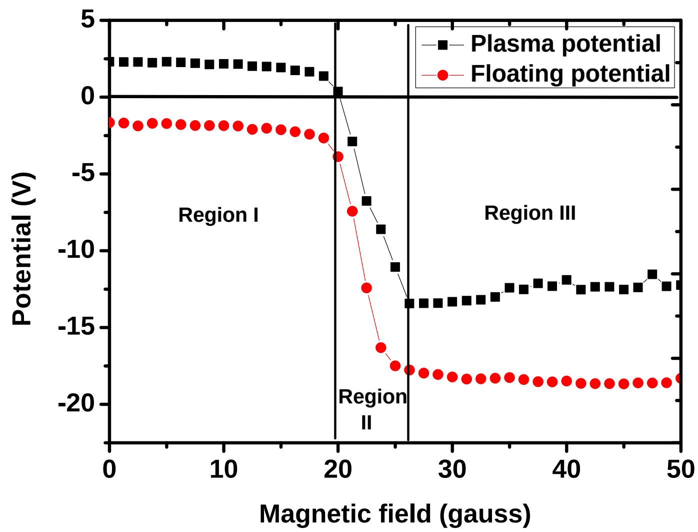

Figure 5.6: *Variation of plasma potential and floating potential in the bulk plasma with increasing magnetic field at constant voltage of 500 V and pressure* 7×10^{-2} *mbar.*

observation, when the applied magnetic field is beyond 25 *Gauss*, confirms the presence of a localized bright anode spot or fireball. Formation of this anode fireball is basically due to the ionization caused by electrons which got accelerated in the electron sheath. Therefore the formation of electron sheath is a pre-requisite for the presence of anode fireball. Putting everything in order, it can be summarized that, the discharge current increases with the increase in external magnetic field, up to certain value, and then start decreasing over the range of few Gauss during which period, the potential profile suggest the evolution of the electron sheath from the existing ion sheath. Finally, the fireball appears at the anode and it enhances the effective electron collection area of the anode and hence the current starts to increase once again. Therefore the increase in discharge current is due to the combined effect of increased ionization and increased electron collection area.

To understand the role of magnetic field in the transition from ion sheath to electron sheath, we can evoke the model used by Baalrud *et.al.*[14]. The criterion for formation of particular type of sheath as discussed above can be written in more useful way as the ratio of the surface areas collecting electrons and ions respectively.

This is because the particle flux to any surface is a function of the local density and temperature of that particle. Building upon this fact, Baalrud *et.al.* have concluded that the ion sheath will form when the ratio $A_e/A_i > 1.7\sqrt{2.3m_e/m_i}$, where A_e and A_i are electron and ion collection area, respectively and m_e and m_i are electron and ion masses respectively. For electron sheath formation, the condition turns out to be $A_e/A_i < \sqrt{2.3m_e/m_i}$.

In absence of the magnetic field the whole cube of the anode collects the current. And hence, the area of full anode has to be considered. In this case the area ratio (A_e/A_i) is 17×10^{-3} which is greater than that required for ion sheath formation and hence an ion sheath would form. Now, applying the external magnetic field results in a better confinement of the electrons in the plasma, thereby reducing the electron loss to the walls and accordingly the discharge current increases initially. However once the electrons are sufficiently magnetized they follow the field lines and miss the anode except for the two side faces where the magnetic field lines penetrate the anode. This effectively reduces the area of the anode to 128 mm^2 and the ratio of electrode surface areas reduces to 8×10^{-3} which satisfies the criterion for the formation of electron sheath. Hence the experimental observation can be explained by the reasoning that with the increasing magnetic field the effective electron collecting area reduces thereby reducing the electron current [89].

5.1.4 Electron temperature and plasma density

The changes in the background plasma density and electron temperature were measured using a single Langmuir probe. Fig. 5.7 shows the variation of plasma density and electron temperature with externally applied magnetic field values at a constant discharge voltage of 500 V and background pressure of 7×10^{-2} $mbar$. It is observed that the electron temperature increases in region II and III. The increase in electron temperature due to the presence of electron sheath has been reported earlier [13]. It can be explained as follows. At the low values of externally applied magnetic field i.e in region I, the electron sheath is absent and the plasma is bound by ion sheath on every surface. By nature, ion sheaths have negative potential with respect to the plasma. This structure, therefore reflects electrons back into the plasma and only those electrons which have sufficient energy to overcome the barrier are lost to the walls. Hence, the high energy electrons are selectively removed from the system and this results in over population of low energy electrons in the plasma leading to lower electron temperature. In regions II and III, however, the electron sheath replaces the ion sheath at the plasma anode interface and therefore all of the electrons can be lost to it irrespective of their energy. Further, the electron loss in the radial direction is greatly reduced because of the externally applied magnetic field. This mitigates the effects that existed in region I, leading to increased temperature due to better confinement of electrons. Fig. 5.7 shows reduction in plasma density when electron sheath forms near the

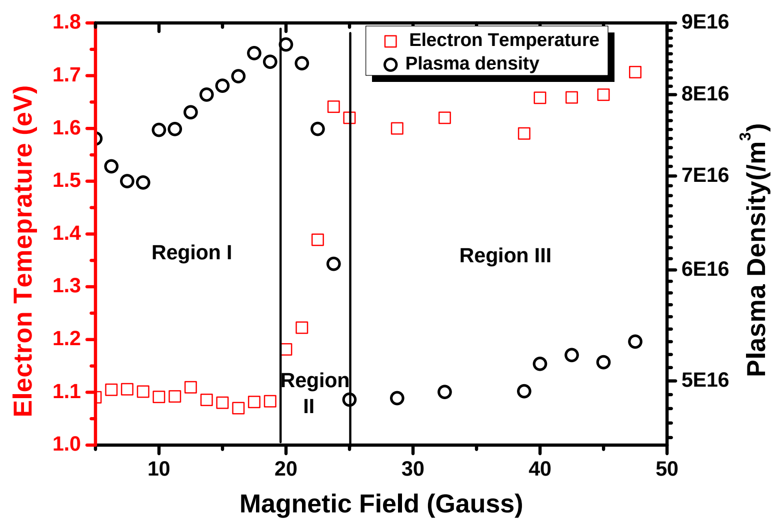

Figure 5.7: *Variation of bulk plasma density and electron temperature with increasing magnetic field.*

anode. As soon as electron sheath formation takes place, the electrons from the background plasma gets drained to the anode. There is a severe electron loss to the anode. Hence the bulk plasma density decreases. Similar type of plasma density reduction in response to the electron sheath formation on the positively biased plate has been observed [42] earlier. The steady increase in plasma density in region III can be attributed to increased ionization in anode spot and better confinement by the magnetic field. The electron Larmor radius of 1 eV electrons at the external magnetic fields of 20 and 40 $Gauss$ are calculated to be 1.2 and 0.6 mm respectively; which are much smaller than typical electron - argon mean free path of 10 mm at 10^{-2} mbar. Though the physical distance between the two cathodes and the cathodes and anode are 40 mm and 20 mm respectively; considering the cathode sheath (of around 5 mm size), the effective distances are only 30 mm and 15 mm respectively. However, still these distances are very much higher than the above mentioned Larmor radii and hence, the confinement effect can be well observed at the applied magnetic field of $20 - 40$ $Gauss$.

Langmuir probe measurements of plasma parameters, in presence of external magnetic field could sometimes be erroneous. Proximity of the probe to the anode may also affect the results to some extent. Therefore, it may be advisable to verify the observations using an independent non-invasive diagnostics. Hence Optical Emission Spectroscopy (OES) of the discharge was also carried out to complement the results obtained with the probe. The results of OES are described in the following section.

5.1.5 OES and photodiode measurement during sheath transition

In the present set of experiments, optical emissions were collected at side-on locations (perpendicular to discharge axis) using a light collection system. The optical probe has Plano convex lens (diameter: 50 mm and focal length of 150 mm) assembled in a small tube with a SMA (Sub Miniature version A) termination for connecting a 0.6 mm silica fiber (numerical aperture : 0.22). In the experiment reported here the light collection system was placed such that it collects the radiations from the bulk plasma only. The spectra were recorded with a 0.5 meter imaging spectrograph (Acton research corp., USA) having a 1200 l/mm grating and equipped with a CCD (Charge Coupled Device) detector(Princeton instruments, USA). All the recordings were obtained by setting entrance slit at 50 micron for which the achievable wavelength resolution is $\sim$ 0.05 nanometer. The argon spectra (400 nm to 900 nm) were obtained at an applied voltage of 500 V and a background pressure of $6-9\times10^{-2}$ $mbar$ for a range of magnetic fields varied from 0 to 50 $Gauss$. The example spectra is shown in the Fig. 5.8. Intense neutral argon lines (Ar I) as well as ionic argon lines (Ar II) are observed. Apart from this, spectral lines corresponding to the excited neutral hydrogen atoms is also observed. As the operating pressure is very low, assuming that the argon atoms are excited

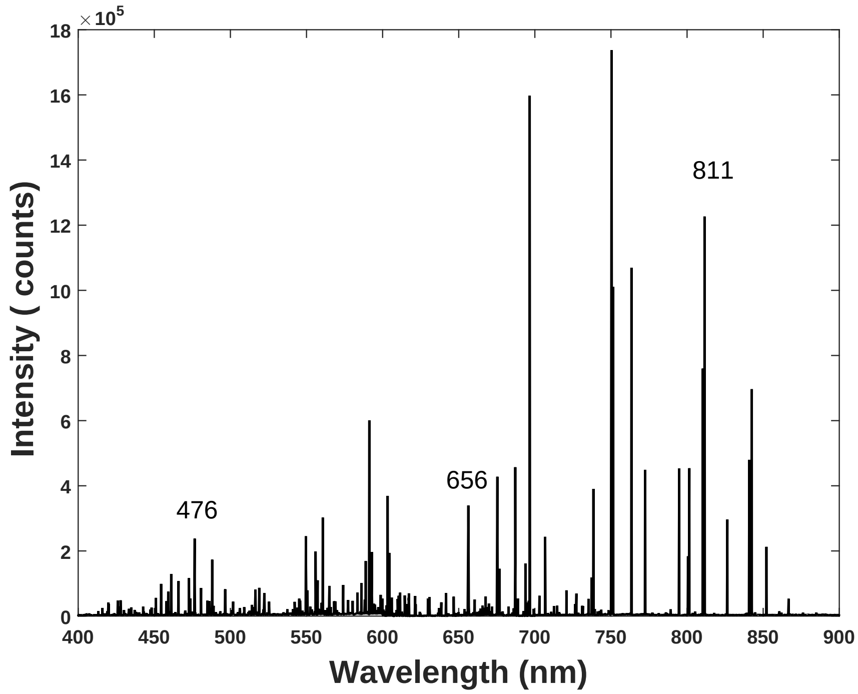

Figure 5.8: *Typical Argon spectra showing Ar*II, H* and Ar*I emission lines.*

by electron impact excitation and decayed radiatively by spontaneous decay, it can be shown that the observed intensity and hence the density of excited neutrals depends on plasma density and very weakly influenced by plasma temperature via reaction rate [90]. In such a case, observed intensity of the spectral lines should decrease in region II of Fig. 5.7. For this purpose, the intensity of spectral lines of excited neutral argon lines(Ar I: 811 nm, transition $3p^5(^2P_{3/2})4s - 3p^5(^2P_{3/2})4p$), ionic argon line (Ar II: 476 nm, transition $3s^2 3p^4(3_P)4s - 3s^2 3p^4(3_P)4p$) and also the Balmer alpha line(H I: 656.3 nm, transition $2p - 3d$) are chosen and the intensity variation with applied magnetic field is plotted in Fig. 5.9.

It can be observed that the intensity of spectral lines from all three different species i.e (Ar*I, Ar*II and H*), increase initially in region I and decrease in region II and again start to rise in region III confirming the observations shown in earlier sections.

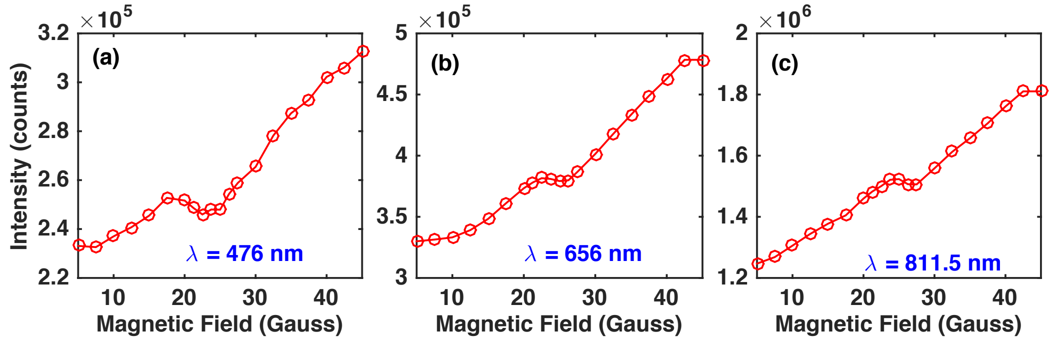

Figure 5.9: *Line Intensity variation of (a)* 476 *nm Argon II line (b)* 656 *nm Hydrogen I line and (c)* 811.5 *nm Argon I line with increasing magnetic field.*

5.1.6 Spatio temporal measurements of plasma parameters

As discussed in previous sections, the various plasma parameters like plasma potential, plasma density, electron temperature as well as intensity of emission lines get influenced during the anode sheath transition from ion sheath to electron sheath. However, the temporal variation of these parameters, as shown in Fig. 5.10, with magnetic field during this transition give more insight of the phenomenon taking place in the discharge. In order to capture the transition phenomenon, the fast variation of magnetic field from 75 $Gauss$ to 0 $Gauss$ in 100 ms (as shown in Fig. 5.10(a)) was carried out by suddenly switching off the current passing through the electromagnetic coil meant for producing the external magnetic field. The discharge current (shown in Fig. 5.10(b)), ion saturation current (shown in Fig. 5.10(c)), floating potential (shown in Fig. 5.10(d)) as well as intensity of spectral lines (shown in Fig. 5.10(e)) were measured simultaneously during the magnetic field variation at a fixed discharge voltage of 600 V and operating pressure of 9×10^{-2} $mbar$. The high speed silicon photo diode (DET 10A) was used to detect the integrated light signal of the emitted argon spectral lines. The spectral response of this diode is good enough to capture the light in the required wavelength range of $600 - 850$ nm in which intense argon spectral lines were recorded using spectrometer as shown in Fig. 5.8. The ion saturation current and floating potential were measured using a single Langmuir probe and the results essentially indicate the variation of plasma density and plasma potential, respectively.

It is clear from the Fig. 5.10, that the discharge current, ion saturation current

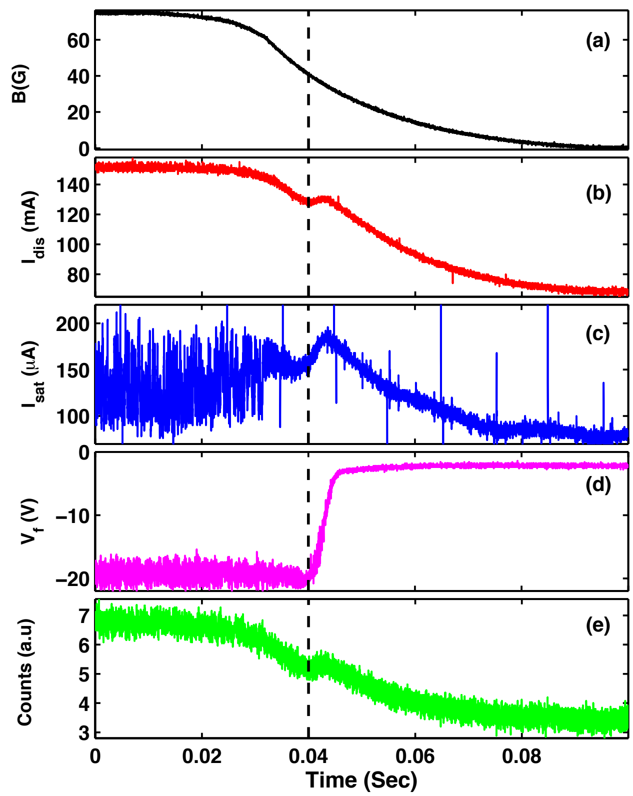

Figure 5.10: *The real time signal of (a) Magnetic field (b) Discharge current (c)Ion saturation current (d)Floating potential and (e) Intensity of light at 600 V and pressure* 9×10^{-2} *mbar.*

as well as intensity of emitted spectral lines shows similar behaviour during the decay of magnetic field from 75 *Gauss* to 0 *Gauss*. Even though the magnetic field is continuously decreasing, at a critical magnetic field of $\sim$ 40 *Gauss*, all these three parameters increases initially and then decreases at the same time when the transition from electron sheath to ion sheath takes place. At a given set of discharge parameters, the discharge current and the ion saturation current are the direct measure of plasma density. The population of excited species of argon neutrals in the plasma and hence intensity of emitted argon lines depends on the plasma density [90]. Therefore, it can be concluded that with the decrease of magnetic field, the plasma density decreases and hence all these parameters like discharge current, ion saturation current and the line intensity follow the same trend of magnetic field except at the time when the transition takes place. It

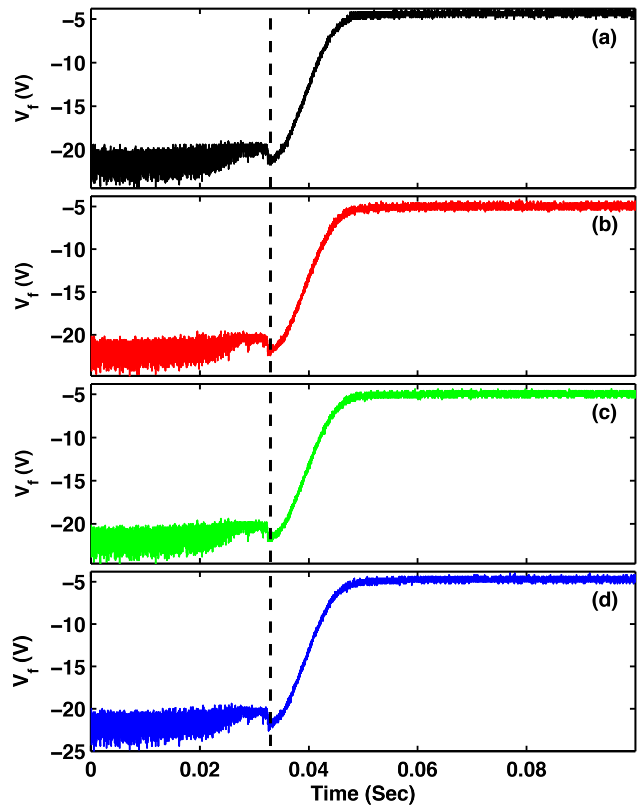

Figure 5.11: *The real time signal of floating Langmuir probes at distance of (a) 10 mm (b) 15 mm (c) 20 mm and (d) 25 mm from the anode during the magnetic field variation.*

is also worth to mention that during the transition of electron sheath to the ion sheath, the spectral line intensity momentarily increases due to the increase of plasma density which essentially follows the same trend of ion saturation current and the discharge current. The signal of the high speed photo diode measurements showed qualitatively similar behaviour to that of argon emission lines as measured by the spectrometer. During the transition the floating potential suddenly jumps from a higher negative value to a smaller negative value, which was otherwise a fixed value in the electron sheath region. All these findings are in line with the steady state measurement of plasma parameters that were discussed in previous sections.

In order to study the spatial variation of this response in the plasma, the floating potential was measured simultaneously at four different places using four identical Langmuir probes which we placed at a distance of 5 *mm* from each other. These probes were mounted below the anode in a direction perpendicular to the magnetic field. Fig. 5.11 shows that all the four probes show the same behaviour of floating potential during the magnetic field variations. These measurement results essentially confirm that the spatial variation in the response of plasma parameters during sheath transition is insignificant.

5.1.7 Theoretical explanation for the electron flux near the anode

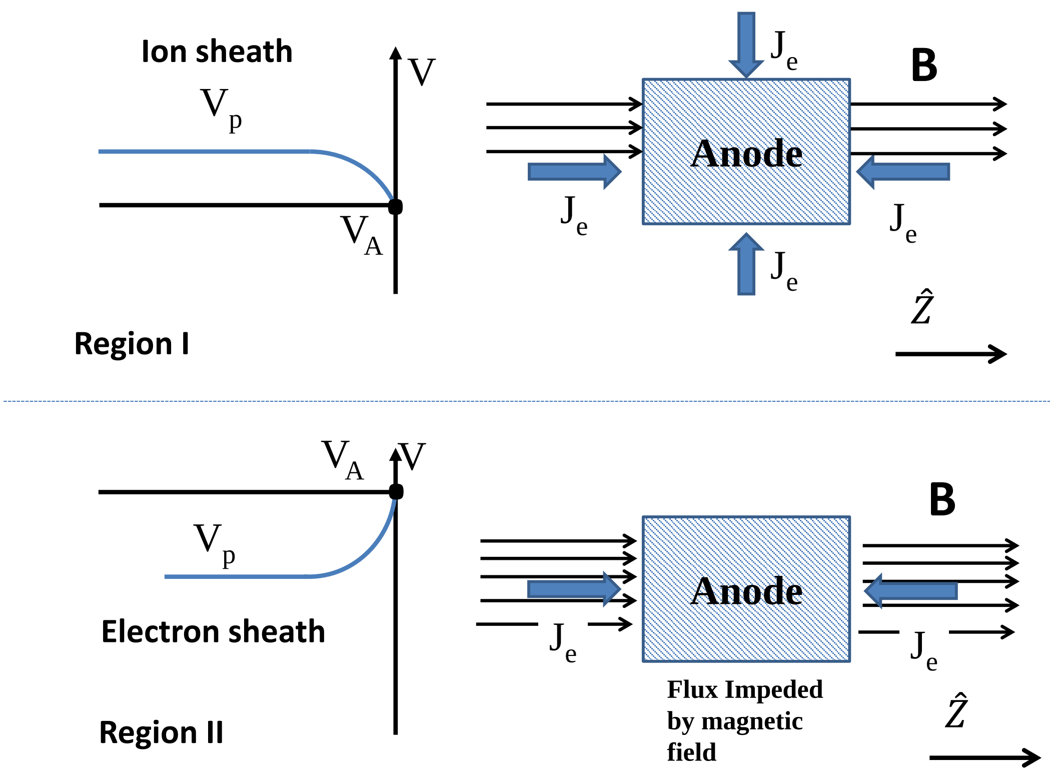

Figure 5.12: *Schematic representation of the perpendicular and parallel electron fluxes entering to the anode sheath.The region I represents low magnetic field where electron sheath is not formed while region II represents electron sheath formation in high magnetic field (i.e.greater than 20 Gauss).*

A schematic representation of the anode surface and particle flow in region I and region II is shown in Fig. 5.12. The particle i.e electron flow or flux is parallel to the magnetic field for two surfaces of the anode while it is perpendicular to the magnetic field for remaining surfaces. In a weakly ionised plasma, the diffusion coefficients for particle flow parallel and perpendicular to the magnetic field are expressed as.

$$D_{\parallel} = \frac{kT_e}{m\nu_c} \tag{5.1}$$

$$D_{\perp} = \frac{D_{\parallel}}{1 + \omega^2/\nu_c^2} \tag{5.2}$$

where $D_{\perp}$ and $D_{\parallel}$ are the perpendicular and parallel diffusion coefficients. m is the mass of electron, kT_e is electron temperature. The $\omega = eB/m$ is electron cyclotron frequency while ν_c is electron neutral collision frequency. The electron flux normal to the field lines is governed by the expression

$$\frac{J}{e} = -D_{\perp}\frac{\partial n}{\partial z} \tag{5.3}$$

In the region I, the electron flux reaching to the anode from all the sides is not disturbed. Thus the thermal electron flux to the anode would carry a current much greater than discharge current. In fact considering the full anode area, the thermal electron current $\sim 100\ mA$ calculated from measured plasma density $\sim 10^{16}\ m^{-3}$ and electron temperature $\sim\ 1\ eV$ is higher than the discharge current $\sim 50\ mA$. Therefore the formation of electron retarding sheath is required to repel excessive electron flux to the anode so that global current continuity is maintained. However, in region II, the electron current reaching to the anode is impeded due to the transverse magnetic field. It is clear from equation 5.2 and equation 5.3 that the diffusion coefficient is going to decrease with the magnetic field and hence the electron current reaching to the anode. In our experimental parameter i.e magnetic field $20 - 50\ Gauss$ and pressure 10^{-2}-$10^{-1}\ mbar$, the ratio ω^2/ν_c^2 is in the range of 1 to 2. It is expected that the electron flux reaching to the anode should reduce considerably in region II. In other words it can be said that when the electron flow is blocked to some of the anode surface, the discharge current should close to the anode at the surface where the electron flow is parallel to the magnetic field.

However a total thermal electron current towards this surface is smaller than the discharge current. The additional electron flux is attracted towards the anode by the electron attracting sheath that appears at the surface. The discharge current closes to the anode via this electron sheath and additional ionisation in it.

5.1.8 Anode glow oscillations

In order to study the stability of discharge during the electron sheath formation, the temporal variation in floating potential was recorded. The Fig. 5.13 shows the time series of floating potential signal for different magnetic field values. It

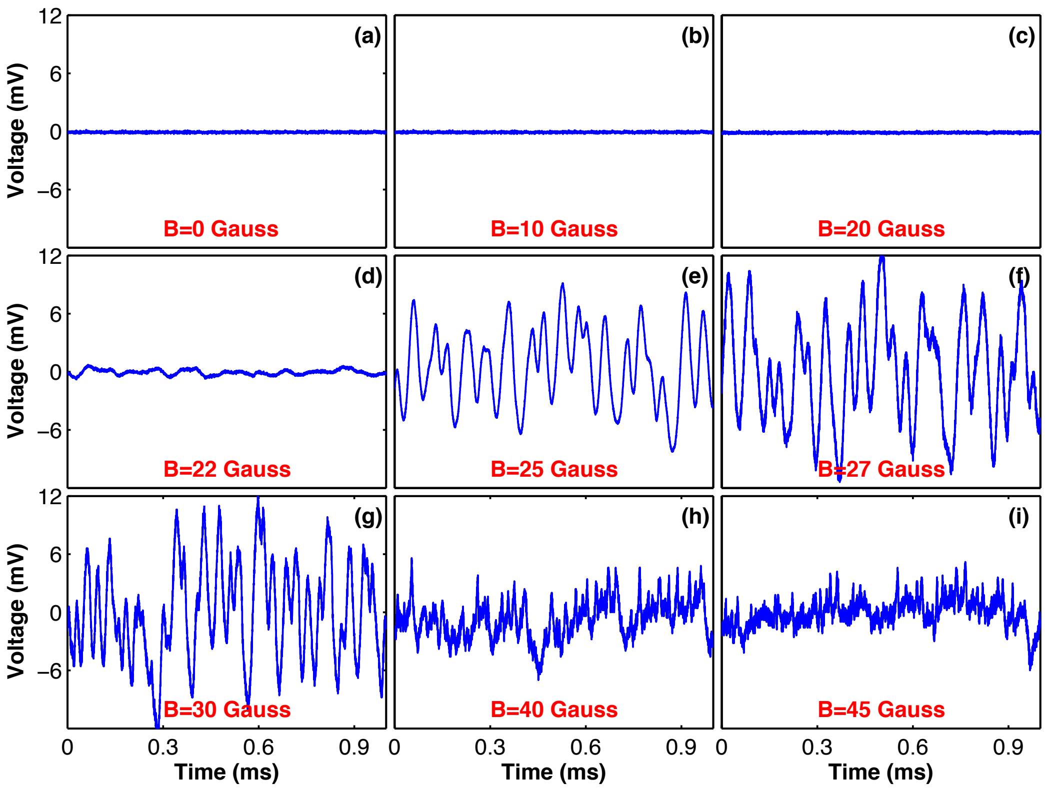

Figure 5.13: *Oscillations of floating potential observed at various magnetic fields.*

is clear from the figure that the discharge is stable upto 20 *Gauss* of applied magentic field and the floating potential signal does not show any fluctuations. However, as soon as the electron sheath formation takes place, the oscillations in the global discharge parameters like floating potential and discharge current are observed. The oscillation frequency is observed to be in the range of $5 - 20\ kHz$. The absence of oscillations in low or zero magnetic field and their appearance with the onset of electron sheath and fireball formation suggests its origin to be in the electron sheath and the ionization inside the sheath. This type of oscillations in the presence of anode spot are well reported [16, 91, 92] and is understood to be the result of repetitive formation and collapse of the double layer structure of the anode spot. The similar oscillations were also observed in the light intensity and ion saturation current when the electron sheath is converted into anode spot at higher magnetic field values. Fig. 5.14 shows the oscillations in light intensity and ion saturation current at a given magnetic field and discharge parameters. It is to be noted that the trend of the oscillations are similar in both the signals. This suggests that the repetitive growth and decay of the fireball is dependent upon the density replenishment from the background plasma.

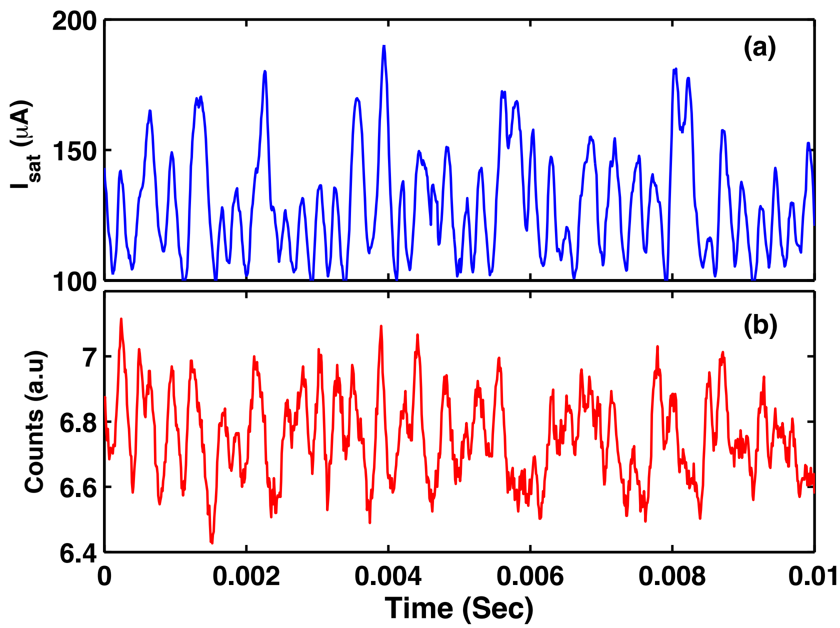

Figure 5.14: *The fluctuations in (a)Ion saturation current and (b) Light Intensity at magnetic field of 50 Gauss.*

5.2 Summary

Magnetic field is shown to induce the formation of the anode spot or fireball on the surface of the anode. This happens primarily due to restricted anode area. The discharge current and emission spectra shows similar behaviour validating the arguments. Measured plasma potential clearly shows that upon increasing magnetic field the anode remains below the plasma potential initially suggesting an ion sheath. However, upon further increase of the magnetic field, the anode potential drops below the plasma potential by about the same value as the ionization potential of the background gas, suggesting formation of anode spot or fireball at the anode surface. The transition can be understood as the result of a restricted electron flow to the anode, which rises the anode potential leading to the formation of electron sheath and eventually to anode spot or fireball. Observed trend of plasma density and electron temperature in the transition region is the result of the location of the formation of the anode spot, which changes local plasma parameters. The anode spot is observed to induce global oscillations in plasma parameters as reported previously by others.

The effect of magnetic field on such type of oscillations has to be studied. In next chapter anode glow is created at low discharge current where the ionisation is produced only near the anode. The experimental results of the effect of externally applied magnetic field on these oscillations are reported in next chapter.

6

Effect of magnetic field on anode glow oscillations

In Chapter 5, the transition from the ion sheath to the electron sheath due to externally applied magnetic field is reported. It is shown that when the electron current to the anode of a discharge is decreased due to the magnetic field, the extra ionisation takes place near the anode so that global current balance is maintained. This suggests that whenever the anode current is not sufficient to balance the global current, the plasma condition near the anode changes. It is known that for fixed anode area, the discharge current and hence the anode current decreases with the reduction in discharge voltage. Therefore it is expected that ionisation should take place near the anode at low discharge voltages also where the discharge current is low. At these voltages, due to very low current, the anode glow will form to maintain the discharge. In past, the low current anode glow mode of DC discharges have been studied experimentally [93]. The sudden transition and associated hysteresis phenomena in discharge current-voltage characteristics has been reported earlier [94–96]. The low frequency oscillations were also observed in the low current region [94–96]. This self-oscillations in the low current regime of thermionic discharges were well explained by Greiner *et al.*[97–99] using nonlinear dynamics, whereas the effect of different discharge parameters on these self-oscillation was later investigated by Ding *et al.*[100]. In another simulation [101] study, three different modes i.e. anode glow mode (AGM), temperature limited mode (TLM) and double layer mode (DLM) have been discussed in electron beam driven collisional plasmas. Therefore the experimental study regarding the formation of such oscillating anode glow at low discharge current and effect of magnetic field on the oscillations was carried out. The anodic plasma was formed at very low curent by controlling the discharge voltage. The transition from stable high current mode to oscillating low current anode glow mode was observed. It is shown that, the nature of oscillations changes from periodic to chaotic at higher magnetic field. The experiments were carried out in modified hollow cathode discharge. In this case a ring anode was used instead of cubical anode. The reason for changing the shape of anode is to create the anode glow in a region where electric and magnetic field are perpendicular to each other in the anode ring. A ring shaped grounded anode (100 mm outer diameter, 95 mm inner diameter and 5 mm thickness) was placed symmetrically in between the parallel plate cathodes. This type of DC plasma source with a ring anode and axial magentic field was also explored as high density plasma source when operated at higher discharge currents [22, 102, 103].

6.1 Experimental results

The experiments were carried out in a modified hollow cathode set-up with ring shaped anode. The schematic of the experimental set-up is shown in Fig. 6.1. The distance between two cathodes was fixed at 40 mm while the anode was kept at the center. The argon plasma was formed between two planar cathodes and ring shaped anode. Initially, at fixed operating pressures, the discharge voltage at which the transition to unstable anode glow takes place was identified. Then the externally applied magnetic field was varied to study the nature of oscillation observed in the floating potential measured by Langmuir probe. The cylindrical Langmuir probe was mounted near the anode ring.

6.1.1 Effect of magnetic field on breakdown voltage

Initially the effect of magnetic field on breakdown voltage was studied in order to ascertain the pressure range in which the magnetic field influences the discharge properties in this electrode configuration. For this present set of experiments, the inter-cathode distance was kept around 40 mm and the anode was placed at an

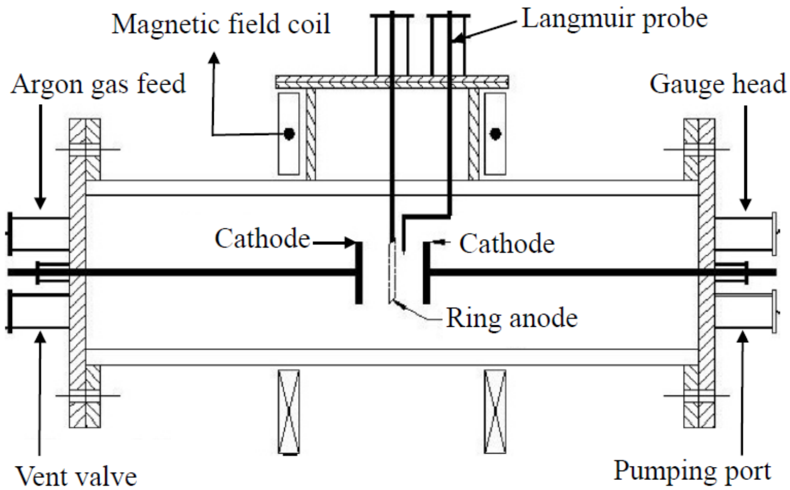

Figure 6.1: *Schematic of the experimental set-up showing ring anode in between the two cathodes.*

equal distance in between two cathodes. The breakdown voltage was measured over a wide range of argon gas pressures (from 0.045 mbar to 4.0 mbar) in absence and presence of external magnetic field of 100 Gauss as shown in Fig. 6.2. It is clear from the figure that at a lower pressure (less than 0.25 mbar), the magnetic field helps the gas to breakdown at lower voltages. On the other hand, magnetic field has no role on the breakdown voltage if the gas pressure becomes higher than 0.50 mbar.

In presence of magnetic field, the residence time of the electrons increases, as a result the lateral diffusion of the electrons reduces and leads to a lower breakdown voltage. The electron-neutral collision frequency at higher pressure regime (0.5 GHz at 0.5 mbar) exceeds the electron gyration frequency (i.e. 280 MHz at 100 Gauss) and hence the electrons remain un-magnetised. It manifests to an insignificant difference in breakdown voltage curves in presence and absence of magnetic field as shown in fig. 6.2. However, below 0.25 mbar pressure, electron gyration frequency becomes comparable or more than the electron-neutral collision frequency and the effect of magnetic field become significant. Hence in this

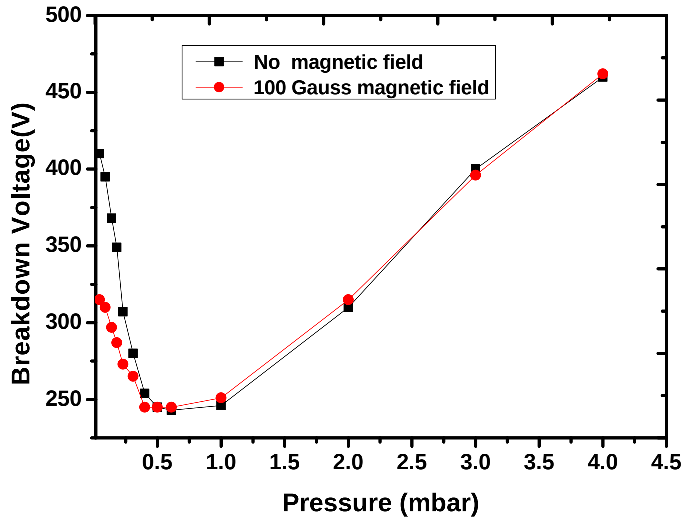

Figure 6.2: *Variation of breakdown voltages with background pressure in absence and presence of magnetic field.*

experimental set-up the operating pressure of less than 0.25 mbar was selected to study effect of magnetic field on anode glow oscillations.

6.1.2 Current mode transition

The current-voltage ($I_d - V_d$) characteristics were measured where the discharge current was very low ($\sim$ few mA). Fig. 6.3 shows $I_d - V_d$ characteristics at two operating pressures (0.10 and 0.15 $mbar$) in absence of external magnetic field. With the increase of discharge voltage, sudden transition to high current mode (HCM) is observed (see point 'c' in Fig. 6.3). However, while decreasing the discharge voltage, the sudden transition back to low current mode (LCM) happens at comparatively lower discharge voltage (see point 'e' in Fig. 6.3), which looks like a hysteresis loop. In addition, floating potential is seen to fluctuate at LCM regime of the hysteresis loop (region between 'b' and 'c' of Fig. 6.3). It is also observed that at low pressure, the voltage required for this transition in discharge current is more. This transition and corresponding hysteresis in the discharge current can be explained as follows:

The LCM is seen when the plasma is concentarted near the anode of a DC glow

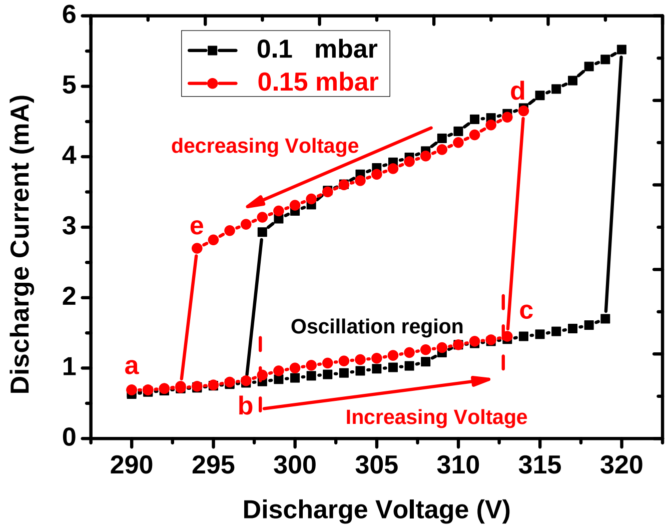

Figure 6.3: *Discharge current (I_d) voltage (V_d) characteristics for two pressures of 0.10 mbar and 0.15 mbar.*

discharge. The anode glow/spot occurs when the current to the anode becomes too small to maintain the discharge. This small amount of current can be attributed due to the smaller size of anode or/and due to the restriction of electrons reaching to anode due to magentic field. The ionization process begins near the anode by frequent collisions of electrons with neutrals [16]. In LCM, ionization takes place mainly near the anode where the energy of the accelerated electrons is higher than the ionization energy of the argon gas atoms. The ions generated in this process rush towards the cathode. If number of ions created by ionization in anode glow region are smaller than that of ions flowing towards the cathode, the LCM state sustains (see a–c in Fig. 6.3). As ion production exceeds, positive charge density in the anode glow region increases. Due to lower mobility of ions, positive potential also increases near the anode, which attracts more electrons from the cathode and leads to more ionization. As a result, anode glow region grows and expands towards cathode. This cascade effect brings a sudden transition (c–d transition) to HCM from LCM regime. The reverse transition from HCM to LCM (point ‘e’ in fig. 6.3) normally takes place at much lower discharge voltage. This leads to a hysteresis loop as shown in Fig. 6.3. The figure essentially signifies that

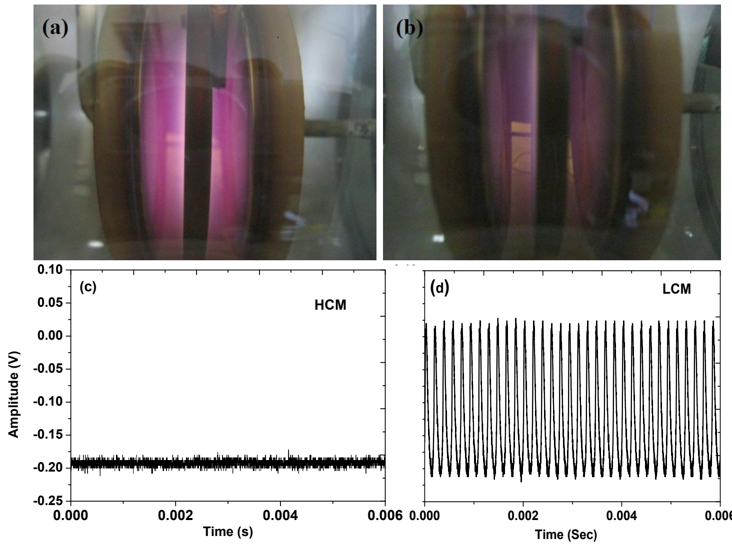

Figure 6.4: *Typical glow and floating potential signals (a) & (c) in HCM and (b) & (d) in LCM regimes, respectively.*

the ionization volume during HCM is much larger than that of LCM. Transition from HCM to LCM occurs only if the ion loss rate overcomes the ion production rate. The discharge is sustained in high current mode due to the continuous ion bombardment on the cathode surface and subsequently secondary electron emission from the cathode. The electrons get accelerated in the cathode sheath and takes part into the ionization process. However in LCM mode, the secondary electron emission reduces from the cathode surface due to low ionization rate. In the case of HCM, the glow covers both the electrodes whereas for LCM the glow confines near the anode ring with low intensity. Fig. 6.4(a) shows the typical glow for HCM while Fig. 6.4(b) shows the same for LCM. Similarly, Fig 6.4(c) shows the floating potential in HCM and Fig 6.4(d) shows the floating potential oscillation in LCM. The oscillations are also observed in the ion saturation region of the Langmuir probe characteristics when the transition to LCM takes place.

The ionization phenomenon near the anode changes the local electric field configuration. The electrons generated near the anode are lost easily to the anode while massive ions create a positive space charge region. The generation and collapse of space charge leads to the oscillating behaviour of plasma parameters.

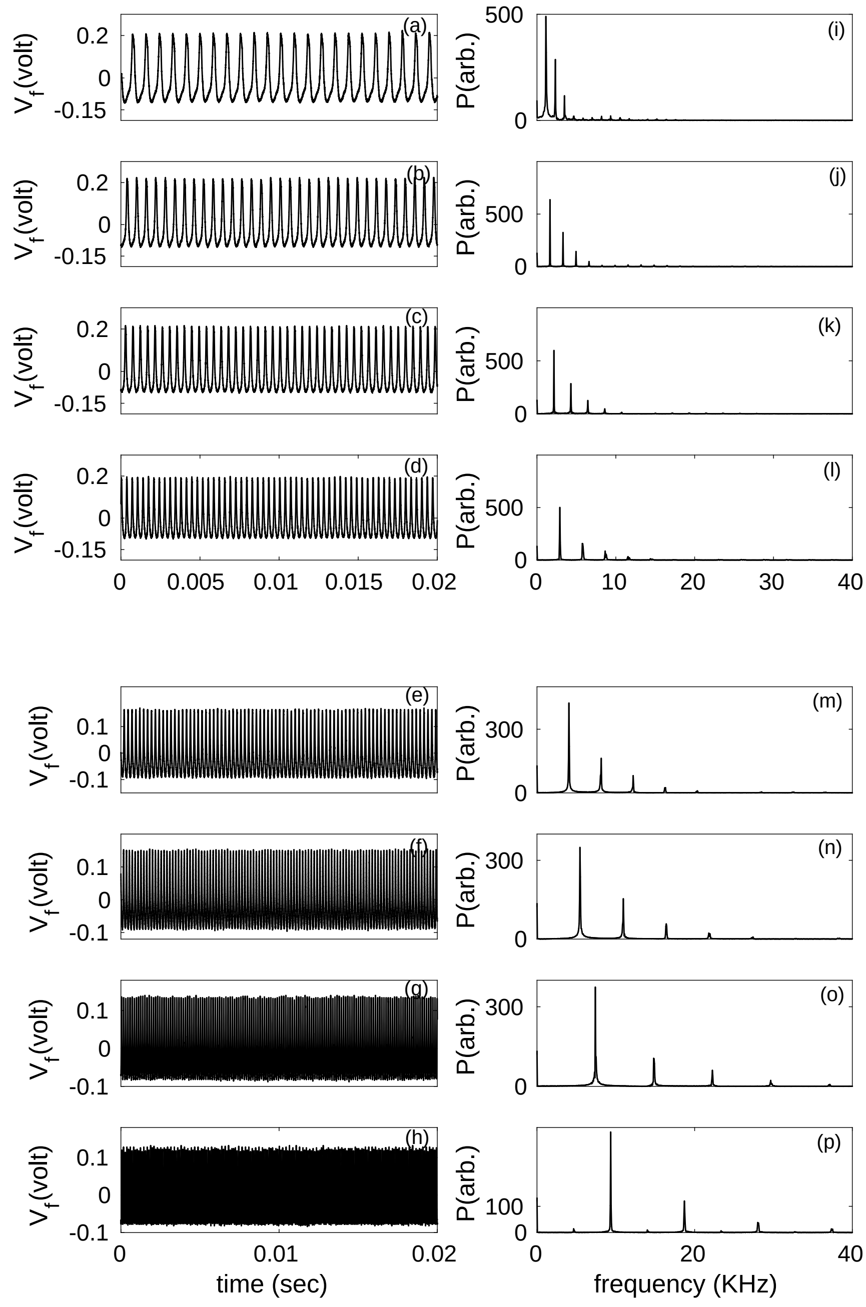

Figure 6.5: *Floating potential oscillations (a–h) and their FFTs (i–p) for different magnetic fields: (a) & (i) 10 Gauss, (b) & (j) 20 Gauss, (c) & (k) 30 Gauss, (d) & (l) 40 Gauss, (e) & (m) 50 Gauss, (f) & (n) 60 Gauss, (g) & (o) 70 Gauss and (h) & (p) 80 Gauss.*

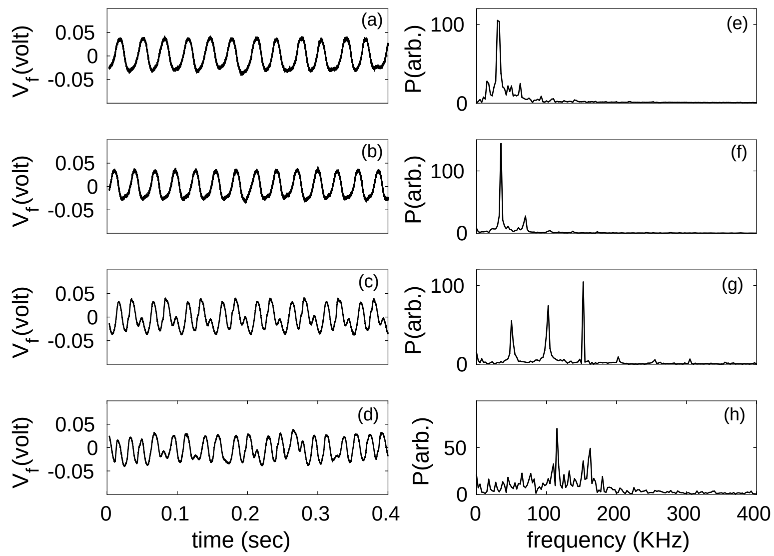

Figure 6.6: *Floating potential oscillations (a–d) and their FFTs (e–h) for different magnetic fields: (a) & (e) 100 Gauss, (b) & (f) 107.5 Gauss, (c) & (g) 112.5 Gauss, and (d) & (h) 120 Gauss.*

6.1.3 Effect of magnetic field on the floating potential oscillations in LCM

As mentioned above, the floating potential and discharge current oscillates when the discharge current transits to LCM. In the present set of experiments, the effect of external magnetic field on these oscillations was investigated over a wide range of magnetic fields. The discharge current (0.95 mA) was kept in LCM by adjusting the discharge voltage at 295 V and background pressure at 0.15 $mbar$. The axial magnetic field was then varied from 10 to 120 $Gauss$ in step of 2.5 $Gauss$. The time series of floating potential oscillations (FPO) measured by Langmuir probe at different magnetic fields were stored in the oscilloscope for further analysis with the help of MATLAB. The floating potential oscillations observed in our experiments are composed of an AC components (∼few mV) with a DC level of ∼few volts. Fig. 6.5(a)–(h) depicts the AC component of the FPOs, whereas Fig. 6.5(i)–(p) represents the corresponding Fast Fourier Transform(FFT) plots, when the magnetic field is increased from 10 to 80 $Gauss$. Similar to Fig. 6.5,

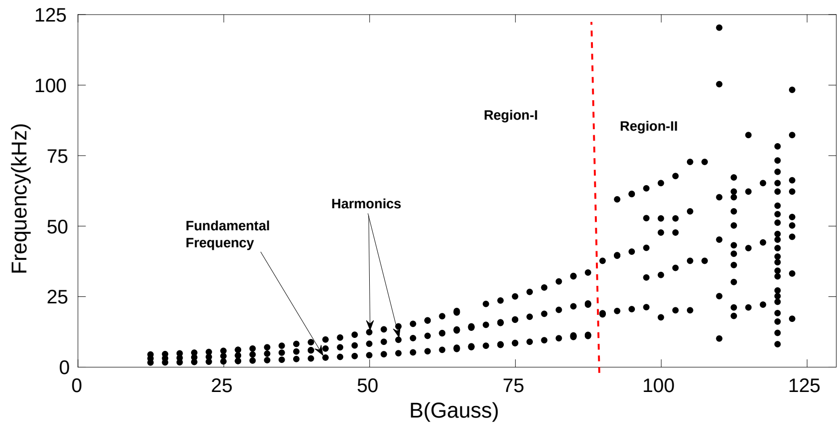

Figure 6.7: *Dominant frequencies obtained from FFT plots for different magnetic fields.*

Fig. 6.6(a)–(d) shows FPOs, and corresponding FFT plots are given in Fig. 6.6(e)–(h) for the increased values of magnetic field from 100 to 120 *Gauss*. At 10 *Gauss* of magnetic field, the floating potential oscillates at very low frequency ∼1.0 kHz. With increasing magnetic field (see Fig. 6.5(i)–(p)) up to 80 *Gauss*, the frequency of oscillation increases upto 10 kHz. At 100 − 120 *Gauss*, oscillations become abruptly chaotic as shown in Figs. 6.6(a)–(d). It is also observed in FFT analysis (see Fig. 6.6(e)–(h) that the dominant peaks are accompanied by smaller peaks which essentially suggest the broadband nature in frequency spectrum indicating the chaotic behaviour in the floating potential oscillation. It infers that the time series gradually changes from periodic to chaotic in nature with increasing magnetic field.

Fig. 6.7 shows the fundamental frequency obtained from the power spectrum as a function of magnetic field. To plot this figure, those frequencies were only considered whose amplitudes were atleast more than 10% of the maximum amplitude of FFT spectrum. Fig. 6.7 clearly shows two regions. In region-I, for a magnetic field below ~ 90 *Gauss*, distinct peaks of fundamental and their harmonics are observed. For an example at 12.5 *Gauss*, the fundamental frequency of oscillations observed is $f \sim 1.50$ kHz, with the first and second harmonics of 3 and 4.5 kHz. With further increasing in magnetic field up to ~ 90 *Gauss*, the frequency of oscillation is found to increase linearly, which essentially signifies that

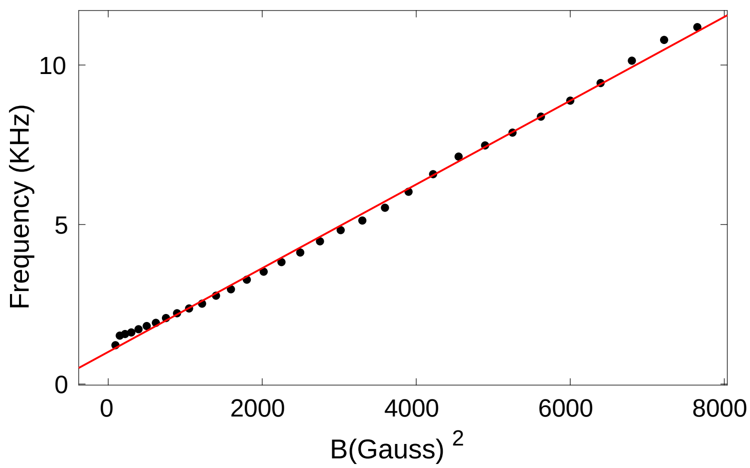

Figure 6.8: *Dependency of fundamental frequency in the periodic region on the magnetic field. Straight line showing best linear fit for region I of fig. 6.7.*

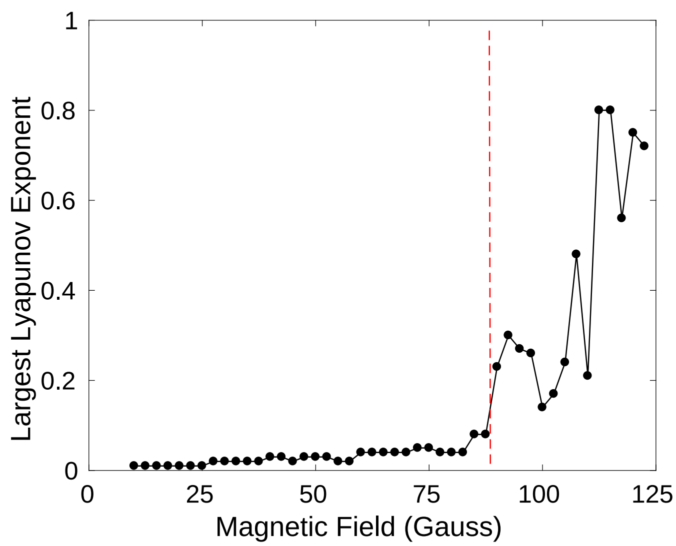

Figure 6.9: *Lyapunov exponent for different magnetic fields.*

the system exhibits periodic behaviour in Region-I. However, beyond 90 *Gauss*, a broadband of frequencies is observed as shown in Region-II. In this region, system shows a characteristic behaviour of chaotic oscillation. This frequency bifurcation diagram reveals the order to chaos transition behaviour of the system.

It is worth mentioning that the range of observed frequency ($1 - 15$ kHz) of periodic oscillations lies below the ion plasma frequency (∼500 kHz) for our discharge conditions. It has already been reported that the dominant frequency increases with the applied voltages in case of anode glow mode[101]. Interestingly in our experiments, we have observed the similar trend of frequency for increasing magnetic field. In the low discharge current mode, a localized anode glow/spot is observed in the anode ring, where the radial electric field is always perpendicular to axial magnetic field. As a result, the radial electron transport across the magnetic field decreases with the increase in magnetic field. The anode region becomes much dominated by the electron population, which helps to increase the anode fall voltage. Hence, the ion production in the anode sheath increases due to the increase in anode fall and therefore the frequency of oscillation increases. The rising part of the wavefront of Fig. 6.4(d) corresponds to the enhancement of ion space charge with time and then it decreases due to loss of ions. With further increase in magnetic field, the rates of creation of ion space charge region and ion loss increases, which results in the increase of oscillation frequency as shown in Fig. 6.7. When the magnetic field is increased beyond 90 *Gauss*, more localized spots appeared covering large area of anode surface as a result the nature of oscillations in the floating potential changes drastically and linear oscillation becomes nonlinear in nature. Fig. 6.8 shows the fundamental frequency is linearly dependent upon square of the magnetic field. The frequency of oscillations increases due to the reduction in anode current. The effective anode area for electron collection decreases with increasing magnetic field. Classically, the transverse electron flux reaching to the anode is dependent upon the square of the magnetic field. Hence the frequency shows linear dependence upon square of magnetic field till 90 *Gauss*.

6.1.3.1 Non-linear time series analysis

It is known from the nonlinear analysis of the oscillation, that the plasma exhibits quasiperiodic–chaotic–quasiperiodic transition, periodic oscillation to chaotic, pe-

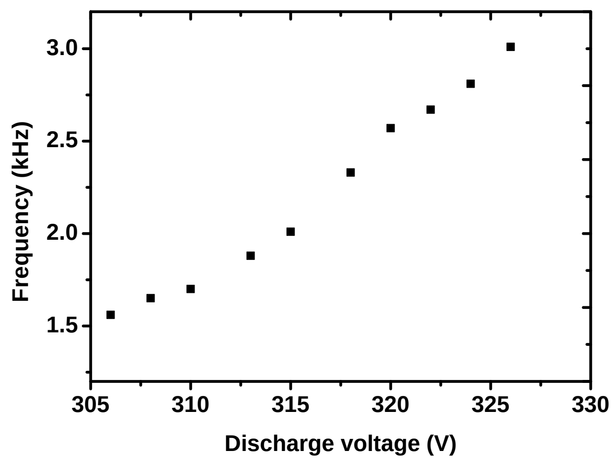

Figure 6.10: *Frequency variation with discharge voltage at constant magnetic field of 25 Gauss at pressure 0.1 mbar.*

riod doubling, period subtraction etc.[104–107]. Largest Lyapunov exponent estimation is a standard tool for confirmation of chaotic behaviour of a time series data or trajectory. Here, to understand the nature of oscillations, the oscillations of the floating potential are quantified using Largest Lyapunov Exponent (LLE)[108]. The algorithm of LLE are described elsewhere [109]. Chaotic dynamical systems are sensitive to initial conditions and exhibit the exponential divergence in the phase space. The divergence can be calculated by using Lyapunov Exponent (LE), which quantifies the nature of oscillations: positive LE indicates the presence of chaotic nature, whereas nearly equal to zero and negative LE values indicates the periodic and limit cycle nature respectively. Fig. 6.9 shows the largest Lyapunov exponent with increasing magnetic field. LLE plot in Fig. 6.9 shows that below 90 *Gauss*, the LLE is around zero which indicates periodic nature while higher value of LLE for higher magnetic fields indicates chaotic nature. A sudden jump in the LLE plot around 90 *Gauss* indicates a transition from order to chaos behaviour which is in the agreement with the frequency spectrum results. In addition to the earlier observations [110], it is seen in our experiments that the non-linear oscillations in plasma has also a dependency on external magnetic field.

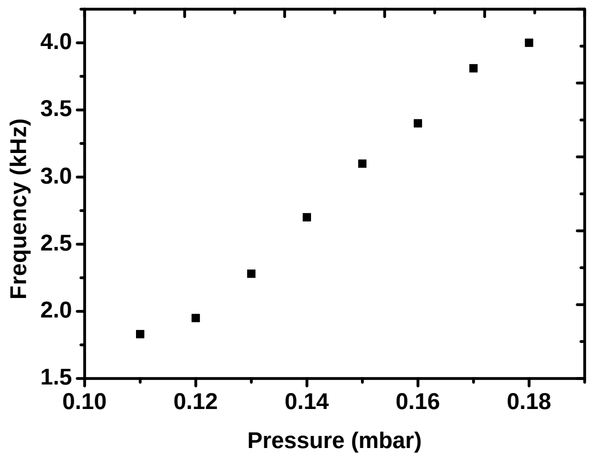

Figure 6.11: *Frequency variation with operating pressure at constant magnetic field of 25 Gauss and discharge voltage of 308 V.*

6.1.4 Effect of operating pressure and discharge voltage on anode glow oscillations in linear region

To further understand the insight of these oscillations, an attempt was made to measure the frequency of floating potential oscillations at different operating pressures and discharge voltages. Here the oscillation frequency was measured at constant magnetic field of 25 *Gauss*. The Fig. 6.10 and Fig. 6.11 show the typical variation of oscillation frequency with discharge voltage and background pressure. The frequency of oscillation with varying discharge voltage for constant magnetic field of 25 *Gauss* and argon gas pressure of 0.1 *mbar* is shown in Fig. 6.10. It shows that the oscillation frequency increases monotonically with discharge voltage. Similarly the frequency of oscillation with varying pressure and at constant magnetic field of 25 *Gauss* and discharge voltage of 308 V is shown in Fig. 6.11. Similar to the discharge voltage, the frequency increases with pressure. Increase in discharge voltage enhances the ion production rate in the anode sheath. Likewise, higher gas pressure causes increase of ion production in the anode sheath region by frequent electron-neutral collision. Thus the increase in discharge voltage and the gas pressure enhances ionisation near the anode which in turn gives higher oscillation frequency. It is also reported in past that the frequency of oscillation in dischrage current for anode glow mode increases with pressure and voltages [97–99]

6.2 Summary

A detailed study on the transition in discharge current mode is reported. The discharge current-voltage characteristic shows two stable regimes, a high discharge current regime and a low discharge current regime. The low current regime exhibits the characteristics similar to the anode glow mode, which shows self-oscillations in floating potential. The effect of external magnetic field, discharge voltage and operating pressure on the anode glow oscillation is studied. It is shown that the frequency of floating potential oscillations increases linearly with the voltage, pressure as well as magnetic field. The observed mode transition and oscillations is the effect of anode glow formation near the anode at low discharge current. The non-linear analysis of these oscillations shows that the periodic to chaotic transition occurs when the magnetic field is increased beyond a threshold value.

7

Conclusions and Future Scope

7.1 Conclusion

The different anode sheath structures are generally studied by using auxiliary electrode in the separately formed background plasma. In the present work, the evolution of anode sheath on the discharge electrode itself is reported. The anode regions of two types discharges i.e hollow cathode cylindrical magnetron and modified hollow cathode Penning discharge are studied. It is shown that the near anode phenomenon can be controlled using the magnetic field in this cross field discharges. The various sheath formation on the anode are demonstrated by controlling magnetic field. The nature and amount of voltage drops near the anode are dependent upon the transverse magnetic field. By varying the magnetic field the anode current is controlled. The transition from ion sheath to electron sheath and further to anode glow has been studied. The impact of this sheath transition on the global plasma parameter is studied by using Langmuir probe and Optical Emission Spectroscopy. The important findings from the thesis work are as following.

1. The B/P ratio plays an important role in the discharge parameters like breakdown properties, discharge current, potential profile etc of Hollow Cathode Cylindrical Magnetron. The transition from positive space charge (strong cathode fall) to negative space charge (strong anode fall) due to magnetic field is experimentally demonstrated. It also verifies previously reported theoretical prediction of transition at low pressure and high magnetic field. The anode fall results in

anode glow/spot formation near the anode.

2. The dimensions of the anode glow depends upon not only voltage and pressure but also on the magnetic field. The anode glow expands with magnetic field. The anode glow is separated from background plasma with a clear potential difference of 10-15 V. The plasma characterisation of the large anode glow confirmed that the plasma density is more near the anode as compared to background plasma.

3. The transition from electron repelling sheath to electron collecting sheath on the anode of modified hollow cathode discharge is demonstrated. The sheath formation is controlled by the magnetic field instead of anode bias. During the anode sheath transition from ion to electron sheath, the plasma density in the background plasma gets depleted while electron temperature increases. The decrease in the plasma density is also reflected in the emitted argon lines as well as total discharge current. However the discharge current as well as plasma density starts increasing again as soon as anode spot formation takes place. The anode spot again showed the oscillation in floating potential as well as discharge current.

4. The other type of anode glow at very low discharge current is also explored where the discharge voltage is less. This type of glow is unstable showing oscillations in floating potential. The frequency of oscillations increases with discharge voltage and pressure. The oscillation frequency of such anode glow is found to increase with magnetic field also. The nature of oscillation is periodic upto particular magnetic field. Beyond which the oscillations become chaotic in nature due to the multiple anode spot formation. The floating potential oscillations in the frequency range $1 - 100$ kHz are observed when the anode spot is formed. These oscillations are related to space charge formation and removal near the anode region.

7.2 Future Scope

7.2.1 Effect of anodic plasma on thin film deposition

The extra ionisation near the anode produces ions which enters into the background plasma. It will be interesting to study the effect of this additional plasma on the growth of thin film. We have performed some preliminary study for copper thin film deposition which shows changes in the morphology of the film. The Fig. 7.1 shows the SEM images of the copper thin film in presence and in absence of anodic glow. The detailed study regarding the effect of anode glow oscillations on the nano structure formation can be carried out in future.

7.2.2 Study of ion acoustic wave during the transition from electron sheath to anode spot

During electron sheath formation the stream of electrons enters into the anode region where plasma density decreases in bulk plasma. However, as soon as the anode spot formation starts, the plasma potential becomes slightly positive. The plasma density also starts increasing after anode spot formation. When the flux of ions suddenly enters into the background plasma, the propagation of ion acoustic wave is expected due to density perturbation. Hence it will be good idea to study the wave propagation during the anode sheath transition. The role of magnetic field on the dynamics of ion acoustic waves can also be investigated.

7.2.3 Effect of $E \times B$ rotation in the anode glow evolution

When the electric field and magnetic field are perpendicular to each other, the effect of $E \times B$ drift velocity can be studied. Even though the electric field near the anode is not sufficiently high, the $E \times B$ rotation will influence the electron dynamics during the anode glow formation.

7.2.4 High density plasma source by using modified hollow cathode discharge

The simple DC discharge with two cathodes and axial magnetic field can be explored as high density plasma source for study like microwave attenuation. As the metallic anode is very small in dimension the microwave attenuation due to metallic surface will be minimum. The high plasma density of the order of 10^{13} m^{-3} to 10^{14} m^{-3} can be achieved with dissipated power of few hundred watts. This source can also be modified for electron source in the fully developed anode spot condition.

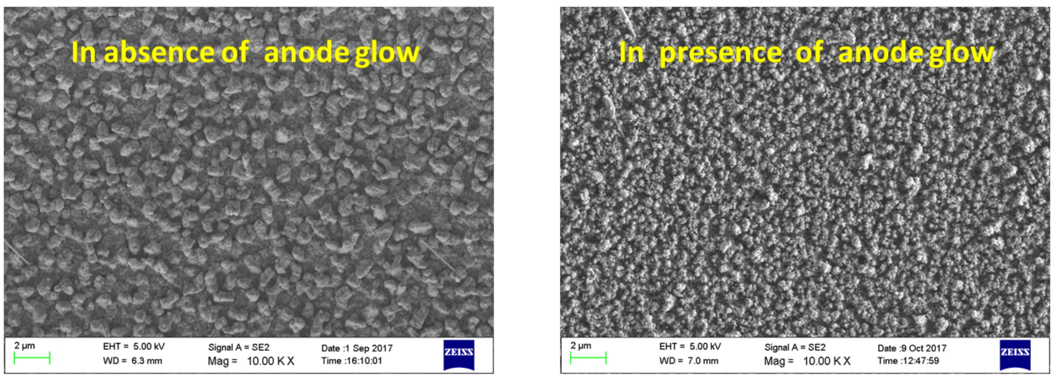

(a) (b)

Figure 7.1: *Scanning Electron Microscopy (SEM) image of copper thin film deposited by using hollow cathode. The Fig.(a)shows surface morphology for film in absence of anode glow and Fig.(b) shows for film in presence of anode glow*

Appendix

The practical formulas for obtaining various length scales and frequency are listed below. Units used for various quantities are as follow,
Plasma density n_e is in cm^{-3}, Electron temperature T_e is in eV, Magnetic field B_0 in $gauss$, Mass of Ion A_R in amu.

- Debye length

$$\lambda_d = 740\sqrt{\frac{T_e}{n_e}}\ cm \tag{7.1}$$

- Plasma frequency

$$\frac{\omega_p}{2\pi} = f = 9000\sqrt{n_e}\ Hz \tag{7.2}$$

- Electron Gyrofrequency

$$f_{ce} = \frac{\omega_{ce}}{2\pi} = 2.8B_0\ MHz \tag{7.3}$$

- Electron Gyroradius

$$r_{ce} = \frac{3.37\sqrt{E}}{B_0}\ \ cm\ \ (E\ \text{ is energy or temperature in eV}) \tag{7.4}$$

- Ion Gyrofrequency

$$f_{ci} = \frac{\omega_{ci}}{2\pi} = \frac{1.52B_0}{A_R}\ KHz \tag{7.5}$$

- Ion Gyroradius

$$r_{ci} = \frac{144\sqrt{EA_R}}{B_0}\ \ cm\ (E\ \text{ is energy or temperature in eV}) \tag{7.6}$$

Bibliography

[1] S N Abolmasov. Physics and engineering of crossed-field discharge devices. *Plasma Sources Science and Technology*, 21(3):035006, 2012. URL http://stacks.iop.org/0963-0252/21/i=3/a=035006.

[2] John A. Thornton. Magnetron sputtering: basic physics and application to cylindrical magnetrons. *Journal of Vacuum Science and Technology*, 15(2): 171–177, 1978. doi:10.1116/1.569448. URL https://doi.org/10.1116/1.569448.

[3] T A van der Straaten, N F Cramer, I S Falconer, and B W James. The cylindrical dc magnetron discharge: I. particle-in-cell simulation. *Journal of Physics D: Applied Physics*, 31(2):177, 1998. URL http://stacks.iop.org/0022-3727/31/i=2/a=004.

[4] T A van der Straaten, N F Cramer, I S Falconer, and B W James. The cylindrical dc magnetron discharge: Ii. the negative space charge mode. *Journal of Physics D: Applied Physics*, 31(2):191, 1998. URL http://stacks.iop.org/0022-3727/31/i=2/a=005.

[5] Stephen Muhl and Argelia PÃĨrez. The use of hollow cathodes in deposition processes: A critical review. *Thin Solid Films*, 579:174 – 198, 2015. ISSN 0040-6090. doi:https://doi.org/10.1016/j.tsf.2015.02.066. URL http://www.sciencedirect.com/science/article/pii/S0040609015001947.

[6] Yuri P Raizer and John E Allen. *Gas discharge physics*, volume 2. Springer Berlin, 1997. URL http://www.springer.com/in/book/9783642647604.

[7] Michael A Lieberman and Alan J Lichtenberg. *Principles of plasma discharges and materials processing*. John Wiley & Sons, 2005. doi:10.1002/0471724254.

[8] D Loffhagen, F Sigeneger, and R Winkler. Study of the electron kinetics in the anode region of a glow discharge by a multiterm approach and monte carlo simulations. *Journal of Physics D: Applied Physics*, 35(14):1768, 2002. URL http://stacks.iop.org/0022-3727/35/i=14/a=319.

[9] J. J. Lowke, J. H. Parker, and C. A. Hall. Electron diffusion under the influence of an electric field near absorbing boundaries. *Phys. Rev. A*, 15: 1237–1245, Mar 1977. doi:10.1103/PhysRevA.15.1237. URL `https://link.aps.org/doi/10.1103/PhysRevA.15.1237`.

[10] I A Porokhova, Yu B Golubovskii, C Wilke, and A Dinklage. Electron distribution function in the anode region of inert gas discharges at low pressures and currents. *Journal of Physics D: Applied Physics*, 32(23):3025, 1999. URL `http://stacks.iop.org/0022-3727/32/i=23/a=308`.

[11] S. Arndt, F. Sigeneger, and R. Winkler. Study of the anode region of a dc glow discharge by a spatially one-dimensional hybrid method. *Plasma Chemistry and Plasma Processing*, 23(3):439–461, Sep 2003. ISSN 1572-8986. doi:10.1023/A:1023278814708. URL `https://doi.org/10.1023/A:1023278814708`.

[12] J Heberlein, J Mentel, and E Pfender. The anode region of electric arcs: a survey. *Journal of Physics D: Applied Physics*, 43(2):023001, 2010. URL `http://stacks.iop.org/0022-3727/43/i=2/a=023001`.

[13] S D Baalrud, N Hershkowitz, and B Longmier. Global nonambipolar flow: Plasma confinement where all electrons are lost to one boundary and all positive ions to another boundary. *Phys. Plasmas*, 14(4):042109, 2007. doi:10.1063/1.2722262.

[14] S D Baalrud, B Longmier, and N Hershkowitz. Equilibrium states of anodic double layers. *Plasma Sources Sci. Technol.*, 18(3):035002, 2009. doi:10.1088/0963-0252/18/3/035002.

[15] EV Barnat, GR Laity, and SD Baalrud. Response of the plasma to the size of an anode electrode biased near the plasma potential. *Phys. Plasmas*, 21 (10):103512, 2014. doi:10.1063/1.4897927.

[16] Bin Song, N D'Angelo, and R L Merlino. On anode spots, double layers and plasma contactors. *J. Phys. D: Appl. Phys.*, 24(10):1789, 1991. doi:10.1088/0022-3727/24/10/012.

[17] L Conde. Ionization instability by energized electrons in weakly ionized unmagnetized plasmas. *Physics of Plasmas*, 11(5):1955–1959, 2004. doi:10.1063/1.1705651.

[18] L. Dorf, Y. Raitses, and N. J. Fisch. Experimental studies of anode sheath phenomena in a hall thruster discharge. *Journal of Applied Physics*, 97(10): 103309, 2005. doi:10.1063/1.1915516. URL `https://doi.org/10.1063/1.1915516`.

[19] Brian N Chapman. *Glow discharge processes*. Wiley, 1980. URL `http://as.wiley.com/WileyCDA/WileyTitle/productCd-047107828X.html`.

[20] J. P. Hobson and P. A. Redhead. Operation of an inverted-magnetron gauge in the pressure range 10^{-3} to 10^{-12}âĂĆmm. hg. *Canadian Journal of Physics*, 36(3):271–288, 1958. doi:10.1139/p58-031. URL `https://doi.org/10.1139/p58-031`.

[21] Reiner Kukla. Magnetron sputtering on large scale substrates: an overview on the state of the art. *Surface and Coatings Technology*, 93 (1):1 – 6, 1997. ISSN 0257-8972. doi:https://doi.org/10.1016/S0257-8972(97)00018-2. URL `http://www.sciencedirect.com/science/article/pii/S0257897297000182`.

[22] E. I. Toader, V. Covlea, W. G. Graham, and P. G. Steen. High-density and low electron temperature direct current reflex plasma source. *Review of Scientific Instruments*, 75(2):382–386, 2004. doi:10.1063/1.1637459. URL `https://doi.org/10.1063/1.1637459`.

[23] L Oksuz and Noah Hershkowitz. First experimental measurements of the plasma potential throughout the presheath and sheath at a boundary in a weakly collisional plasma. *Physical review letters*, 89(14):145001, 2002. doi:10.1103/PhysRevLett.89.145001.

[24] Li Yi-Ren, Ma Jin-Xiu, Zheng Yao-Bang, and Zhang Wen-Gui. Experimental studies of plasma sheath near meshes of different transmissivity. *Chinese Physics B*, 19(8):085201, 2010. doi:10.1088/1674-1056/19/8/085201.

[25] RN Franklin. The plasma–sheath boundary region. *Journal of Physics D: Applied Physics*, 36(22):R309, 2003. doi:10.1088/0022-3727/36/22/R01.

[26] K-U Riemann. The bohm criterion and sheath formation. *Journal of Physics D: Applied Physics*, 24(4):493, 1991. doi:10.1088/0022-3727/24/4/001.

[27] D Bohm. *The characteristics of electrical discharges in magnetic fields ed. By A. Guthrie and R.K. Wakerling*. National nuclear energy series: Electromagnetic Separation Project. McGraw-Hill, 1949. URL `https://books.google.co.in/books?id=KyRRAAAAMAAJ`.

[28] Irving Langmuir. The interaction of electron and positive ion space charges in cathode sheaths. *Physical Review*, 33(6):954, 1929. doi:10.1103/PhysRev.33.954.

[29] K-U Riemann. The influence of collisions on the plasma sheath transition. *Physics of plasmas*, 4(11):4158–4166, 1997. doi:10.1063/1.872536.

[30] Noah Hershkowitz. Sheaths: More complicated than you think a. *Physics of plasmas*, 12(5):055502, 2005. doi:10.1063/1.1887189.

[31] Jin-Yuan Liu, Zheng-Xiong Wang, and Xiaogang Wang. Sheath criterion for a collisional sheath. *Physics of Plasmas*, 10(7):3032–3034, 2003. doi:10.1063/1.1584048.

[32] Bin Song, N D'Angelo, and Robert L Merlino. Stability of a spherical double layer produced through ionization. *Journal of Physics D: Applied Physics*, 25(6):938, 1992. doi:10.1088/0022-3727/25/6/006.

[33] Mircea Sanduloviciu, Catalin Borcia, and Gabriela Leu. Self-organization phenomena in current carrying plasmas related to the non-linearity of the current versus voltage characteristic. *Physics Letters A*, 208(1-2):136–142, 1995. doi:10.1016/0375-9601(95)00715-F.

[34] Silviu Gurlui, Marcel Agop, Mitachi Strat, Georgeta Strat, and Simona Bācāiţā. Experimental and theoretical investigations of anode double layer. *Jpn. J. Appl. Phys., Part 1*, 44(5R):3253, 2005. doi:10.1143/JJAP.44.3253.

[35] R L Stenzel, C Ionita, and R Schrittwieser. Dynamics of fireballs. *Plasma Sources Sci. Technol.*, 17(3):035006, 2008. doi:10.1088/0963-0252/17/3/035006.

[36] M Strat, Georgeta Strat, and S Gurlui. Basic processes in discharge plasma double layers. *Journal of Physics D: Applied Physics*, 32(1):34, 1999. doi:10.1088/0022-3727/32/1/007.

[37] Deli Tang and Paul K Chu. Anode double layer in magnetized radio frequency inductively coupled hydrogen plasma. *Journal of applied physics*, 94(3):1390–1395, 2003. doi:10.1063/1.1589592.

[38] RL Stenzel, J Gruenwald, B Fonda, C Ionita, and R Schrittwieser. Transit time instabilities in an inverted fireball. i. basic properties. *Physics of Plasmas*, 18(1):012104, 2011. doi:10.1063/1.3533437.

[39] V Lapuerta and E Ahedo. Dynamic model of a plasma structure with an intermediate double-layer, formed outside an anodic plasma contactor. *Physics of Plasmas*, 7(6):2693–2703, 2000. doi:10.1063/1.874113.

[40] L Conde, C Ferro Fontan, and J Lambás. The transition from an ionizing electron collecting plasma sheath into an anodic double layer as a bifurcation. *Phys. Plasmas*, 13(11):113504, 2006. doi:10.1063/1.2388265.

[41] Codrina IonitÌğă, Dan-Gheorghe Dimitriu, and Roman W Schrittwieser. Elementary processes at the origin of the generation and dynamics of multiple double layers in dp machine plasma. *Int. J. Mass Spectrom.*, 233(1):343–354, 2004. doi:10.1016/j.ijms.2004.01.009.

[42] Binita Borgohain and H. Bailung. Ion and electron sheath characteristics in a low density and low temperature plasma. *Physics of Plasmas*, 24(11):113512, 2017. doi:10.1063/1.5006133. URL `https://doi.org/10.1063/1.5006133`.

[43] Brett Scheiner, Scott D Baalrud, Benjamin T Yee, Matthew M Hopkins, and Edward V Barnat. Theory of the electron sheath and presheath. *Phys. Plasmas*, 22(12):123520, 2015. doi:10.1063/1.4939024.

[44] Brett Scheiner, Scott D. Baalrud, Matthew M. Hopkins, Benjamin T. Yee, and Edward V. Barnat. Particle-in-cell study of the ion-to-electron sheath transition. *Physics of Plasmas*, 23(8):083510, 2016. doi:10.1063/1.4960382. URL https://doi.org/10.1063/1.4960382.

[45] Brett Scheiner, Edward V. Barnat, Scott D. Baalrud, Matthew M. Hopkins, and Benjamin T. Yee. Theory and simulation of anode spots in low pressure plasmas. *Physics of Plasmas*, 24(11):113520, 2017. doi:10.1063/1.4999477. URL https://doi.org/10.1063/1.4999477.

[46] RL Stenzel, J Gruenwald, B Fonda, C Ionita, and R Schrittwieser. Transit time instabilities in an inverted fireball. ii. mode jumping and nonlinearities. *Physics of Plasmas*, 18(1):012105, 2011. doi:10.1063/1.3533440.

[47] S Torven and D Andersson. Observations of electric double layers in a magnetised plasma column. *Journal of Physics D: Applied Physics*, 12(5):717, 1979. URL http://stacks.iop.org/0022-3727/12/i=5/a=012.

[48] D Andersson. Double layer formation in a magnetised laboratory plasma. *Journal of Physics D: Applied Physics*, 14(8):1403, 1981. URL http://stacks.iop.org/0022-3727/14/i=8/a=008.

[49] Tao An, RL Merlino, and N D'Angelo. Cylindrical anode double layers ('firerods') produced in a uniform magnetic field. *Journal of Physics D: Applied Physics*, 27(9):1906, 1994. doi:10.1088/0022-3727/27/9/014.

[50] Deli Tang and Paul K. Chu. Anode double layer in magnetized radio frequency inductively coupled hydrogen plasma. *Journal of Applied Physics*, 94(3):1390–1395, 2003. doi:10.1063/1.1589592. URL https://doi.org/10.1063/1.1589592.

[51] S Chauhan, M Ranjan, M Bandyopadhyay, and S Mukherjee. Droplet shaped anode double layer and electron sheath formation in magnetically constricted anode. *Phys. Plasmas*, 23(1):013502, 2016. doi:10.1063/1.4939029.

[52] Steven L Cartier and Robert L Merlino. Anode-type double layers in a nonuniform magnetic field. *Phys. Fluids*, 30(8):2549–2560, 1987. doi:10.1063/1.866093.

[53] B E Cherrington. The use of electrostatic probes for plasma diagnosticsâĂŤa review. *Plasma Chem. Plasma Process*, 2(2):113–140, 1982. doi:10.1007/BF00633129.

[54] I. H. Hutchinson. *Principles of Plasma Diagnostics:*. Cambridge University Press, Cambridge, 2 edition, 007 2002. ISBN 9780511613630. doi:10.1017/CBO9780511613630. URL https://www.cambridge.org/core/books/principles-of-plasma-diagnostics/93578947341481B0F9169D598D535E76.

[55] Noah Hershkowitz. 3 - how langmuir probes work. In Orlando Auciello and Daniel L. Flamm, editors, *Plasma Diagnostics*, pages 113 – 183. Academic Press, 1989. ISBN 978-0-12-067635-4. doi:http://dx.doi.org/10.1016/B978-0-12-067635-4.50008-9. URL http://www.sciencedirect.com/science/article/pii/B9780120676354500089.

[56] R.H. Huddlestone and S.L. Leonard. *Plasma diagnostic techniques*. Pure and applied physics. Academic Press, 1965. URL https://books.google.co.in/books?id=Eb08AAAAIAAJ.

[57] Michael A Lieberman and Alan J Lichtenberg. *Principles of plasma discharges and materials processing*. John Wiley & Sons, 2005. URL http://as.wiley.com/WileyCDA/WileyTitle/productCd-0471720011.html.

[58] E. O. Johnson and L. Malter. A floating double probe method for measurements in gas discharges. *Phys. Rev.*, 80:58–68, Oct 1950. doi:10.1103/PhysRev.80.58.

[59] Muhammad Yasin Naz, Abdul Ghaffar, NU Rehman, S Naseer, and Muhammad Zakaullah. Double and triple langmuir probes measurements in inductively coupled nitrogen plasma. *Progress In Electromagnetics Research*, 114: 113–128, 2011. doi:10.2528/PIER10110309.

[60] J P Sheehan, Yevgeny Raitses, Noah Hershkowitz, Igor Kaganovich, and N J Fisch. A comparison of emissive probe techniques for electric potential measurements in a complex plasma. *Phys. Plasmas*, 18(7):073501, 2011. doi:10.1063/1.3601354.

[61] J P Sheehan and N Hershkowitz. Emissive probes. *Plasma Sources Sci. Technol.*, 20(6):063001, 2011. doi:10.1088/0963-0252/20/6/063001.

[62] Irving Langmuir. The pressure effect and other phenomena in gaseous discharges. *Journal of the Franklin Institute*, 196(6):751–762, 1923. doi:10.1016/S0016-0032(23)90859-8.

[63] Robert F Kemp and JMs Sellen Jr. Plasma potential measurements by electron emissive probes. *Review of Scientific Instruments*, 37(4):455–461, 1966. doi:10.1063/1.1720213.

[64] L Dorf, Y Raitses, and NJ Fisch. Electrostatic probe apparatus for measurements in the near-anode region of hall thrusters. *Review of scientific instruments*, 75(5):1255–1260, 2004. doi:10.1063/1.1710698.

[65] Yu B Golubovskii, I A Porokhova, V P Sushkov, M HolÃŋk, P Kudrna, and M TichÃ¡. Electron kinetics in cylindrical discharges of magnetron configurations. *Plasma Sources Science and Technology*, 15(2):228, 2006. URL http://stacks.iop.org/0963-0252/15/i=2/a=007.

[66] H A Blevin and S C Haydon. The interpretation of breakdown characteristics of electrodeless discharges in transverse magnetic fields. *Proceedings of the Physical Society*, 81(3):490, 1963. URL http://stacks.iop.org/0370-1328/81/i=3/a=315.

[67] S N Sen and A K Ghosh. Variation of townsend's second coefficient in electrodeless discharge. *Proceedings of the Physical Society*, 79(1):180, 1962. URL http://stacks.iop.org/0370-1328/79/i=1/a=322.

[68] S N Sen and A K Ghosh. Variation of townsend's second coefficient in an electrodeless discharge in crossed electric and magnetic fields. *Proceedings of the Physical Society*, 79(2):293, 1962. URL http://stacks.iop.org/0370-1328/79/i=2/a=307.

[69] S N Sen and A K Ghosh. Breakdown of an electrodeless discharge in crossed electric and magnetic fields. *Proceedings of the Physical Society*, 80(4):909, 1962. URL http://stacks.iop.org/0370-1328/80/i=4/a=313.

[70] Shou-Zhe Li and Han S. Uhm. Influence of magnetic field on the electrical breakdown characteristics in cylindrical diode. *Physics of Plasmas*, 11(7): 3443–3448, 2004. doi:10.1063/1.1737743. URL https://doi.org/10.1063/1.1737743.

[71] Marija RadmiloviÄĞ-RadjenoviÄĞ and Branislav RadjenoviÄĞ. The effect of magnetic field on the electrical breakdown characteristics. *Journal of Physics D: Applied Physics*, 39(14):3002, 2006. URL http://stacks.iop.org/0022-3727/39/i=14/a=019.

[72] R. Rane, M. Bandyopadhyay, M. Ranjan, and S. Mukherjee. Controllable transition from positive space charge to negative space charge in an inverted cylindrical magnetron. *Physics of Plasmas*, 23(1):013514, 2016. doi:10.1063/1.4940326. URL https://doi.org/10.1063/1.4940326.

[73] L Pekker. Longitudinal distribution of plasma density in the low-pressure glow discharge with transverse magnetic field. *Plasma Sources Science and Technology*, 4(1):31, 1995. URL http://stacks.iop.org/0963-0252/4/i=1/a=004.

[74] W. D. Gill and Eric Kay. Efficient low pressure sputtering in a large inverted magnetron suitable for film synthesis. *Review of Scientific Instruments*, 36(3):277–282, 1965. doi:10.1063/1.1719553. URL https://doi.org/10.1063/1.1719553.

[75] E Passoth, P Kudrna, C Csambal, J F Behnke, M TichÃ¡, and V Helbig. An experimental study of plasma density determination by a cylindrical langmuir probe at different pressures and magnetic fields in a cylindrical magnetron discharge in heavy rare gases. *Journal of Physics D: Applied Physics*, 30(12): 1763, 1997. URL http://stacks.iop.org/0022-3727/30/i=12/a=013.

[76] E Passoth, J F Behnke, C Csambal, M TichÃ¡, P Kudrna, Yu B Golubovskii, and I A Porokhova. Radial behaviour of the electron energy distribution function in the cylindrical magnetron discharge in argon. *Journal of Physics D: Applied Physics*, 32(20):2655, 1999. URL http://stacks.iop.org/0022-3727/32/i=20/a=312.

[77] Sankar Moni Borah, Arup Ratan Pal, Heremba Bailung, and Joyanti Chutia. Optimization of plasma parameters for high rate deposition of titanium nitride films as protective coating on bell-metal by reactive sputtering in cylindrical magnetron device. *Applied Surface Science*, 254(18):5760 – 5765, 2008. ISSN 0169-4332. doi:https://doi.org/10.1016/j.apsusc.2008.03.047. URL http://www.sciencedirect.com/science/article/pii/S0169433208006065.

[78] S. M. Rossnagel and H. R. Kaufman. Charge transport in magnetrons. *Journal of Vacuum Science & Technology A*, 5(4):2276–2279, 1987. doi:10.1116/1.574434. URL https://doi.org/10.1116/1.574434.

[79] A Todoran, M Mantel, A BÃĺs, C Vachey, and A Lacoste. Control of particle flux and energy on substrate in an inverted cylindrical magnetron for plasma pvd. *Plasma Sources Science and Technology*, 23(6):065039, 2014. URL http://stacks.iop.org/0963-0252/23/i=6/a=065039.

[80] Steven L Cartier and Robert L Merlino. Anode-type double layers in a nonuniform magnetic field. *Phys. Fluids*, 30(8):2549–2560, 1987. doi:10.1063/1.866093.

[81] EV Barnat, GR Laity, and SD Baalrud. Response of the plasma to the size of an anode electrode biased near the plasma potential. *Phys. Plasmas*, 21 (10):103512, 2014. doi:10.1063/1.4897927.

[82] S D Baalrud, B Longmier, and N Hershkowitz. Equilibrium states of anodic double layers. *Plasma Sources Sci. Technol.*, 18(3):035002, 2009. doi:10.1088/0963-0252/18/3/035002.

[83] John B Boffard, R O Jung, Chun C Lin, and A E Wendt. Optical emission measurements of electron energy distributions in low-pressure argon inductively coupled plasmas. *Plasma Sources Science and Technology*, 19 (6):065001, oct 2010. doi:10.1088/0963-0252/19/6/065001. URL https://doi.org/10.1088%2F0963-0252%2F19%2F6%2F065001.

[84] P.J. Cullen and V. MilosavljeviÃĎâĂą. Spectroscopic characterization of a radio-frequency argon plasma jet discharge in ambient air. *Progress*

of Theoretical and Experimental Physics, 2015(6), 06 2015. ISSN 2050-3911. doi:10.1093/ptep/ptv070. URL https://dx.doi.org/10.1093/ptep/ptv070.

[85] Vladimir MilosavljeviÄĞ, Niall MacGearailt, P. J. Cullen, Stephen Daniels, and Miles M. Turner. Phase-resolved optical emission spectroscopy for an electron cyclotron resonance etcher. *Journal of Applied Physics*, 113(16):163302, 2013. doi:10.1063/1.4802440. URL https://doi.org/10.1063/1.4802440.

[86] I. A. Porokhova, Yu. B. Golubovskii, J. Bretagne, M. Tichy, and J. F. Behnke. Kinetic simulation model of magnetron discharges. *Phys. Rev. E*, 63:056408, Apr 2001. doi:10.1103/PhysRevE.63.056408. URL https://link.aps.org/doi/10.1103/PhysRevE.63.056408.

[87] R. Rane, P. Bandyopadhyay, M. Bandyopadhyay, and S. Mukherjee. Experimental investigation of near anode phenomenon in inverted cylindrical magnetron discharge. *Physics of Plasmas*, 25(6):063516, 2018. doi:10.1063/1.5025220. URL https://doi.org/10.1063/1.5025220.

[88] S Chauhan, M Ranjan, M Bandyopadhyay, and S Mukherjee. Droplet shaped anode double layer and electron sheath formation in magnetically constricted anode. *Phys. Plasmas*, 23(1):013502, 2016. doi:10.1063/1.4939029.

[89] R. Rane, S. Chauhan, P. Bharathi, K. Nigam, P. Bandyopadhyay, and S. Mukherjee. Electron sheath evolution controlled by a magnetic field in modified hollow cathode glow discharge. *Physics of Plasmas*, 25(9):093509, 2018. doi:10.1063/1.5038907. URL https://doi.org/10.1063/1.5038907.

[90] Hans R Griem. *Principles of Plasma Spectroscopy*. Cambridge University, 2005. doi:9780521619417.

[91] M A Mujawar, S K Karkari, and M M Turner. Properties of a differentially pumped constricted hollow anode plasma source. *Plasma Sources Sci. Technol.*, 20(1):015024, 2011. URL http://stacks.iop.org/0963-0252/20/i=1/a=015024.

[92] Neeraj Chaubey, S Mukherjee, A N Sekar Iyengar, and A Sen. Synchronization between two coupled direct current glow discharge plasma sources. *Phys. Plasmas*, 22(2):022312, 2015. doi:10.1063/1.4913227.

[93] H Klostermann, F Greiner, T Klinger, and A Piel. Stable and unstable discharge modes of a multipole confined thermionic gas discharge at low pressure. *Plasma Sources Science and Technology*, 3(2):134–141, may 1994. doi:10.1088/0963-0252/3/2/003. URL https://doi.org/10.1088%2F0963-0252%2F3%2F2%2F003.

[94] Robert L. Merlino and Steven L. Cartier. Hysteresis in a lowâĂŘpressure argon discharge. *Applied Physics Letters*, 44(1):33–34, 1984. doi:10.1063/1.94593. URL https://doi.org/10.1063/1.94593.

[95] R. Timm and A. Piel. Hysteresis and transition to chaos in a thermionic plasma discharge. *Contributions to Plasma Physics*, 32(6):599–611. doi:10.1002/ctpp.2150320603. URL https://onlinelibrary.wiley.com/doi/abs/10.1002/ctpp.2150320603.

[96] R. A. Bosch and R. L. Merlino. Sudden jumps, hysteresis, and negative resistance in an argon plasma discharge. i. discharges with no magnetic field. *BeitrÃďge aus der Plasmaphysik*, 26(1):1–12. doi:10.1002/ctpp.19860260102. URL https://onlinelibrary.wiley.com/doi/abs/10.1002/ctpp.19860260102.

[97] F. Greiner, T. Klinger, H. Klostermann, and A. Piel. Experiments and particle-in-cell simulation on self-oscillations and period doubling in thermionic discharges at low pressure. *Phys. Rev. Lett.*, 70:3071–3074, May 1993. doi:10.1103/PhysRevLett.70.3071. URL https://link.aps.org/doi/10.1103/PhysRevLett.70.3071.

[98] F. Greiner, T. Klinger, and A. Piel. Nonlinear dynamical behavior of thermionic low pressure discharges. i. simulation. *Physics of Plasmas*, 2(6):1810–1821, 1995. doi:10.1063/1.871335. URL https://doi.org/10.1063/1.871335.

[99] T. Klinger, F. Greiner, A. Rohde, and A. Piel. Nonlinear dynamical behavior of thermionic low pressure discharges. ii. experimental. *Physics of Plasmas*, 2(6):1822–1836, 1995. doi:10.1063/1.871336. URL https://doi.org/10.1063/1.871336.

[100] W.X Ding, T Klinger, and A Piel. Low-frequency current oscillations in a linear hot-cathode discharge. *Physics Letters A*, 222(6):409 – 414, 1996. ISSN 0375-9601. doi:https://doi.org/10.1016/S0375-9601(96)00661-5. URL http://www.sciencedirect.com/science/article/pii/S0375960196006615.

[101] Hae June Lee and Jae Koo Lee. Mode transition and nonlinear self-oscillations in the beam-driven collisional discharge plasma. *Physics of Plasmas*, 5(8):2878–2884, 1998. doi:10.1063/1.873009. URL https://doi.org/10.1063/1.873009.

[102] E. I. Toader and V. N. Covlea. Enhanced magnetic ionization in hydrogen reflex discharge plasma source. *Review of Scientific Instruments*, 76(3):033502, 2005. doi:10.1063/1.1866236. URL https://doi.org/10.1063/1.1866236.

[103] E I Toader and W G Graham. Plasma parameter characterization of a reflex plasma source operating in oxygen. *Plasma Sources Science and Technology*, 9(3):288–294, jul 2000. doi:10.1088/0963-0252/9/3/306. URL https://doi.org/10.1088%2F0963-0252%2F9%2F3%2F306.

[104] Gopi Kishan Sabavath, Pankaj Kumar Shaw, A. N. Sekar Iyengar, I. Banerjee, and S. K. Mahapatra. Experimental investigation of quasiperiodic-chaotic-quasiperiodic-chaotic transition in a direct current magnetron sputtering plasma. *Physics of Plasmas*, 22(8):082121, 2015. doi:10.1063/1.4928902. URL https://doi.org/10.1063/1.4928902.

[105] P. Y. Cheung and A. Y. Wong. Chaotic behavior and period doubling in plasmas. *Phys. Rev. Lett.*, 59:551–554, Aug 1987. doi:10.1103/PhysRevLett.59.551. URL https://link.aps.org/doi/10.1103/PhysRevLett.59.551.

[106] P. Y. Cheung, S. Donovan, and A. Y. Wong. Observations of intermittent chaos in plasmas. *Phys. Rev. Lett.*, 61:1360–1363, Sep 1988.

doi:10.1103/PhysRevLett.61.1360. URL https://link.aps.org/doi/10.1103/PhysRevLett.61.1360.

[107] J. Qin, L. Wang, D. P. Yuan, P. Gao, and B. Z. Zhang. Chaos and bifurcations in periodic windows observed in plasmas. *Phys. Rev. Lett.*, 63:163–166, Jul 1989. doi:10.1103/PhysRevLett.63.163. URL https://link.aps.org/doi/10.1103/PhysRevLett.63.163.

[108] Holger Kantz and Thomas Schreiber. *Nonlinear time series analysis*, volume 7. Cambridge university press, 2004.

[109] Md. Nurujjaman, Ramesh Narayanan, and A. N. Sekar Iyengar. Parametric investigation of nonlinear fluctuations in a dc glow discharge plasma. *Chaos: An Interdisciplinary Journal of Nonlinear Science*, 17(4):043121, 2007. doi:10.1063/1.2815818. URL https://doi.org/10.1063/1.2815818.

[110] BORNALI SARMA, SOURABH S. CHAUHAN, A. M. WHARTON, and A. N. SEKAR IYENGAR. Continuous wavelet transform analysis for self-similarity properties of turbulence in magnetized dc glow discharge plasma. *Journal of Plasma Physics*, 79(5):885âĂŞ891, 2013. doi:10.1017/S0022377813000639.